Polymer Derived Silicon Carbide Ceramics for Nuclear Applications

Shelly Arreguin

A dissertation

submitted in partial fulfillment of the

requirements for the degree of

Doctor of Philosophy

University of Washington

2015

Reading Committee:

Rajendra Bordia, Chair

Chuck Henager Jr.

Brian Flinn

Lucien Brush

Program Authorized to Offer Degree:

Materials Science and Engineering

University of Washington

Abstract

Polymer Derived Silicon Carbide Ceramics for Nuclear Applications

Shelly Arreguin

Chair of the Supervisory Committee:

Professor Rajendra Bordia

Materials Science and Engineering

The next generation of nuclear fission and fusion reactors depends upon the development of high performance structural materials. Silicon carbide (SiC) is being considered for a variety of nuclear reactor components because it possesses outstanding physical and chemical properties, including: high thermal conductivity, high temperature stability, chemical inertness, extreme hardness and small neutron capture cross-section. However, when exposed to energetic particles, SiC is observed to experience various radiation induced defects such as: vacancy clusters, dislocation loops and network dislocations at lower temperatures and swelling of the material causing voids/cavities at higher temperatures. Recent studies have shown nanostructured interfaces and nanoscale grains are more radiation damage tolerant. Polymer derived ceramics (PDCs) provide a unique route to develop SiC ceramics with nanostructural features that can help mitigate radiation defects. A novel class of SiC ceramics with controlled microstructures has been developed through tailoring of the molecular architecture of the starting precursor (allylhydridopolycarbosilane, Starfire® SMP-10). Nanostructural features in the form of graphene layers were incorporated via excess carbon from the addition of divinylbenzene (0-5 wt%) to the liquid SMP-10. It was observed that with increasing concentration of carbon, the 6H SiC (hexagonal) phase formed at the expense of 3C SiC (cubic). The utilization of PDCs also made possible the addition of sintering additives at the molecular level through a hydroboration reaction of SMP-10 with decaborane. This allowed the boron additives to be contained within the SiC grains, as opposed to on the grain boundaries, as is observed in traditional ceramic processing. Finally, these materials were irradiated using ion accelerator facilities located at the Environmental Molecular Sciences Laboratory at the Pacific Northwest National Laboratory. AFM results indicate that utilizing PDC processing routes vs. traditional ceramic routes yielded a significant decrease in the amount of swelling from point defect accumulation due to radiation bombardment. This research contributes to current priorities in designing materials for the next

generation of nuclear power plants that are anticipated to have minimal waste, decreased risk of proliferation and increased accident damage tolerance.

Table of Contents

Figures

Tables

Acknowledgements

This extended educational experience of continuous questioning was in a huge part inspired by my undergraduate research experiences at the University of Colorado at Boulder (CU). The motivation I received from Professor Rishi Raj (Mechanical Engineering, CU) and Professor Cortlandt Pierpont (Chemistry, CU) gave me the vision to move forward in my pursuit of science. During my time as a graduate student, I had the pleasure of doing research across 3 continents, 4 countries and 5 laboratories. As such, this body of work would not have been possible without assistance from the: Pacific Northwest National Laboratory (PNNL), Institute of Inorganic Chemistry Slovak Academy of Sciences (IICSAS), Technische Universität Wien (TU) and University of Queensland, Centre for Microscopy and Microanalysis. I am forever grateful to have had such wonderful opportunities to learn and expand my horizons…

The powder processing and densification of the PDC SiC was accomplished at the IICSAS and TU. At the IICSAS, I would like to thank Professor Pavel Sajgalik for inviting me as a visiting scholar to perform this work. My background in Chemistry had a huge impact on the thought processes that went into the polymeric portions of this research. Admittedly though, prior to my time at the IICSAS I didn't know how to effectively think about the densification of SiC and SiC/Si_3N_4 ceramics. However, with the help of Dr. Zoltan Lences, I learned the necessary parameters to obtain dense, crack free SiC and SiC/Si_3N_4. I also learned that hot presses are very finicky and can have any number of problems at a given time. Needless to say, at one point the hot presses were all down and I still had samples to process and little time remaining. As such, I received a most welcome offer from Dr. Thomas Konegger from TU to use their hot press for the remaining samples. Arne Ziebell (graduate student at TU) helped me successfully densify my SiC materials (crack free, of course). Without the efforts of the folks from the IICSAS and TU, I would not have known the novelty of the SiBC powders I developed during my Ph.D.

The great majority of the last two years of my Ph.D. research was conducted at PNNL. With that, I would especially like to thank Dr. Chuck Henager Jr. for always having an open door and being a hugely encouraging mentor, as well as vastly expanding my ideas in developing radiation resistant materials. I would also like to thank: Dr. Nancy Washton for the MAS-NMR results as well as her mentorship both personally and professionally (we'll figure out the boron), Dr. Birgit Schwenzer for being an amazing CSM and taking time to discuss forks in the road, Dr. Yongsoon Shin for showing me the ropes upon arrival, Dr. Weilin Jiang and Dr. Shuttha Shutthanandan for assistance with the ion accelerator experiments, Dr. Zihua Zhu for the Nano-SIMS and ToF-SIMS work, Dr. Jonathan Suter and Dr. Martin McBriarty for all things AFM, Timothy Roosendaal for assisting me with the 1600°C hot press work, Matt Westman for various thermal analysis techniques, Sandeep Manandhar for assistance with SRIM/TRIM and Dr. Danny Edwards for preliminary TEM analysis. I would also like to give a HUGE, Huge shout out to Clyde Chamberlain for all the assistance with machining and polishing, both the porous and dense SiC samples (and for epic conversations about boots and motorcycles). Finally, I would like to thank Donna Feaster for general help and assistance with everyday everything's… All of you at PNNL have significantly enriched my graduate research experience...

My final months as a graduate student were spent at the University of Queensland (UQ), Centre for Microscopy and Microanalysis (CMM). I would like to thank Professor John Drennan for inviting me to the CMM to use the TEMs for my analysis, as well as being a most excellent host

(even if we did almost end up in Tasmania on a jet ski…). With the help of Dr. Graeme Auctherlonie, I became very efficient at HRTEM and zoning relatively small grains (less than 100 nm). This was done to understand the crystal structure (boron carbide dps, too easy…) as well as visualize the defects associated with ion irradiation. Graeme also helped me considerably with STEM EELS to know the location and size of the boron grains within the SiC. Graeme was also very welcoming of me to the lab and Oz in general. When not too busy in the dark TEM rooms we would go for Wednesday Bubbles, as well as epic bush walking excursions on weekends. Additionally, I would like to thank: Dr. Hui Diao for all the TEM sample prep using the FIB, Eunice Grinam for video assistance for the Australia Academy of Sciences, Dr. Anya Yago and Dr. Kevin Jack for XRD analysis, Dr. Zhi Zhang for general TEM guidance and Jill Prescott for further culturing me in Aussie language. My time at the UQ was a most rewarding experience and the knowledge I gained here will continue to assist me in my future career.

At the University of Washington I would like to thank my committee members: Professor Lucien Brush, Professor John Sorensen, Professor Jiangyu Li, Dr. Chuck Henager (PNNL) and special thanks to Professor Brian Flinn, for not only serving on my committee but also directly assisting me in the lab on numerous occasions. I would also like to thank: Dr. Ashley Tracey and Dr. Ryan Toivola for assisting me with FTIR, Dr. Scott Braswell for working with me on SEM/EDS, Dr. Gary Weber for the electron beam curing of SMP-10, Dr. Betzaida Batalla for always lending an ear (R.I.P. con mucho turismo) and the MSE staff: Bichtien Thac, Karen Wetterhahn and Kathy Elkins for going above and beyond (even if it was last minute). I would also like to thank the following members of the Bordia group for passing on their infinite wisdom my way before checking out: Dr. Cliff Leslie Dr. Nikolas Hrabe, and Dr. Kaishi Wang.

Finally, I would like to give a huge thank you to my advisor Professor Raj Bordia. Raj always encouraged the writing of proposals, which perhaps in the beginning was a seemingly impossible task, whereas now simply a necessary reality. Furthermore, Raj always forwarded along interesting and novel opportunities to enhance our education beyond the lab, such as conferences, advanced schools, etc… As such, I became more involved in the scientific community (nuclear specifically) and began searching for more ways I could contribute to not only scientific societies but public outreach as well. Ultimately, Raj allowed a lot of freedom in the research process, which has very much fostered my development as an independent scientist.

Last, but most certainly not least… I would like to give an extra special thanks to Dr. Kevin Strong Jr., a Ceramicist from Alfred who is always willing to share his wealth of knowledge with me, as well as entertain my hypothetical ceramic questions. Moreover, he always read and re-read proposals that I was working on, as well as listened endlessly to presentations I was about to give. I learned so much from him and continue to do so… I only hope I provided the same sort of support back his way…

This research was supported in part by:

- DoE-Nuclear Energy University Program Award # 10-918
- National Science Foundation East Asia and Pacific Summer Institute, 2015
- International Center for Materials Research Fellowship, 2012
- Washington NASA Space Grant, 2009

Dedication

To the unconventional conventionalists of the Darkside of the Watermelon…

Chapter I Introduction

The demand for nuclear energy has increased due to rising costs of fuel oil and natural gas, along with increasing energy demands worldwide. In addition, the negative long-term effects of greenhouse gases associated with fossil fuel usage are being recognized. The global community is facing the challenges of maintaining sovereign nation security, reducing greenhouse gases, and also addressing the issue of climate change. Nuclear power is well established as a safe, clean option to reduce greenhouse gases from electricity production and has the potential of displacing fossil fuel based plants as the primary source of electric power. In the US nuclear power currently yields 20% of the electrical power and 16% worldwide.[1] However, there is a pressing need to develop technologies and solutions to improve reliability and extend the life of current reactors. In addition, there is a need to develop new reactor designs and fuel cycles, which will improve fuel utilization, minimize the risk of proliferation and further increase accident damage tolerance.

The potential for accident scenarios and leakages are of significant importance in the development of new nuclear power plants. Sites such as Fukushima, Japan (natural disaster accident), Hanford, WA, USA (legacy waste from weapons production), Chernobyl, Ukraine (nuclear power plant accident) and Dounreay, UK (nuclear fuel leak) remain challenging environmental cleanup locations. Varying methods of remediation are required due to differences in radionuclides as well as respective locations, which impact transport mechanisms through the environment. The history of these sites, in conjunction with the US lacking an operational repository, impacts decisions on the development of next generation nuclear reactors. Furthermore, there is also concern that nuclear reactors, their facilities and their fuel can be

misused in the development of weapons. Therefore threat of proliferation, waste disposal issues and increasing accident damage tolerance are key issues driving next generation nuclear reactor designs.

High temperature reactors (HTR) are leading candidates in Generation IV reactor design concepts. They are being designed to operate at increased temperatures such that fuel will be used more efficiently to have greater energy yield with decreased production of waste. HTRs have the ability to operate at a temperature up to 800°C in the short term and above 900°C in the longer term.[2] The capability of achieving these goals requires the development of advanced materials that will have increased radiation damage tolerances with the ability to tolerate high temperatures in the neutron environment. Advanced metallic and ceramic materials are currently being investigated for a variety of applications in these Generation IV reactor concepts.[1] Specifically, SiC ceramics are being considered for a variety of next generation nuclear reactor components because they possess outstanding physical and chemical properties, including high-thermal conductivity, high-temperature stability, chemical inertness, extreme hardness, and small neutron capture cross-section.[3,4] SiC ceramics have many potential nuclear applications including the development of Tristructural-isotropic (TRISO) fuel, storage of inert gas fission products and the replacement of zircaloy cladding in light water reactors (as SiC is observed to have reduced exothermic reactions with water or steam compared to zircaloys).[5] It is also a barrier for fission product diffusion in gas-cooled fission reactors,[6] an inert matrix for the transmutation of plutonium and other transuranics,[7] and is also used in fusion first wall applications.[8] The usage of SiC in specialized reactor components assists in the achievement of innovative reactor design

concepts that will further extend the safety and proliferation resistant operation of nuclear reactors.

In summary, nuclear energy plays a key role in providing the world with clean, affordable electricity. In order to maintain continued support for this abundant source of energy the safety, reliability, efficiency and lifetime of current and future nuclear reactor designs must be advanced. The design criteria will be such that increased accident damage tolerance and ability to operate at higher temperatures is realized. The development of advanced structural materials like SiC will play a large role in achieving these goals.

Chapter II Background

Next generation nuclear fission and fusion reactor designs are anticipated to operate under high radiation fluxes, elevated temperatures, intense productions of transmutant elements (particularly, H and He) and high stresses. In order for these new operating conditions to be feasible it is necessary to develop advanced structural materials that are able to withstand these conditions. Structural materials in the first demonstration fusion reactor are expected to satisfactorily operate up to damage levels approaching 100 displacement per atom (dpa) or higher,[9] whereas the first-generation (late 1950s) fission reactor plants required materials to withstand a maximum damage of one dpa. It is also well known that materials in a fusion reactor will encounter He atoms either through an (n,α) reaction or directly through implantation from plasma generated helium.[2] This increased generation of helium and hydrogen transmutation by fusion absorption causes cavity swelling in current structural materials and thus embrittlement of the exposed materials.

At various temperatures there are different degrees and clusters associated with swelling of the materials under irradiation. At lower temperatures, the defect cluster accumulation in the matrix tends to produce high hardening with embrittlement and localized deformation creating high stress concentrations at the grain boundaries. At high temperatures, formation of helium cavities at grain boundaries can lead to severe intergranular embrittlement Figure II-1.[4]

Figure II-1 Helium accumulation at the grain boundaries [10]

Therefore, the microstructure of the ceramic materials including their grain boundaries must be designed to mitigate these severe neutron radiation effects.

In addition to developing materials for next generation nuclear reactors, the pertinent issue of further increasing accident damage tolerance of current reactors remains a primary goal for the nuclear community.

In history, three nuclear accidents are remembered for their massive impacts: Fukushima nuclear power plant (NPP) (2011), the Chernobyl NPP (1986) and the Kyshtym (Russia) radiation accident (1957). At Chernobyl, radioactivity was released from an operating nuclear reactor that exploded during an experiment scheduled to test a potential safety emergency core-cooling feature. In the case of Kyshtym, the newly developed afterthought of a storage facility for high

level radioactive waste from weapons production was improperly monitored. The cooling system in one of the tanks containing 70-80 tons of liquid radioactive waste failed. The waste began heating itself through decay heat due to its high levels of radioactivity, which resulted in the evaporation and subsequent chemical explosion of the dried waste. The Fukushima NPP failure was due to loss of backup electricity and subsequent loss of cooling in the reactor, leading to meltdown of the fuel rods. The Fukushima incident is explored in greater detail due to its immediate influence on the nuclear community. It can be observed that all these failures were very different in nature and character. However, despite their innate differences, it can be observed that they all had cooling related failures (with Chernobyl and Fukushima both having fuel rod meltdowns) and significant radioecological consequences.

II.1 Fukushima and the Need for Accident Damage Tolerant Materials

On March 11, 2011, a massive earthquake hit the East coast of northern Japan. Shortly following the earthquakes the Onagawa, Fukushima Daiichi, Fukushima Daini and Tokai Daini nuclear power plants (NPPs) were affected and emergency systems were activated.[11] The Tohoku earthquake resulted in a tsunami (~15m high) off the coast of Miyagi Prefecture, Japan.[12] The earthquake and tsunami hit 14 nuclear power reactors in the four NPPs along the Pacific Coast of north-eastern Japan. The tsunami caused loss of power at the Fukushima Daiichi NPP leaving it without any emergency backup electricity. This loss of power led to severe damage resulting in discharge of a large amount of radioactive materials in the environment. In order to prevent future accidents and assure public safety it is important that the mechanisms of failure are thoroughly understood.

As a result of the catastrophic earthquake and tsunami events of Fukushima, three reactors failed at the Fukushima Daiichi NPPs.[13] After much analysis of the Fukushima NPP accident, it was determined that ultimate failure of the reactors from the naturally derived nuclear disaster was due to loss of cooling in the reactor vessels. In order to control the elevation of temperature of the reactors, seawater mixed with boron (a neutron absorbing material) was injected into the reactors in lieu of the ability to utilize cooling water. The discharge and pumping of water into and out of reactor cores and spent fuel pools to cool them down, led to a situation where water containing large quantities of radioactive materials flowed out into the ground below. Additionally, it was later discovered that highly radioactive water was flowing into the ocean from a crack in the outlet at unit 2.[12] This led to radioactivity from Fukushima to be released directly into the ocean from waters that were used to cool the NPPs.[14]

During the process to cool the reactor cores, it can be noted that more than 10,000 tons of comparatively low level contaminated water from the radioactive waste treatment facility was discharged into the sea to make room for the storage of the highly radioactive wastewater[15] used to cool the reactors. As a result, water with a high contamination of radiation was found in these reactors. It is presumed that the total activity of radioactive materials released into the water would be approximately 4.7×10^{15} Bq.[16] This wastewater discharge event has caused transboundary concerns. Contamination of oceans, soils, air and coastal discharge sites from the release of radionuclides is evident, but the extent of the concentration still remains unclear.

In addition to the release of radionuclides into the ocean and groundwater, it was also released into the atmosphere. This was from the loss of cooling in the reactor cores causing the zircaloy fuel rods to react with steam in the high temperature environment that developed from decay heat in the reactor cores. This reaction resulted in the formation of hydrogen and the subsequent buildup of hydrogen pressure leading to the eventual explosions that damaged multiple reactor buildings. This resulted in the release of radionuclides being blown directly into the atmosphere. A preliminary estimate made by the Nuclear Safety Commission of Japan indicated that 150 PBq of ^{131}I and 12 PBq of ^{137}Cs were spewed into the atmosphere from March 2011 to April 5, 2011[17] (a much larger quantity than what was released into the oceans from the low level wastewater). These radionuclides were then eventually deposited by rainfall and incorporated into surface water and agriculture crops.

This release of radionuclides into the environment caused global concern due to concentrations of NPP discharge of ^{137}Cs reaching 50 million times preexisting ocean levels of ^{137}Cs.[18] Radioactive ^{134}Cs, ^{137}Cs and ^{131}I have since been detected in drinking water, foods, milk, in several prefectures of Japan and as a result their distribution becoming highly regulated.[19] This disturbance of adding radiation from ^{137}Cs and ^{131}I to the environment posed potential human health issues due to possible cancer risks associated with the nuclear accident. However, studies of the radiological impact of Fukushima on countries outside Japan such as Korea [15] and Greece[20] were noted to be practically negligible. In addition to abiotic factors, average dose rates for biota in the coastal zone in the vicinity of the NPP suggested that internal doses to fish and mollusks resulted primarily from cesium exposure. This release of radionuclides into the marine

environment has caused increased public anxieties in regards to both eating seafood and the potential risk factor associated with using nuclear energy in the production of electricity.

The infrequency of nuclear power plant (NPP) accidents coupled with potential global effects on ecosystems and human health make engineering critical reactor components (i.e. fuel cladding) a high priority for the nuclear community. The zircaloy fuel rods used in the Fukushima reactors are of the same type currently employed in all US light water reactors. Despite the prior and current reliable use of zircaloy fuel cladding in their 50 years of development and commercial operation, new materials may further enhance accident damage tolerance. The leading candidate for replacement of the zircaloy cladding is SiC, due to its inert matrix, high strength at high temperatures, radiation resistance and superior creep properties. By replacing current fuel rods with SiC, the reactors are anticipated to possess enhanced damage tolerance. In addition, in the next generation of nuclear reactors, the usage of SiC may allow the possibility of burning fuel at higher temperatures, thus increasing reactor efficiency and reducing waste produced.

II.2 Fuel Cycles & Non-proliferation

The feasibility of next generation nuclear reactors will require the implementation of advanced fuel cycles to sustainably use uranium for many years to come. Nuclear fuel cycles consist of multiple stages including: uranium mining, enrichment and fuel fabrication, in reactor usage in the production of electricity, recycling/reprocessing of fuel and disposal of spent fuel in a geologic repository. The three fuel cycles under consideration are: once through (open), open-modified, and full recycle/fully closed systems. Advanced fuel cycles have distinctive features in

both their reactor type and spent fuel reprocessing. For example, Advanced Recycling Reactor (ARR) and High Temperature Gas Reactor (HTGR) designs are such that continuous recycling of the spent fuels takes place.[21] Whereas Light Water Reactor (LWR) spent fuel can be reprocessed for the production of electricity through plutonium recovery useful in mixed oxide fuels (MOX).[21] For the recycling technology, Uranium Extraction (UREX) and Pyrochemical (PYRO) processes are adopted for recycling oxide and metal fuels, respectively.[21] These advanced fuel cycle strategies have been initiated in the United States of America's (USA) Department of Energy (DOE) to increase energy security, reduce the risk of nuclear proliferation, encourage clean energy development, and improve the environment through closing of the fuel cycle.

Currently, the United States, along with a majority of other nuclear energy producing countries, use the once through (open) fuel cycle in their reactors. The open system utilizes the mined ore to develop fuel that is then used in a reactor for the production of electricity. Once the fuel is spent, it is then sealed and sent to a "geologic repository" (which currently in the USA is on the reactor site) without any reprocessing as shown in Figure II-2**.**

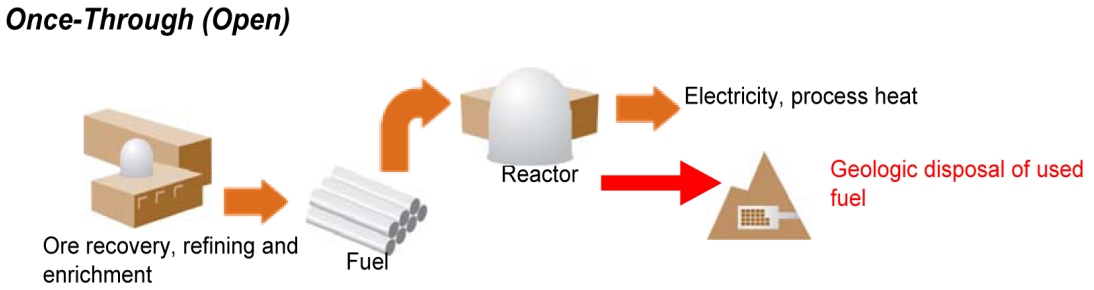

Figure II-2 Open system currently employed in all US reactors and most other countries [22]

From a technological standpoint this is a highly inefficient process. However, from a non-proliferation view this technology poses a reduced risk of proliferation. This is understood due to the Secure, Transportable, Autonomous Reactor proposal stating that as the fuel remains constantly sealed and that no separation of the fuel material takes place, the process inherently contributes to non-proliferation.[23] Simply put, there are less points to divert nuclear waste such that it has the potential of being used in an activity not relevant to nuclear power. However, when the fission products' radiation decays, the storage offers a high risk in proliferation because it can be viewed as a plutonium mine. In the long term, this cycle uses up more uranium, reducing the supply for future generations. Therefore, without adopting better fuel cycles there will be increased waste, with longer lifetimes, less efficient reactors and less repository space.

In the modified open fuel cycle the fuel is used in a reactor for the production of electricity, it is then reprocessed such that separation of actinides can be used again in the production of electricity. A schematic of this process is shown in the

Figure II-3:

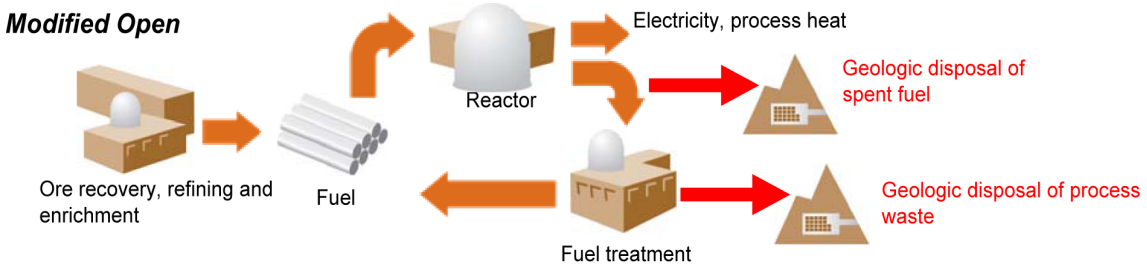

Figure II-3 Modified open fuel cycle schematic indicating reprocessing of spent fuel [22]

The waste produced from the modified open fuel cycle is such that only fission products and minor actinides remain after completion of the cycle. The ability to recycle in a manner that does not produce separated plutonium can also further avoid proliferation risks.[24] However, recycling is proving to be uneconomical today, given current plentiful supplies of uranium at low and stable prices. Of course when reserves are decreased this situation will inevitably change and will make partial or fully closed fuel cycles more viable options.

Further increasing the recycling of the spent fuel is being implemented with the design of a full recycle/fully closed system. This system is similar to the open modified system (

Figure II-3) with the exception that all actinides are separated from the used fuel and burnt in appropriate reactors leaving the remaining waste containing only gaseous fission products to be captured for geologic disposal. A schematic of this process is shown in Figure II-4

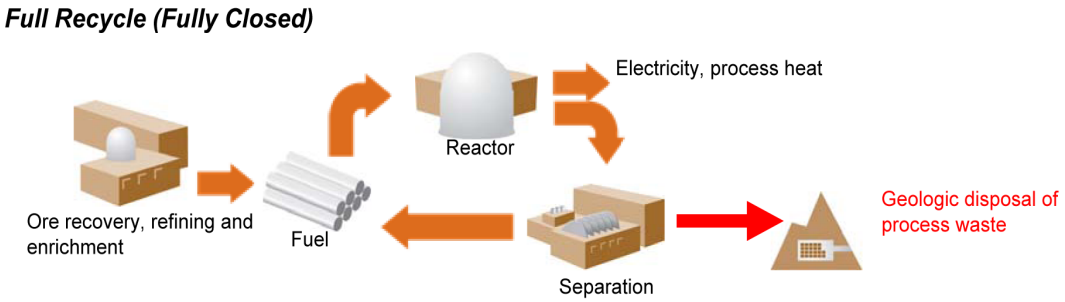

Figure II-4 Ideal fully closed fuel cycle minimizing waste [22]

A few of the benefits to recycling of the waste include: low volume of high-level radioactive, lower toxicity, and the potential to be processed into more suitable forms for final disposal. However, proliferation risks with this cycle remain, due to the potential of diverting material in the reprocessing stages of the cycle. Consequently, the fuel cycle facilities of proliferation concern will then be directed toward the reprocessing facilities. The reprocessing units will require similar basic technology for producing low-enriched uranium (LEU) for LWR fuel (with enrichments typically in the 4-5% range) or high-enriched uranium (HEU) for weapons (technically defined as ^{235}U enrichment above 20%, but in reality greater than 90% for weapons programs).[25] Increased securities in the reprocessing facilities will be of the utmost necessity when utilizing this fuel cycle scenario in order to minimize the risk of proliferation.

The once-through and closed fuel cycle systems offer different barriers to proliferation risks. The fundamental difference between the two options is that in the once-through cycle the spent fuel is stored once it has produced energy in the reactor, while in the closed cycle the spent fuel is reprocessed: the fissile uranium and plutonium, and also the actinides for transmutation are extracted and utilized to fabricate new fuel. The once through open fuel cycle waste facilities need lifetime monitoring, whereas reprocessing facilities for the fully closed systems pose continuous proliferation risks. Over the next 50 years, the once through open fuel cycle is considered the most economical and proliferation resistant choice for commercial reactors. [26] Therefore, the design and implementation of advanced reactors and fuel cycles which improve efficiency and increase accident damage tolerance are the focus of ongoing research and development.

II.3 TRISO Fuel Pellets in Very High Temperature Reactors

As discussed previously, open fuel cycle reactors in comparison to closed/modified cycles, have relatively low efficiency due to the accumulation of large volumes of nuclear waste. More advanced nuclear reactors, which are currently under investigation, are expected to allow more efficient and safer use of nuclear energy. In the aforementioned fuel cycles and next generation reactor designs, the fuel and its cladding are important safety barriers. As is the location in which radioactive fission products are being restrained such that they remain contained within their respective volume. Therefore, the selection of fuel cladding and capsule material is based on many design constraints, including: neutron absorption cross section, service temperature, mechanical strength, toughness, neutron radiation resistance, thermal expansion, thermal conductivity, and chemical compatibility.

Tristructural-isotropic (TRISO) coated fuel particles are explored here due to their ability to allow very high fuel burnups that will allow increased efficiency of the fuel. They are designed for use in very high temperature reactors such as Pebble Bed Reactors (PBR), Gas Turbine Modular Helium Reactor, Fixed Bed Nuclear Reactor and even potentials in CANada Deuterium Uranium (CANDU) reactors.[27] TRISO coated fuel particles are not only the fuel, but also the final waste form, as the goal is to retain fission products in the capsule indefinitely. The TRISO fuel is a micro fuel particle consisting of a fuel kernel composed of UOX in the center, coated with four layers of three isotropic materials. The four layers consist of a) a porous buffer layer

made of carbon, b) a dense inner layer of pyrolytic carbon, c) a ceramic layer of SiC (to retain fission products at elevated temperatures and to give the TRISO particle more structural integrity) and d) a dense outer layer of PyC as shown in Figure II-5 [28]

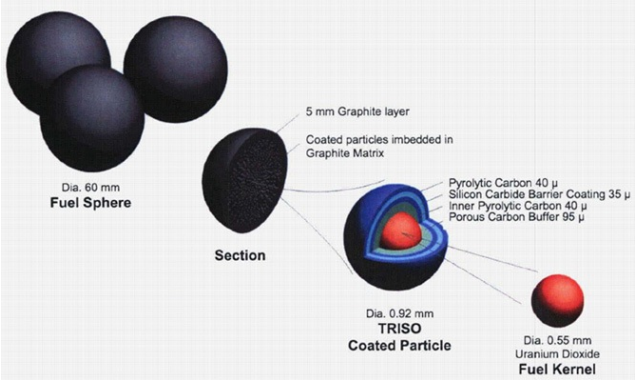

Figure II-5 TRISO fuel pellets for pebble bed reactors [28, 29]

The design of the TRISO particle fuels is such that they have the ability to withstand and utilize the very high temperatures experienced in the PBRs. The ceramic layer, composed of SiC, functions as a miniaturized pressure vessel that retains all fission products. The SiC layer begins to lose its integrity above ~1600°C, and therefore this temperature is indicative of the maximum fuel temperature for an accident scenario.[26,29] The composite materials in the TRISO particles were designed such that the they are not prone to chemical attack leaving these materials efficient for both fuel use and allowing for significantly less complicated storage processes once the fuel is spent.[28, 29]

After irradiation, each pebble is observed to contain between 7 and 9 g of low enriched uranium (LEU), up to 9.6% ^{235}U and after irradiation between 80 and 90 GWd/MT (Gigawatt-days per

metric tonne) contains less than 0.12 g of plutonium and less than 8.2 g of residual uranium containing 3.8% ^{235}U with ^{232}U, ^{234}U and ^{236}U.[29] The safeguards related to the TRISO particles is currently being evaluated in a bulk accountancy of the plutonium in the "used fuel".[28, 29] The safeguards are somewhat debatable due to plutonium dilution being below the limits of the IAEA consensus of provisional guidelines for termination of safeguards on measured discards.[29] However, due to the understood radiation hazard of the PBR used fuel and its potential use in radiological sabotage is one reason why safeguards cannot be terminated. Although plutonium concentrations may be sufficiently low, residual uranium minor isotopes of ^{232}U and ^{236}U do not meet IAEA provisional guidelines for eliminating safeguards.[28, 29]

The TRISO fuel particles are considered ideal in both their ability to reach very high temperatures leading to increased reactor efficiency and their inherent increased proliferation resistance. The leftover spent fuel in the pebble reactors poses a potential risk of utilizing the ^{232}U and ^{234}U. However, to utilize these two isotopes would require extensive reprocessing and blending in order to dilute the significant quantities of ^{236}U. The high amount of ^{236}U limits the attractiveness of re-enrichment of PBR used fuel as fuel for thermal-neutron spectrum research reactors, if not production reactors. However, the likely high content of ^{232}U would also discourage its utility in both research reactors and nuclear weapons due to the radiological penalty of handling such material.[29] These various factors inherently make reprocessing very costly; however, a more significant consideration is that reprocessing technologies for these coated fuel pellets have not progressed beyond laboratory-scale demonstrations.[29] The significant complications required to utilize the minimal amount of usable weapons grade materials allows for much debate as to how much cost should be associated with safeguarding these seemingly

proliferation resistant materials. The successful implementation of the intrinsically safe and nearly proliferation resistant PBRs is highly dependent on the ability to process the TRISO fuels. Despite their small sizes, they are inherently a highly important structural material in the future of nuclear energy technology.

II.4 Silicon Carbide Ceramics for Next Generation Nuclear Reactors

SiC ceramics are being considered for a variety of next generation nuclear reactor components because they possess outstanding physical and chemical properties, including: high-thermal conductivity, high-temperature stability, chemical inertness, extreme hardness, and small neutron capture cross-section.[3] Specifically, several studies have demonstrated that continuous SiC fiber reinforced SiC matrix (SiC/SiC) composites are attractive materials for nuclear applications due to their physical and chemical properties and additionally their stability under irradiation.[9] The optimized composites under current investigation consist of stoichiometric SiC matrices and fibers.[9] Due to the low chemical reactivity of SiC it is being proposed as also an ideal cladding material for advanced light water reactors.[30] It is additionally a barrier for fission product diffusion in gas-cooled fission reactors[6], and an inert matrix for the transmutation of plutonium and other transuranics.[7] Studies of He-implanted SiC materials for fusion materials revealed that inert gases in SiC are highly immobilized. For example, thermal release of helium generated in neutron- irradiated SiC does not occur until above 1200 K.[31] Further, Xe and Kr have been shown to have extremely low mobilities in SiC at low temperatures and only become mobile above 1200°C.[32] Due to these low mobilities it appears that SiC is also an ideal candidate for use

as a material to store and retain radioactive inert gases (i.e. its utilization in TRISO fuel particle applications). A primary benefit of using SiC and its composites for nuclear applications is the potential lack of severe effects of neutron irradiation. In addition SiC has other well-known advantages such as the retention of strength and chemical inertness up to very high temperatures and the inherent low activation/low decay heat properties.[33] Although SiC has inherent radiation damage tolerance due to its covalent bonding, it still undergoes unacceptable dimensional changes in certain temperature regimes. This is due to the Si and C interstitials being extremely mobile even at moderate temperatures leading to phase-transitions and superstructure formation.[34,35] Studies on SiC/SiC composites for the US-DOE Fusion Materials Program have clearly demonstrated that SiC has good radiation resistance. These same studies have also clarified the damage mechanisms at lower temperatures (T<1000°C), where point defect induced dimensional changes are significant and at higher temperatures void swelling and He-bubble accumulations appear Figure II-6.[36,37,38]

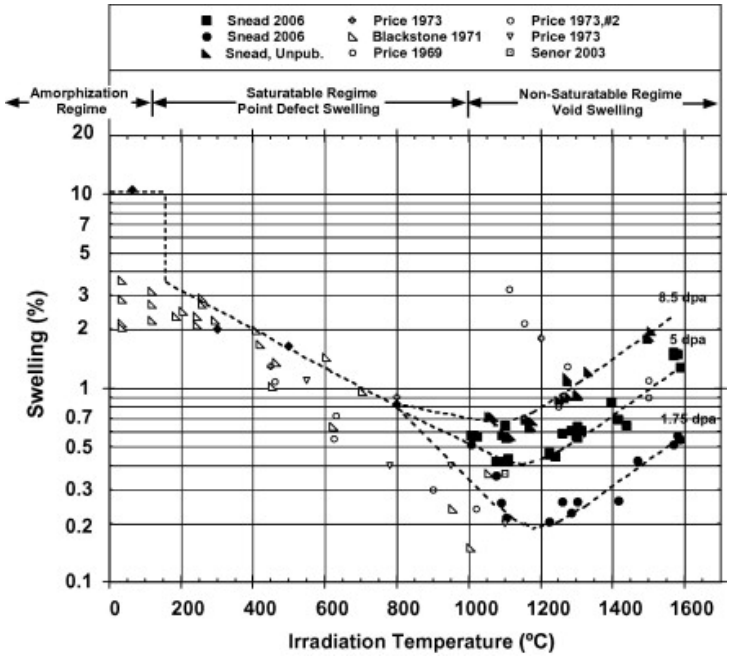

Figure II-6 Irradiation Swelling Temperature Regime [38]

In order to further improve the performance of SiC in nuclear environments, compositions and microstructures that are tolerant to these damage modes need to be developed.

II.4.1 Silicon Carbide Topology and Low Temperature Radiation Induced Amorphization

When exploring SiC for nuclear applications it is important to address the relationship of topological disorder to irradiation-induced amorphization of SiC. The topology of the ceramic structure governs the possibility of alternative structural rearrangements.[39] The topology of a material is based on the atomic arrangement of the network structure where the number N, of polyhedral of order A share a vertex {A,N}. The SiC ceramic adopts a network structure that features vertex sharing of four SiC_4 tetrahedra.[39] It is shown in Figure II-7 that SiC exhibits a {4,4} topological arrangement, which is highly constrained compared to SiO_2 {4,2} and slightly more than Si_3N_4 {4,3}.[40]

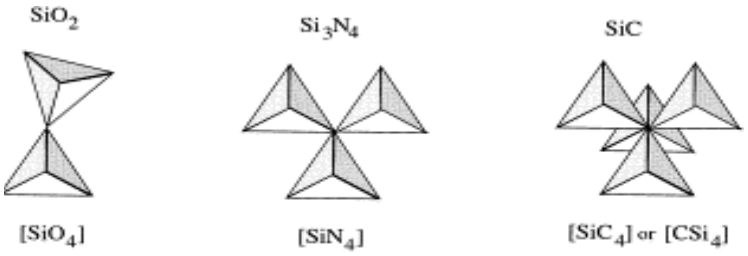

Figure II-7 Vertex Sharing schemes of SiO_2, Si_3N_4, SiC [40]

The structural freedom is dependent upon the redundancies in the connectivity of the structure.[41,42] The degree of structural freedom, f, is represented by the number of degrees of freedom from each vertex, V, equal to the dimensionality, d, of the structure less the number of constraints, h, imposed by connections to neighboring elements.

$$f = d - C\left\{\delta - \left[\frac{\delta(\delta+1)}{2V}\right]\right\} - (d-1)(\left(\frac{Y}{2}\right) - [(p-1)d - (2p-3)](\frac{Z}{p})$$

Equation II.1 Degree of structural freedom (f) [33,39,40,42]

Where δ is the dimensionality of the structuring polytope itself, Y is the fraction of edge-sharing vertices and Z is the fraction of vertices sharing p-sided interfaces.[33,39,40,42] Based on these parameters one can deduce the degree of structural freedom, f, for SiC is decreased compared to SiO_2 (with f = -3 for SiC and f = 0 for SiO_2). These parameters are significant in the consideration of radiation bombardment of the material. The degree of freedom can help predict how easily a material is likely to transform to the metamict state (irradiation-induced loss of crystallinity). SiC with an over constrained structure is more likely to maintain a crystalline state in comparison to the under constrained SiO_2 structure, which is more free to adopt an aperiodic configuration.[43] In addition to network structure, the melting point, ionicity and homologous crystallization temperature are additional properties important for loss of crystallinity.[39]

It has been demonstrated that SiC experiences metamictization through single ballistic displacements.[39] This is caused from the recoiling of atoms from the matrix inducing disorder in the structure. SiC is observed to amorphize at room temperature at ~0.6 dpa; however, remaining

crystalline at 1000K to doses up to 100 dpa.[39] This higher temperature observation is likely due to thermal energy being a driving force for atomic rearrangement in the SiC matrix and thus preferring the lower energy crystalline state. However, at these higher doses and temperatures, void swelling due to alpha particle emission becomes the dominant damage mechanism.[39]

Studies on neutron irradiation have shown that the formation volume increase of Frenkel pairs contributes to the volume swelling under irradiation.[44] Frenkel defects are a type of point defect in a crystal lattice that forms when an atom or cation leaves its place in the lattice. It creates a vacancy and situates itself in an interstitial site not occupied by an atom as shown in Figure II-8.

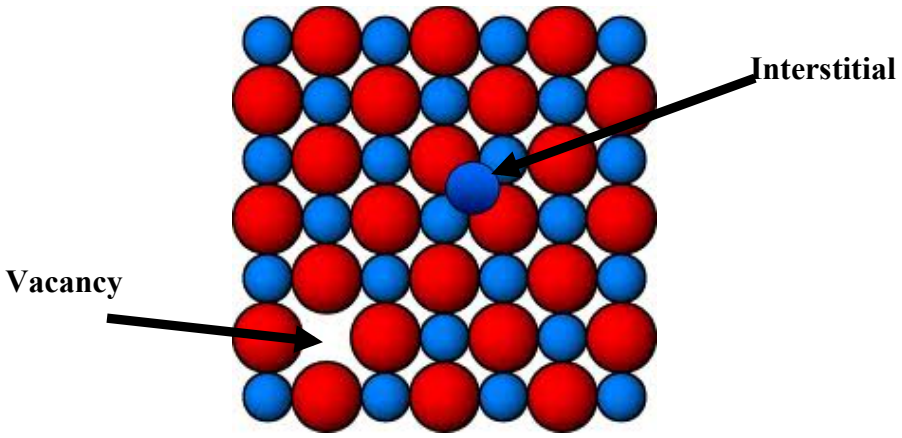

Figure II-8 Frenkel defect in a crsystalline lattice

Molecular dynamic simulations have confirmed that except for the C_{Si} antisite, all other defects cause the cell to expand. It has been confirmed that there is a factor of 3-4 higher number of displaced C atoms than Si atoms.[45] This is due to a smaller atomic mass and a lower displacement threshold energy for C atoms on the C sublattice than those of Si atoms on the Si sublattice.[45] If the interstitials were sufficiently mobile they would reduce their strain energy by

forming interstitial dislocation loops.[46] The interstitial atoms and vacancies produced in both components of SiC have an effective charge, which makes them very efficient traps for either electrons or holes.[47]

Due to the many structural rearrangements in irradiation induced SiC one could question whether a crystalline or amorphous starting structure would be ideal for nuclear applications. There is possibility that starting with amorphous SiC could lead to a "self assembly" of the matrix that is determined by radiation fluence as well as operating reactor temperature. Starting with an amorphous material would also allow for more ease of mobility of Si and C within the system as opposed to starting with an already over constrained crystalline structure. It would therefore, be useful to compare defect aggregation in both amorphous and crystalline SiC before and after irradiation. In addition, recent studies on other materials have shown that nanostructured and nanoscale grains are more damage tolerant.[48, 49] This phenomena has not been investigated for SiC but it is anticipated that with addition of a carbon nanodomain, there is potential for recombination of Frenkel defects thus mitigating radiation damage. The investigation of nanostructured SiC is therefore a significant goal of this research.

II.4.2 Swelling of Silicon Carbide During High Temperature Radiation Bombardment

The microstructural changes associated in materials under both high temperature and radiation is important in the consideration of using SiC as a high temperature reactor material. In a fusion reactor, He is predicted to be produced in SiC at a rate of ~1500-2000 ppmHe/CMWy (megawatt years) by transmutation reactions with concurrent displacement damages of 10-15 dpa

(MWy/m^2).[50] The (n,α) reactions (i.e. neutron absorbed, alpha particle emitted) occurring from 14 MeV neutrons, result in the large accumulation of helium atoms in materials.[51] This excess helium is caused from the release of alpha particles from the (n, α) reaction. It is well known from the emission spectrum of the alpha particles that they are simply energetic (E_α 4 - 9 MeV) helium atoms.[52] Extensive production of helium and hydrogen is known to occur in SiC as a result of nuclear trans-mutations from fusion neutrons.[37] Helium and other inert gases introduced into solid materials are known to agglomerate due to their extremely low solubility (nearly zero).[52] Therefore, when the concentration of gas is high, bubble formation and swelling is observed.[53] This volume expansion, or swelling, is a well-known irradiation-induced damage phenomenon.

Displacement of lattice atoms from the matrix is a major contributor to accumulation of various other defects important when considering SiC as a material for the high temperature radiation environment.[54] Under high temperature (1000-1500°C) irradiation studies at Oak Ridge National Laboratory, both irradiation-induced vacancies and interstitial atoms were shown to migrate freely and form defect clusters leading to progressive swelling with temperature and irradiation fluence, the so-called void swelling regime.[55] The helium effect is important because helium interacts with the radiation point defects and impurities. Helium and other inert gases introduced into solid materials have also been known to agglomerate due to their extremely low solubility. The cavity swelling and dislocation evolution may cause unstable volume expansion and lead to irradiation creep thus altering the physical and/or mechanical properties of the structural material. Swelling potentially determines the low-temperature limit (point defect swelling) and high-temperature life-time (cavity swelling) of the design window of SiC.[56]

At higher temperatures parallel with gas escape, the combination and accumulation of mobile defects tends to lead to larger defects such as bubbles, voids and cavities.[54] Recovery from swelling has also been shown to take place at even higher temperatures. Although complete recovery during long hours of annealing at 1000 K usually doesn't occur due to trapped gases contained within the SiC lattice structure.[57] Cavity formation tends to be the result of this supersaturated vacancy migration. These cavities are shown to occur during radiation bombardment with increasing temperatures. The effects of the void swelling regime can be seen in Figure II-9. At 1050°C the onset of cavity formation from helium migration is shown to occur sparsely and only present at the grain boundaries. Further increasing the temperature to 1300°C the appearance of spherical voids in the matrix in addition to the grain boundaries is observed. At 1460°C the void formation has evolved from spherical to tetrahedral voids.[45]

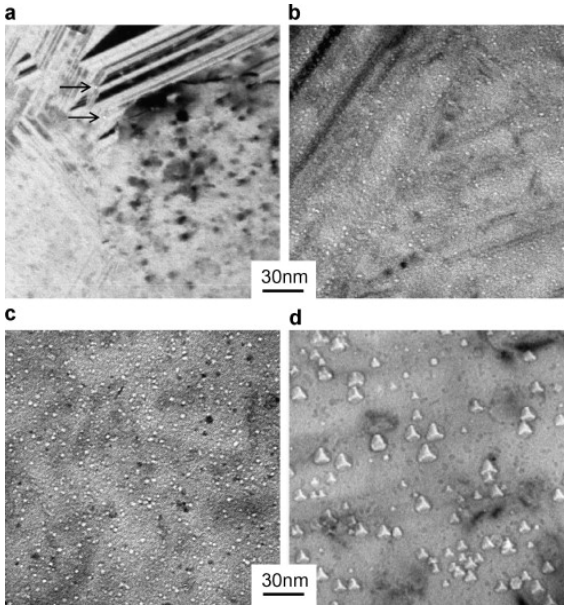

Figure II-9 Cavity microstructures in β-SiC irradiated at (a. 1050 °C, 4.9dpa, b. 1300 °C, 9.3 dpa, c. 1400 °C, 9.4 dpa, d. 1460 °C, 5.6 dpa[58]

These tetrahedra voids are noted to form at the facets of the Si {111} planes in SiC. It can be noted that the {111} planes in the Zinc Blende crystal structure (Figure II-10) of β-SiC are the areas of highest atomic packing densities.

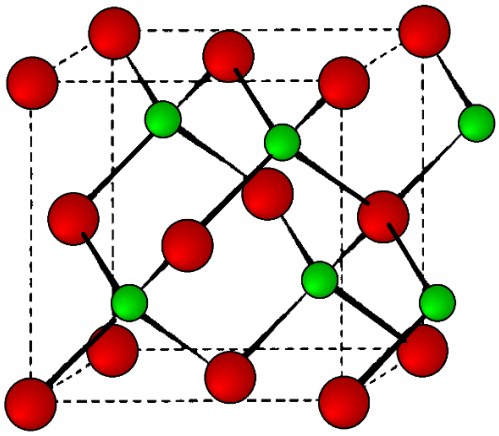

Figure II-10 Zinc blende crystal structure of β-SiC

It can be appreciated that Si atoms are 1.5 times larger than carbon atoms making the Si {111} plane an area of increased resistance for diffusion of the helium atoms. The tetrahedral void swelling is thought to occur because there is more surface area here than in a spherical void for a given volume. This is likely a necessary space in which to contain He if the concentration is increased during prolonged higher temperature reactions. The increased volume of the tetrahedral void implies that the free surface energy of the faceted surfaces is lower than other surfaces.[59] Most materials displaying {111} faceted voids, have void shapes that are either octahedral and/or {110} truncated octahedra because of their lower surface area than the tetrahedra for a given volume.[45] However, ab initio studies of the energetics of He in SiC

determined that the trapped tetrahedral sites surrounded by four Si atoms were preferential to C tetrahedral sites due to decreased formation energies for a single He interstitial. It can be noted that when locating four He atoms in the carbon tetrahedral site that they were spontaneously stabilized into silicon tetrahedral sites.[54] This therefore implies that the preferable site for He within the SiC matrix is the Si tetrahedral interstitial site. It is possible that the introduction of layers in the form of a carbon nanodomain in the SiC matrix can mitigate these defects by minimizing mobility (a demonstrated approach in improving radiation resistance of metals) Figure II-13 and Figure II-12.

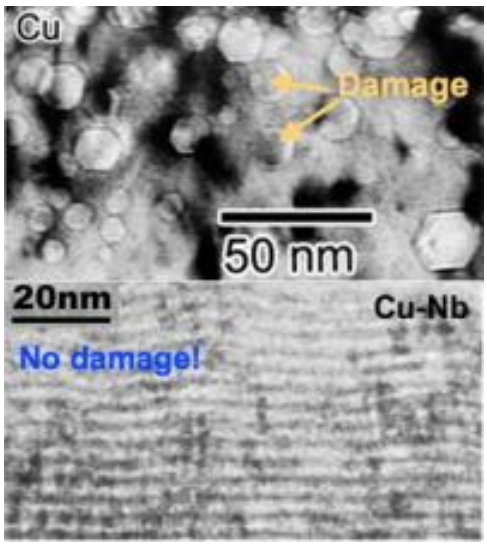

Figure II-11 Nanocomposite of Cu & Nb, radiation damage contained by interfaces between the Cu & Nb layers [60]

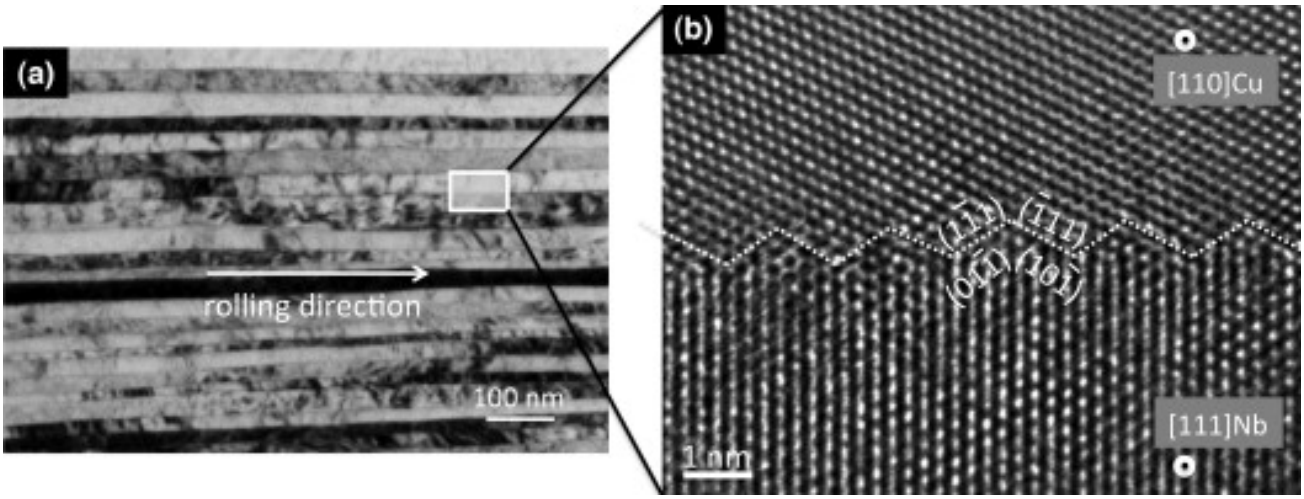

Figure II-12 Nanolayered materials for mitigating radiation defects in metals [61]

Additionally, the initial prevention of amorphization from Frenkel defects through the recombination of defects with nanostructured SiC could also assist in decreasing the amount of He migrating into the matrix. This would therefore provide the possibility of decreasing microstructural defects from helium migration causing cavity swelling. The development of nanostructured SiC through this research will further the understanding of how these defects can be effectively mitigated and lead to the advancement of nuclear materials for next generation nuclear applications Figure II-13.

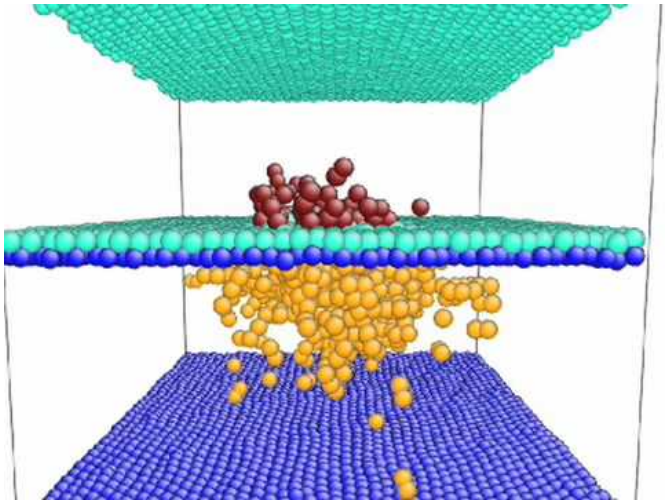

Figure II-13 Hypothesis: Incorporation of nanostructured interfaces within SiC will more easily allow annihilation of radiation-induced point defects [62]

One can argue that this tetrahedral void swelling phenomenon is driven by the attempted recovery of the crystalline phase from the amorphous phase during low temperature irradiation. There is possibility that re-crystallization of the radiation induced amorphized SiC at increasing temperatures with trapped He in the system causes the He to migrate from the grain boundaries and defect sites to the energetically favorable sites within the SiC matrix (i.e. the Si {111} planes). The crystallization would of course have to be confirmed through TEM investigations. Ideally an understanding of whether these effects can be mitigated through varying degrees of crystallinity can allow an understanding of the role of crystallinity and microstructures in radiation damage of SiC.

II.4.3 Irradiation Creep Deformation of SiC

Creep is the time dependent deformation of materials at constant stress and normally occurs at high temperatures. Irradiation creep mechanisms in ceramics are strongly dependent upon defect mobility (i.e. grain boundary defect, vacancies and cluster defects). Irradiation leads to point and line defects, which can migrate under stress leading to enhanced creep. Irradiation induced creep has been considered as additive to thermally induced creep. Irradiation creep dominates at lower temperatures [63] but also occurs at higher temperature when the defect sites' mobility increases with increasing temperatures. Therefore, irradiation creep is an important materials phenomenon due to it being a major contributor to the dimensional instability at lower temperatures where thermal creep doesn't readily occur. It is also an interesting phenomenon for brittle ceramics because it may seemingly cause a relaxation or redistribution of the stresses. Such as in the appearance of dislocation loops commonly observed in TEM analysis after neutron irradiation creep testing.[64]

Irradiation creep is an important property for SiC because it often determines the design limits for temperature, stress loading, and neutron fluence. Irradiation creep is studied through a bend stress relaxation (BSR) experiment by preparing thin strips of SiC with approximate dimensions of 40 mm x 0.1 mm x 1.0 mm to study their irradiation creep at elevated temperatures. A BSR irradiation creep experiment can be used such that the thin strips are bent to a fixed radius during irradiation Figure II-14 [65]

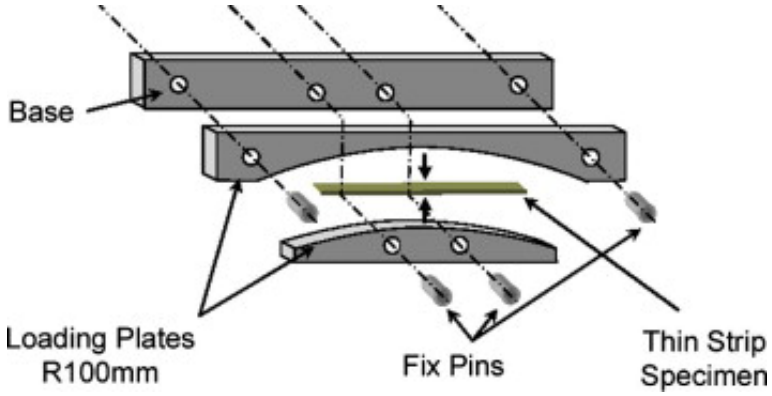

Figure II-14 Fixture of BSR experiment [65]

The initial and final stresses σ_0 and σ_a, respectively are calculated using the measured initial (constrained) bend radius (R_0), the unconstrained residual bend radius after irradiation (R_a), specimen thickness (t) and literature values for temperature dependent elastic modulus.

$$\sigma_0 = \frac{Et}{2R_0}, \sigma_a = \frac{Et}{2}\left(\frac{1}{R_0} - \frac{1}{R_a}\right)$$

Equation II.2 Initial and Final Stresses [65]

Normally, creep deformation occurs in three stages, transient creep where the strain rate decreases with time, steady state creep where strain increases at a constant rate with time and tertiary creep in which creep rate increases with time. Previous studies have shown that creep strains for CVD SiC were dominated by transient creep at temperatures below ~950 °C, and steady state creep at higher temperatures.[64] Irradiation creep of SiC however is currently very poorly understood. It has been observed that at lower temperatures, transient creep is the primary concern. Transient creep strain being more pronounced at the onset of radiation and

decreasing with increasing dosage.[65] It can therefore be implied that there is a relationship between irradiation creep and the saturation-swelling regime that are both occurring at these low temperatures. The strain induced from transient irradiation creep is anticipated to be beneficial in relaxing stresses.[65]

II.4.4 Summary of Nuclear Applications

Based on a review of the literature we can conclude:

a) Silicon carbide is an attractive material for next generation nuclear reactors both for structural components and storage of radioactive gases

b) There is need to further improve both the low temperature and high temperature defect stability of SiC in a radioactive environment

c) There is need to develop a robust processing approaches to develop SiC in a variety of physical forms i.e. both dense & porous (discussed further in Chapter II)

d) Irradiation creep and its effects on the microstructure is a poorly understood phenomenon and is dominated at lower temperatures

e) Nanostructured SiC has the potential to be more radiation resistant than large grain SiC at both high and low temperatures

II.5 Polymer Derived Ceramics

Polymer derived ceramics (PDCs) are Si based polymers that thermally decompose to a ceramic. This approach allows the possibility to molecularly control and design the composition of the resultant ceramic. Common precursors and the resultant ceramics are: polycarbosilane resulting in silicon carbide (SiC); polysiloxanes resulting in silicon oxycarbides (SiOC); and polysilazanes resulting silicon carbonitrides (SiCN) Figure II-15.[66,67]

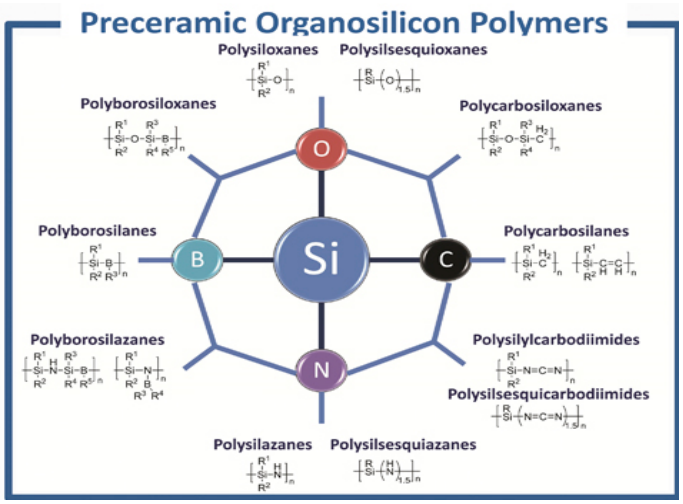

Figure II-15 Polymeric Precursors [66]

This work focuses on the development of SiC and therefore it is necessary to utilize a preceramic polymer from the polycarbosilane family. Specifically, allylhydridopolycarbosilane (SMP-10) developed by Starfire Systems Figure II-16, SMP-10 is an ideal preceramic polymer since its decomposition leads to stoichiometric SiC.

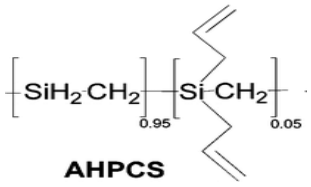

Figure II-16 Allylhydridopolycarbosilane (SMP-10)

The PDC processing route involves the transition of an inorganic/organic polymer → an amorphous solid → a crystalline ceramic Figure II-17.[68]

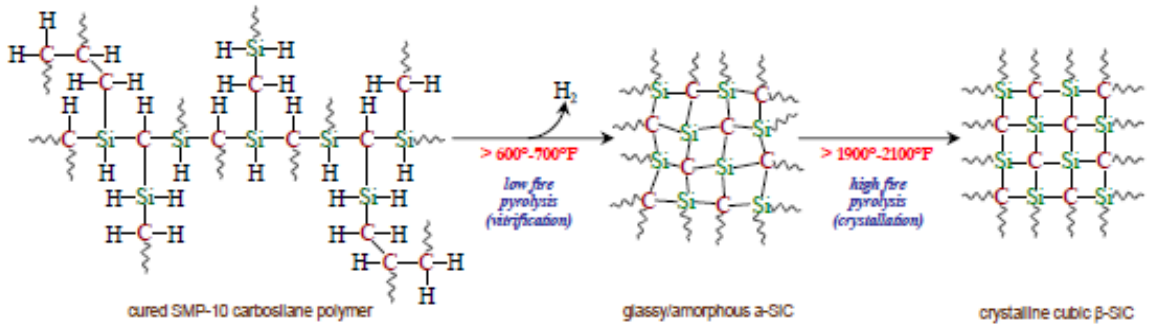

Figure II-17 Schematic of the polymer to ceramic transformation of SMP-10. [68]

Beyond the basics of PDC processing, there are several methods which can be used to tailor the microstructure, polytype, pore structure and density of the resultant ceramic. Some of the important parameters include: degree of crosslinking (thermal, crosslinking agents, e-beam, UV, etc…), mixing of polymeric precursors, foaming agents (for porous materials), dopants (for multicomponent ceramic systems), and crystalline nanoparticles (to function as a seed for crystal growth).[66] This ability to fine-tune the composition and microstructure of the ceramic system, as well as allow novel shaping of the material are arguably the most distinctive advantages of using

PDC processing methods over traditional ceramic processing routes (e.g. powder processing) Figure II-18.

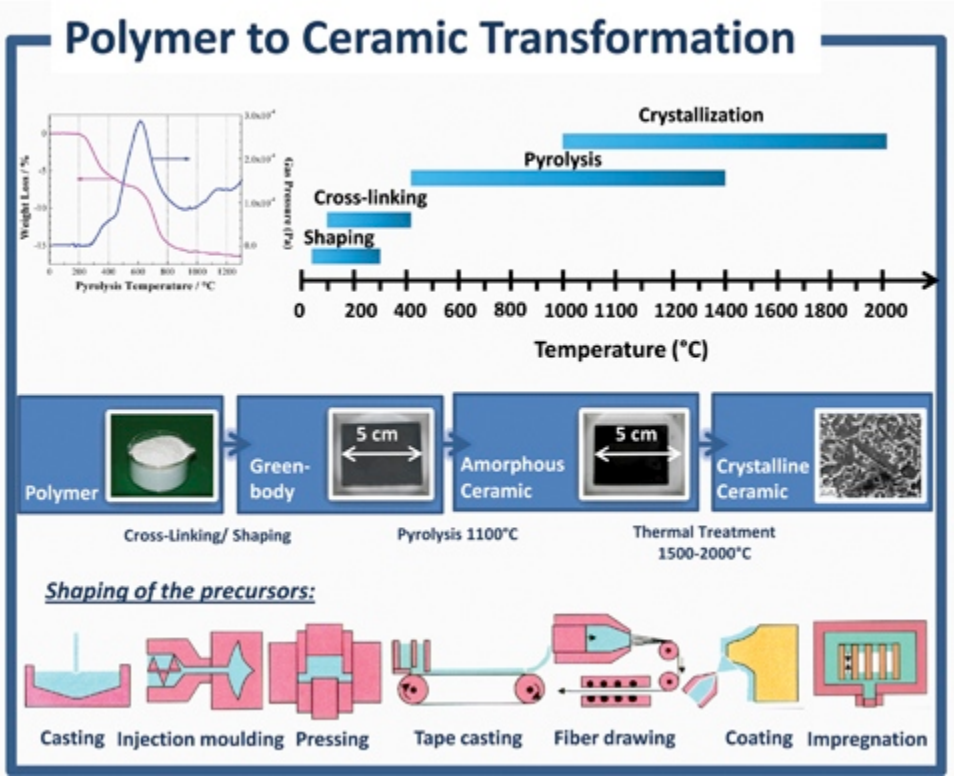

Figure II-18 Advantages of PDC processing [66]

The PDC processing approach allows the generation of interpenetrating interfaces within the material.[69] This work will exploit these nanodomains in their potential to mitigate radiation defects. PDCs also have the unique ability of being resistant to crystallization at high temperatures.[70] Their extremely stable amorphous phases provide an opportunity to investigate their stability in the radiation environment. Boron containing Si-C-N based polymeric precursors are shown to have even further increased thermal stability and are expected to remain amorphous up to 2200°C with the added benefit of enhanced creep resistance.[70] An additional advantage of PDCs is their unique formability that cannot be achieved through traditional ceramic processing routes as shown in Figure II-19.

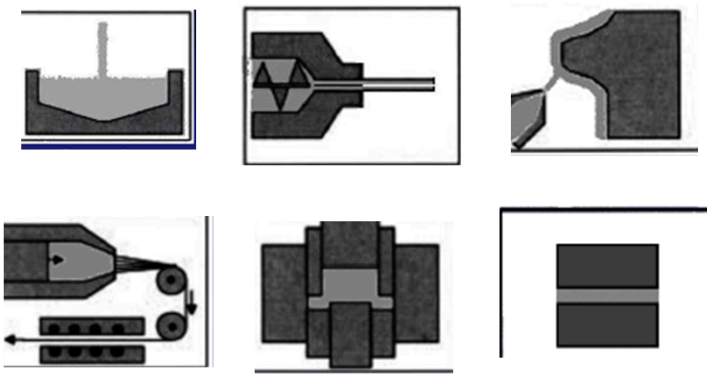

Figure II-19 PDCs can be used in a variety of processing methods.[71]

A novel feature of PDCs is their ability to generate nanosized grains due to the devitrification processes associated with crystallization of the amorphous phase.[66] In addition the ability to utilize conventional polymeric processing to shape the material make this an attractive processing route.[66,72] This approach allows for the production of unique shapes not easily processed using powder processing methods, such as continuous fibers[73] and unique porous structures.[74,75] SiC fibers being one of the older and more successful applications of PDCs as this is the only means of obtaining long continuous SiC fibers.[76] It is also possible to load the polymer with a filler for multicomponent phases in the final ceramic.[77,78,68] PDCs also have the ability for use in joining applications[79], which will be of considerable importance for the advancement of SiC/SiC composites as structural materials for fusion reactors. Due to this reasoning, this work seeks to develop precursor derived SiC with graphene nanodomains that will function as centers for point defect recombination in the mitigation of radiation defects.

II.5.1 Crosslinking the Preceramic Polymer

Crosslinking is one of the most critical manufacturing steps in PDC processing. This is because crosslinking ensures shape retention and therefore is inherently important when considering the development of coatings, fibers, porous materials and composites. In addition, crosslinking of the polymeric chains prevents the loss of low weight oligomers during the pyrolysis process leading to higher ceramic yield and lower porosity.[76] It is therefore crucial to effectively crosslink the material to minimize mass loss during pyrolysis and thus increase the ceramic yield.[66,72] Crosslinking is not only essential in curing the thermoset preceramic polymers, but this step also allows for the possibility to open up the polymer chains leading to modification of the chemical composition of the resultant ceramic. One way in which the chemical composition of the precursors can be modified is through crosslinking the material in the presence of oxygen.[76] Oxygen crosslinking can occur via a free radical mechanism of Si-H and Si-CH_3 as follows: [80]

$$\text{Si-H} + \text{CH}_3\text{-Si} + \text{O}_2 \rightarrow \text{Si-O-CH}_2\text{-Si} + \text{H}_2\text{O}$$

The oxygen therefore functions as a catalyst in effectively crosslinking the preceramic polymer. Crosslinking of polycarbosilanes in the presence of oxygen has also been found to occur via free radical mechanisms, the oxidation of Si-H can be shown in Figure II-20

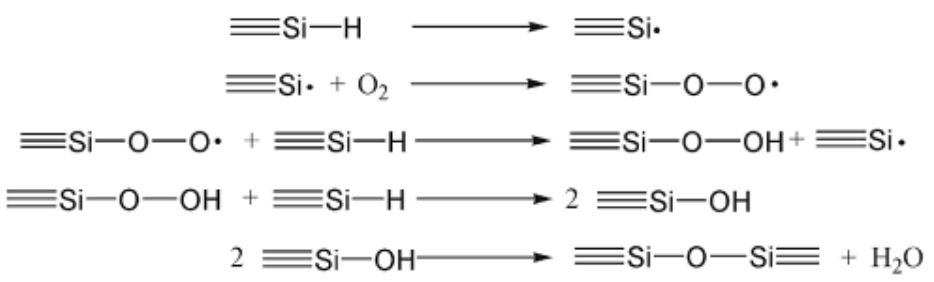

Figure II-20 Oxidative Crosslinking of a polycarbosilane via radical mechanism [76]

Since oxygen is easily incorporated into the polymer, it is necessary to crosslink the preceramic polymer in an inert environment.

There are a multitude of ways to crosslink preceramic polymers: catalyst assisted (transition metals, peroxides), e-beam, UV, thermal, etc...[66,76] The specific crosslinking method is dependent upon the expectations of the resultant ceramic. For example electron beam curing is an ideal route to maximize the degree of crosslinking between the chains. Using an e-beam to cure the polymer allows the severing of bonds and thus creating more possible crosslinks than other methods. However, this method requires specialized equipment and is usually limited to thin sections due to the limit of the depth of penetration. Therefore, this method is commonly used for think sections such as developing fully dense amorphous SiC fibers, a similar situation exists when considering UV curing options for PDCs.[81]

In this work, the goal is to develop SiC with an enhanced ceramic yield as well as minimize oxygen concentration from handling the SMP-10 preceramic polymer. In general, crosslinking of SMP-10 involves the opening of a C=C bond during thermal heat treatment to link with another

polymer chain. This process is often assisted with the help of a free radical initiator such as dicumyl peroxide as shown in Figure II-21.[68] The crosslinking of the chains generates more covalent bonding through the release of hydrogen in the process.

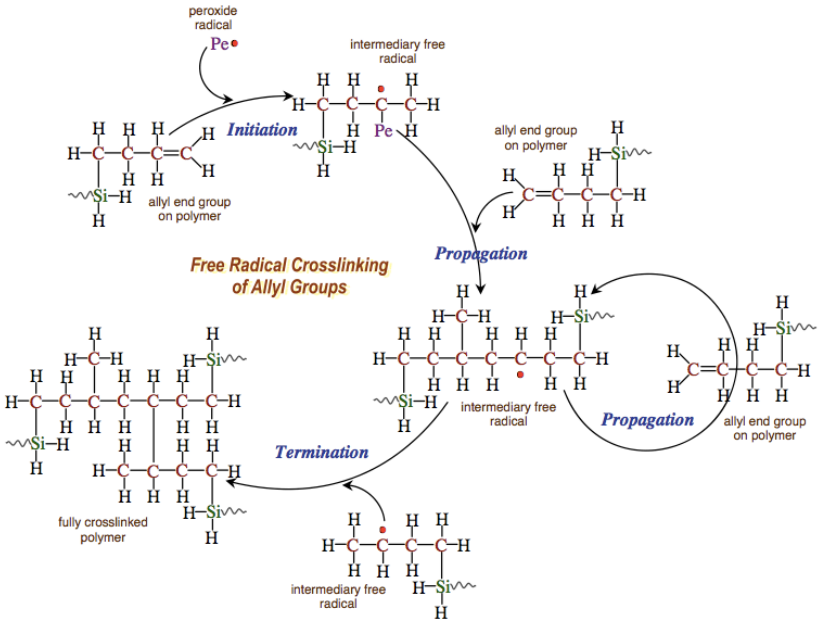

Figure II-21 Crosslinking of SMP-10 w/ peroxide initiator [68]

Through increasing the degree of crosslinking in the system, more of the lower weight oligomers in the system can be maintained and therefore the ceramic yield enhanced. In addition, in this approach, oxygen is not needed for the crosslinking of the SMP-10 polycarbosilane. This method involving the thermal, catalyst-assisted crosslinking can be successfully accomplished in an inert environment leading to the minimization of oxygen contamination in the resultant SiC ceramic system.

Crosslinking is often the first step in controlling the microstructure of the resultant ceramic. The microstructure can be further manipulated through tailoring of the polymer chemistry.[72] The degree of crosslinking, the type of polymers used as well as any additives (such as crosslinking agents, dopants, and filler systems (inert and active)) are some of the many processing variables to control the composition and microstructure of the ceramics.[66]

II.5.2 Amorphous to Crystalline Transition

Pyrolysis of the crosslinked polymer is accomplished through thermal degradation of the polymer releasing hydrocarbons and low weight oligomers. In polycarbosilanes it is understood that pyrolysis of the crosslinked materials usually is completed between 800-1000°C. Following pyrolysis of polycarbosilanes an amorphous silicon carbide material is obtained as illustrated in Figure II-22.[76] During the pyrolysis process (i.e. beyond the crosslinking temperatures) the polycarbosilanes transform into inorganic materials with the elimination of Si-H, Si-CH_3 and Si-CH_2-Si as determined using DTA (endothermic) and TGA/MS analysis techniques.[76]

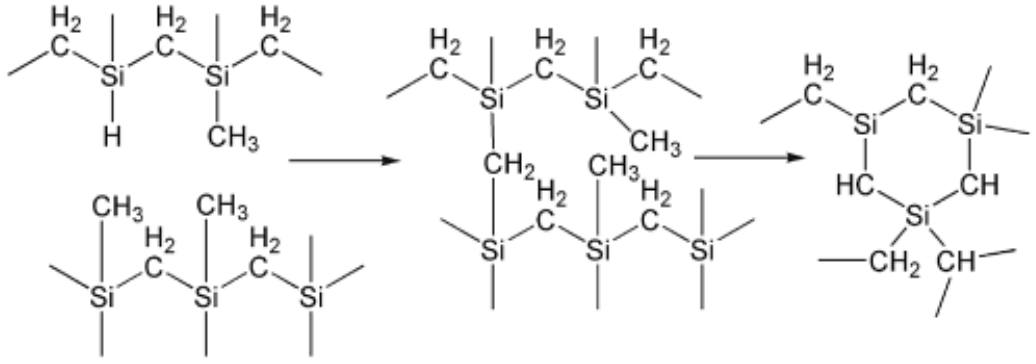

Figure II-22 Transformation of Preceramic Polymer into Amorphous Covalent Ceramics [76]

The amorphous phases of PDCs are known to be extremely thermally stable, up to 2200°C in some cases.[70] The functionality of amorphous vs. crystalline SiC or some degree thereof has not been considered in the nuclear literature due to traditional ceramic processing constraints. However, with the exploitation of the amorphous to crystalline transition that occurs during PDC processing, there is possibility to explore varying degrees of crystalline SiC and its functionality in the nuclear environment. In order for amorphous or partially crystalline SiC to be studied effectively for its radiation stability it is necessary that the monolith be homogeneous. This is important in case of any radiation-induced crystallinity, in which possible misalignments in regions of non-uniformity could densify at different rates in comparison to a homogeneous counterpart.

The nucleation of the crystalline grains from the amorphous phase occurs when exposed to elevated temperatures. In polycarbosilanes the transition from amorphous silicon carbide to crystalline silicon carbide usually begins to occur at ~1400 °C.[66] This is due to the lower energy state of the crystalline phase in comparison to the amorphous phase. Crystal growth occurs at these elevated temperatures due to the increase in atomic mobility, which leads to the crystallization of the amorphous phase.[82] The occurrence of devitrification in traditional glasses yields nanosized grains; this is also the case for PDCs. This is another significant reason PDCs were explored in this research rather than more traditional methods of ceramic processing. The ability to control the crystal nucleation and growth from the amorphous to crystalline state would result in a significantly different nanostructure and hence different mechanical and radiation resistant properties.

The amorphous to crystalline transition occurring during processing is pertinent when determining processing parameters for the development of silicon carbide. For the nuclear applications of polymer derived silicon carbide ceramics, it is also relevant to consider the crystalline to amorphous transition that takes place due to high energetic particle radiation in SiC. Polymer derived SiC ceramics are relatively new materials (in comparison to other methods of preparing fully dense SiC) especially in the nuclear community. Therefore their functionality in the radiation environment has not been characterized. It would be ideal to understand the kinetics of vitrification of the PDCs from high energetic particle radiation. The crystallization of PDC SiC likewise needs to be studied as function of temperature and additives. This will help develop an understanding of what methods promote or hinder the crystallization of the amorphous state.

II.5.3 Nanodomain of SiC Polymer Derived Ceramics

The PDC processing route is an ideal way to produce nanospaced interfaces within the matrix. These interfaces will be designed to mitigate radiation damage by enhancing local recombination of defects at these engineered interfaces.[83,84] Previous Raman spectroscopy studies of irradiated SiC revealed the presence of homonuclear Si-Si bonds leading to a disordered crystalline SiC phase.[85] This research proposes the utilization of a carbon interface to recombine the defects formed during radiation bombardment. There is possibility that this carbon interface will lead to the prevention of these homonuclear Si-Si bonds through recombination.

The stoichiometry of the Si and C of the SMP-10 preceramic polymer can be adjusted by mixing it with a high carbon content polymer such as divinyl benzene (DVB). This has been done in SiOC PDCs and has the ability to manipulate the preceramic polymer in order to generate a predictive amount of "free carbon" as shown in Figure II-23.[34]

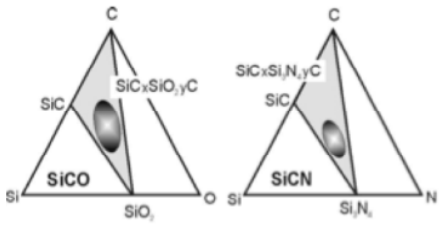

Figure II-23 Schematic of the phase relationship of the Si-O-C and Si-C-N system [34]

The amount of DVB used will allow for precise control over the free carbon introduced into the system. SiOC studies have shown that when the precursors are converted to ceramics, the excess carbon forms homogeneously dispersed graphene layers with nano-domains estimated at 1 to 5 nm as shown in Figure II-24.[69]

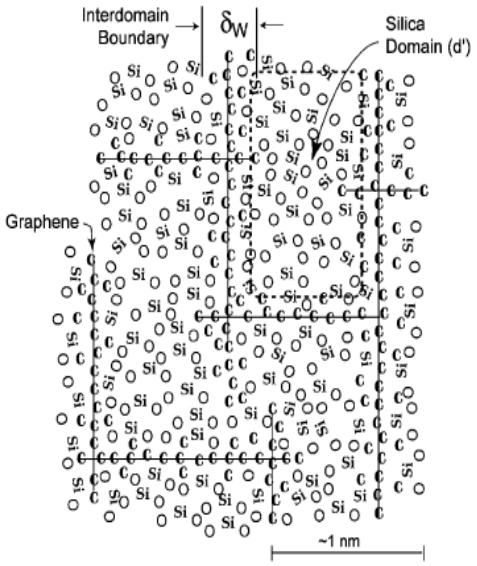

Figure II-24 Schematic representation of the proposed organization of the SiOC system.[69]

The amount of the carbon in the precursor and the processing temperature leads to the formation of either turbostratic nanocarbon domains or percolating graphene stacks (for high carbon content) as is demonstrated in Figure II-25.[69, 86, 87]

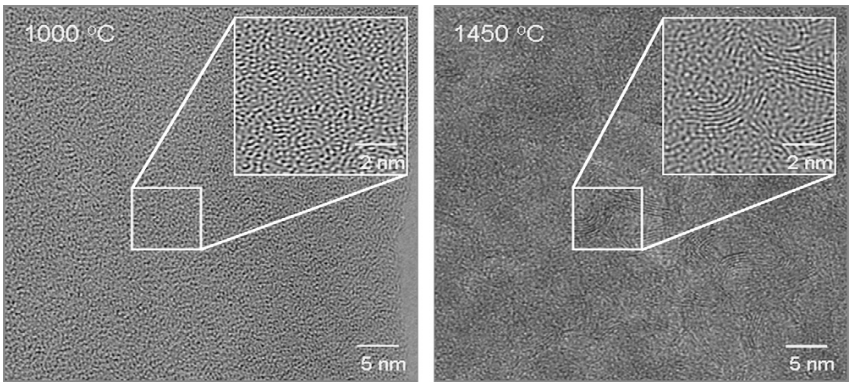

Figure II-25 TE*M image of turbostratic SiOC structure at 1000 °C and 1450 °C* [88]

This research will explore the nanodomain size using various concentrations of divinylbenzene in the SMP-10 precursor after hot pressing the samples to 2100 ^{0}C in argon with a very low partial pressure of oxygen. The nanodomain size can be estimated by small angle X-Ray scattering (SAXS). The results on the domain size will be compared to the predictions of the model presented in [69]. An important question that has not been considered in the literature is the effect of temperature on the domain size. The crystalline phases can be determined by X-Ray diffraction and the state of free carbon by Raman Spectroscopy.[89,90] The experimental results will provide quantitative information on the effect of temperature and C/Si ratio in the precursor on phases and nanostructure in the ceramic, which will be used to develop processing protocols for specific nanostructures with full crystallinity.

Significant advances in nuclear energy technology can be achieved by development of these tailored nanostructures in a high temperature capable material such as SiC has the potential to allow for increased radiation resistance as others have shown for oxides.[91,92,93,94] SiC offers a highly attractive combination of high temperature capability, and low neutron activation.[48] This study postulates that by making Si-C based materials with nanostructured features, the radiation damage resistance of SiC will improve relative to that for SiC produced using chemical vapor infiltration (CVI) or chemical vapor deposition (CVD) provided that stoichiometry can be maintained for the SiC-regions. The C-nanodomains in our proposed materials will act as point defect recombination centers to reduce defect densities and radiation damage.

II.5.4 Boron Doping in Polymer Derived Ceramics

SiBC polymer derived ceramics have not been fully characterized nor studied in depth. However, previous studies on SiBCN PDCs have shown that the temperature stability is improved by the addition of boron. The amount of free carbon in SiCN thermodynamically controls the degradation of Si_3N_4. This degradation is expected to start at temperatures above $T = 1484$ °C due to the carbothermal reduction of Si_3N_4.[95]

$$Si_3N_4 + C \rightarrow 3SiC + 2N_2$$

This reaction leads to the formation of SiC and a mass loss due to N_2 evolution. Without the presence of free carbon Si_3N_4 is stable up to 1884 ˚C at ambient N_2 pressure. The decomposition reaction of Si_3N_4 proceeds as follows: [95]

$$Si_3N_4 \rightarrow 3Si + 2N_2$$

Boron addition has been shown to inhibit the crystallization of SiC and Si_3N_4 up to 2200°C.[70] Insertion of boron at the molecular level also improves high temperature stability, oxidation resistance and creep properties of the PDCs.[66] The main reason for the increased stability of SiBCN materials is currently poorly understood. However, it is believed that addition of the BCN phase into the system encapsulates the Si_3N_4 phase and acts as a diffusion barrier preventing the SiC and Si_3N_4 reaction as shown in *Figure II-26*. [96]

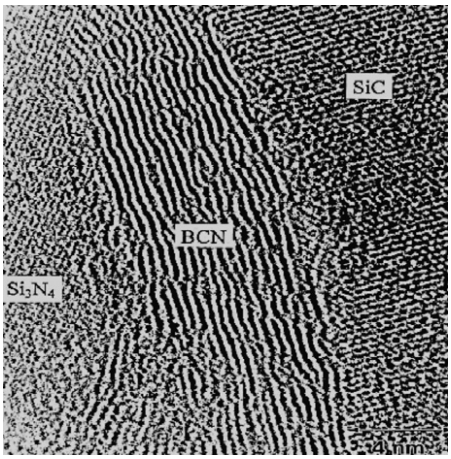

Figure II-26 HRTEM SiC and Si_3N_4 grain boundaries surrounded by BCN [96]

Although SiBCN has been well studied, SiBC structures have not yet been investigated to any appreciable extent. Doping the polycarbosilane SMP-10 polymer with boron has the potential of increasing the high temperature stability as it does with SiBCN. Another beneficial role of boron is that of a sintering aid. It is well known that boron is an ideal sintering aid for the densification of powder processed SiC.[65] Boron is typically added to SiC powder by dry ball milling with B_4C or amorphous Boron with carbon additions. Boron has been shown to reduce grain boundary energy while carbon is known to reduce the surface SiO_2 layer.[97] In this study boron will be added at the molecular level using decaborane. The densification of precursors as is examined both with and without boron will be investigated. The densification as well as the radiation resistance of the PDC SiC that has had boron added directly to the precursor vs. added to the powder will be compared in this research. This will give substantial insight as to the effects of PDC processing methods vs. more traditional routes in generating SiC and its stability after exposure to ion irradiation

II.5.5 Porous Ceramics from Precursors

As mentioned in II.3 porous materials have applications in nuclear materials for usage in TRISO fuel pellets. Additionally, porous SiC is the primary candidate as a flow channel insert for dual coolant blanket concepts in fusion reactors as shown in Figure II-27 and Figure II-28.[98]

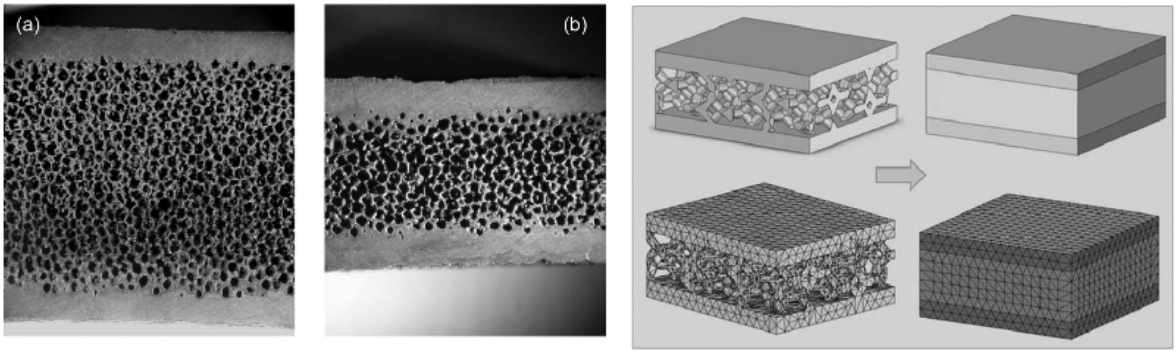

Figure II-27 Silicon carbide foams for flow channel inserts[99]

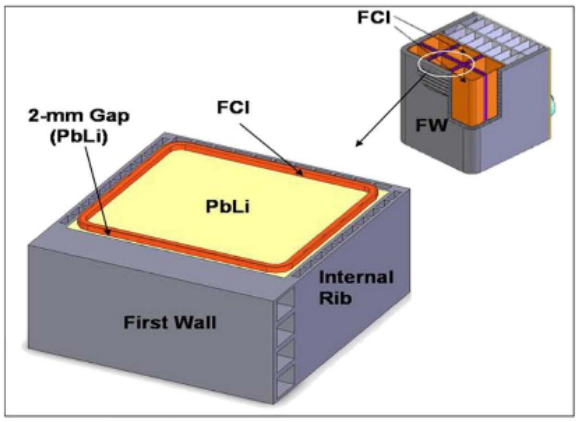

Figure II-28 Location of SiC Flow channel inserts for fusion reactors [99]

SiC is an attractive material for this application due to its excellent thermal, mechanical and chemical stability at high temperatures as well as their low thermal expansion, high thermal

shock resistance, low corrosion by liquid metal, low activation and good resistance to neutron irradiation.[100] In addition to the nuclear field, porous ceramics find numerous applications in other areas such as filtration (gases, molten metals, etc…), radiant burners, catalyst supports, biomedical devices, kiln furniture, reinforcement for metal matrix composites, thermal protection systems, solid oxide fuel cells, heat exchangers, among others…[101] The production of ceramic materials from preceramic polymers offers unique opportunities to engineer the porosity using conventional polymeric/plastic forming techniques in lieu of more traditional ceramic processing routes. There have been a variety of manufacturing methods that can be utilized to introduce porosity into polymer derived ceramics including: replica of polyurethane foam, direct blowing of a ceramic suspension (with extrinsic or intrinsic pore formers), the use of sacrificial fillers, controlled pyrolysis of preceramic bulk components and extrusions. [76,101] The variety of plastic forming technologies allows for the possibility to tailor the porosity and pore morphology of a ceramic to suit specific applications.

Ceramic foams are a specific class of porous ceramics that typically have highly interconnected porosities with cell sizes ranging from a few nanometers to several millimeters.[76] An example of how processing parameters can be tailored for varying porosity can be seen in Figure II-29. In this specific example, a silicone resin (SR) preceramic polymer (polymethylsiloxane) was utilized to form a Si–O–C amorphous ceramic upon heating.[101] Three different porosities were achieved in these ceramics by varying the method: (a) macro-cellular ceramic foams; (b) micro-cellular ceramic foams; (c) high porosity ceramic components.

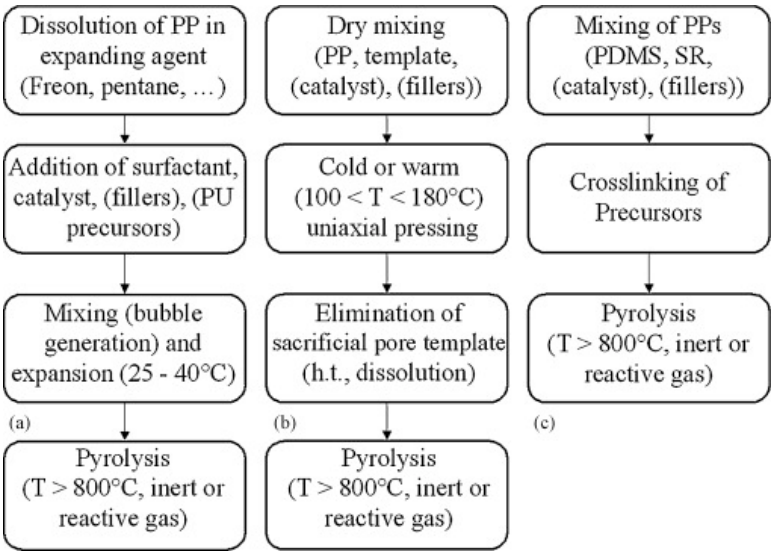

Figure II-29 Processing parameters for tailoring porous PDCs [101]

In Figure II-30 it can be seen how these different methods of processing can change pore morphology (open/closed celled, size, density) within the structures.

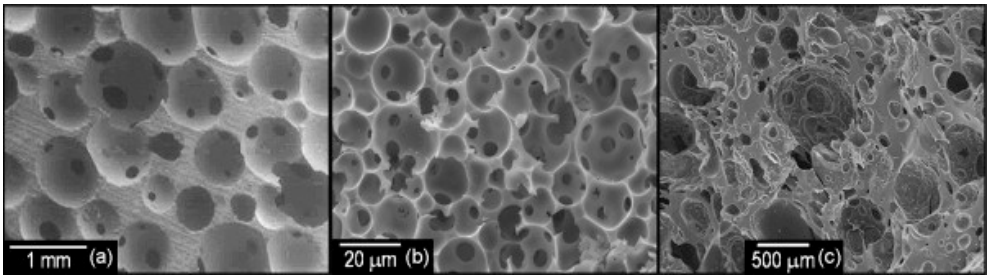

Figure II-30 (a) Macro-cellular open cell foam; (b) micro-cellular open cell foam and (c) high porosity sample [101]

Utilizing direct foaming either closed or open-cell foams can be manufactured with both macro and microcellular porosity. The commonality in all foaming is the utilization of gas bubbles (often referred to as blowing agents) in a preceramic polymer solid, melt or solution followed by

final curing of the polymer. Either intrinsic or extrinsic blowing agents can be utilized to generate the foam. Extrinsic agents generate the porosity due to their low boiling point liquids (e.g. dichloromethane or freon) or added components, which form gases during their decomposition (azodicarbonamide, hydrazine, carbazides, etc…). Oftentimes, the addition of a low boiling point liquid can yield an open-celled network containing density gradients. The addition of solids which typically decompose ~250 °C and release gases such as nitrogen, carbon dioxide, carbon monoxide or ammonia lead to the generation of large amounts of porosity in the curing polymeric precursor. [102]

The mixing of precursors of varying molecular architectures is showing promise for fabricating larger components with blended macroporosity.[101] This can allow for a blend of pore morphologies in the resultant ceramic monolith due to variations in weight loss, shrinkage and gas evolution from the starting precursors. Therefore the resulting pore morphology can be somewhat inhomogeneous and also contain both open and closed cells. In contrast, intrinsic blowing agents generate porosity through a chemical reaction or phase separation occurring between components in the liquid system.[76] This was previously observed when using a structure terminating hydroxyl and ethoxy group that react to form alcohol and water in the temperature range of 200-300°C as shown in Figure II-31. This allowed in situ foaming without requiring the necessity of additional foaming agents.

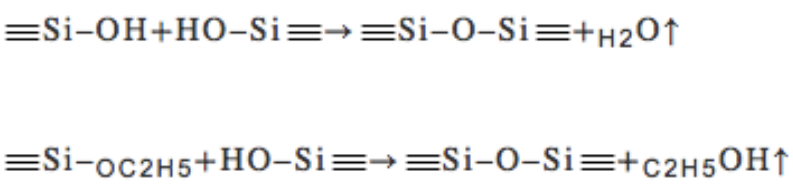

Figure II-31 Polycondensation reaction of polysilsesquioxane [103]

In this reaction, H_2O and C_2H_5OH act as intrinsic foaming agents and the foam structure will be stabilized by the concurrent viscosity increase due to crosslinking of the polymer melt. The microstructures can be further tailored to optimize the associated properties (e.g. mechanical, magnetic, electrical, storage) by loading the polymer with reactive or inert filler particles.[104] In order to utilize fillers (reactive or inert) it is necessary to optimize the foaming temperature (curing time). The polymer melt viscosity can also be varied to control the sedimentation kinetics of the filler powder particles and thus the rise of gas bubbles in the polymer melt during foaming. Once the thermoset foam has been cured it is necessary to pyrolze it in order to convert the polymeric foam into a ceramic foamed monolith.

A wide range of processing routes has been investigated for the production of cellular ceramics for various applications. This research has focused on a foaming method that incorporate both intrinsic (tailoring the molecular architecture of the starting preceramic polymer) and extrinsic (using the foaming agent azodicarbonamide) to control the pore morphology of SMP-10 in the production of monolithic open porosity silicon carbide foam systems.

II.6 Silicon Carbide Ceramics

Silicon carbide ceramics are promising candidates as high-temperature structural materials. This is due to their high thermal shock resistance, high hardness and resistance to aggressive chemicals and abrasion.[97,105] Silicon carbide rarely exists in nature, but has been produced on the industrial scale for numerous years through utilization of the Acheson method from silica and coke. In this technique two solid electrodes are connected with graphite powder, followed by a mixture of silica and coke placed in the surrounding vicinity. The mixture is electrically heated to produce SiC: [97]

$$SiO_2 + 3C \rightarrow SiC + 2CO$$

The SiC is then ground and refined to produce powders suitable for densification (ultrafine-grained powders).[97] These powders are then typically hot pressed as SiC is fundamentally a difficult material to sinter. In general, for densification to occur, parameters such as temperature, applied pressure, average particle size and gaseous atmosphere must be considered. In order for sintering to take place, there must be a decrease in the free energy of the system. The curvature of the free surfaces, the applied pressure and a chemical reaction are some of the primary driving forces for sintering ceramic particles.[106] In the consideration of SiC, virtually no sintering is observed when a pure SiC powder compact is heated. This can be attributed to the covalent bonding characteristics of SiC and the high grain boundary to surface energy. Whenever this exceeds a certain critical value, a solid will fail to densify due to lack of the necessary energy gain when surfaces are replaced by grain boundaries.[107] The densification of SiC requires the use of very high temperatures and pressures in an inert environment.[108] In order to densify these

materials it is also necessary to utilize sintering additives. In many cases this is in the form of liquid-forming additions.[109] The use of yttria or other rare earth oxidies, Al_2O_3 or AlN as sintering additives leads to the formation of a silicate liquid phase in which $Si0_2$ exists on the surface of the SiC particles.[110] This liquid phase will reduce the sintering temperature to values less than 1900 °C in comparison to the more typical 2100-2200 °C for the solid state sintering of SiC.[108]

It can be appreciated that the sintering of SiC is usually performed at very high temperature up to 2200 °C in the solid state due to covalent bonding.[108] [111] The solid state sintering of silicon carbide can be accomplished through the addition of boron and carbon to submicron sized SiC powders. Boron as a sintering aid is typically in the form of elemental boron (amorphous or crystalline), boron carbide or lithium borohydride.[109] The amount of boron in the SiC system should be in the range of 0.53 parts by weight of boron to silicon carbide. When less than 0.5 is utilized, full densification is not observed; whereas when more than 3.0 parts by weight are implemented, exaggerated grain growth is shown to occur in conjunction with loss of strength and oxidation resistance. The optimum amount of boron utilized in the solid state sintering of SiC was observed to be 1 part by weight per 100 parts of silicon carbide.[112] This is most likely related to the solubility limit of B in SiC. At temperatures of up to 1500°C, boron is shown to exhibit surface diffusion-induced gran growth, thereby facilitating sintering at high temperatures.[97]

The pressureless sintering of silicon carbide with boron is thought to require excess carbon. [113] Small additions of boron are shown to be dependent upon the control over oxygen present during sintering of the SiC. This is evidenced by the presence of uniform, equiaxed grain structures of β-SiC when sufficient oxygen is present allowing detectable particles of SiO_2, whereas uniform elongated grain structures of SiC are observed in the presence of excess carbon. [114] It is generally thought that the carbon is needed to reduce the thin layer of SiO_2, which is considered to be present on the surface of SiC powder particles. It has also been considered that free carbon may enter the SiC lattice, causing the formation of lattice defects in the form of silicon vacancies, which have the possibility to provide an increased rate of diffusion.[111] In order for bulk diffusion to cause densification, it is necessary for both silicon and carbon to diffuse together. Silicon is considered to be rate controlling as it is thought to diffuse slower than carbon.[111] There is possibility that varying the concentration of carbon in the system can alter the overall sintering rate by controlling the silicon diffusion rate.

As previously discussed in this chapter, polycarbosilanes are of considerable interest in developing silicon carbide ceramics. The use of polycarbosilane in the development of silicon carbide is probably most well known for its ability to generate long continuous silicon carbide fibers.[115] However, in order for these fibers to be feasible it is necessary to utilize a preceramic polymer that has a high ceramic yield upon pyrolysis. A catalyst can also be used for crosslinking to not only increase ceramic yield, but also to allow for crosslinking to occur at lower temperatures. [106] The long continuous fully dense SiC fibers are possible due to melt spinning at 250-350 °C [106], where the density is managed due to the decreased fiber thickness allowing for easy escape of the gaseous products released during pyrolysis. Although this

method is functional for thin sections it is not possible to prepare bulk specimens in this manner due to escaping gas within the bulk structure leaving behind a porous pathway. In order to make a dense SiC bulk monolith, a polymer infiltration pyrolysis (PIP) has been developed as shown in Figure II-32:[116]

- Curing of the liquid precursor to obtain a polycarbosilane powder
- Shaping the powders using warm pressing techniques
- Pyrolysis of the green bodies to convert the crosslinked powders into ceramic monoliths
- Polymer infiltration followed by pyrolysis (PIP)

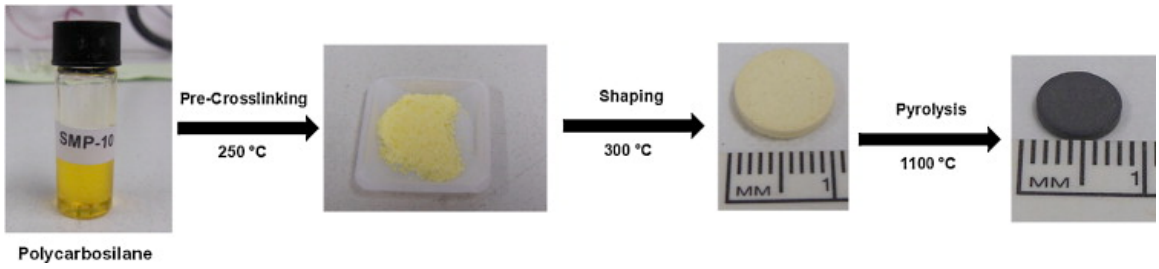

Figure II-32 PIP processing of a polycarbosilane[116]

This method allowed crack free and relatively dense SiC monoliths to be prepared using pressureless sintering. However, the ceramic monoliths were shown to exhibit residual porosities of 15-25%, which can be detrimental to the mechanical properties of the SiC.[116] Therefore, in order for this to be a viable process it will be necessary to do multiple PIP cycles in order to further increase density.

II.6.1 SiC Polytype formation

The fundamental structural unit in all SiC polytypes is a covalently bonded coordination tetrahedron (either SiC_4 or CSi_4). An interesting phenomenon that occurs in SiC is a one-dimensional disorder that allows a variety of stacking sequences known as polytypism.[117] This is the result of more than one crystal structure being thermodynamically stable in a given temperature and pressure regime.[118] A SiC polytype may be considered as an assembly of tetrahedral. In any of the various SiC structures, the SiC tetrahedra are joined to each other at the corners (i.e. two neighboring tetrahedral share a corner atom).[117] The SiC tetrahedron arises out of the tetrahedral bonding between silicon and carbon atoms Figure II-33 where the structure in a) represents a SiC tetrahedron with the c-axis coinciding with the vertical Si-C bond; and b) represents a twinned variant of the SiC tetrahedron. [117]

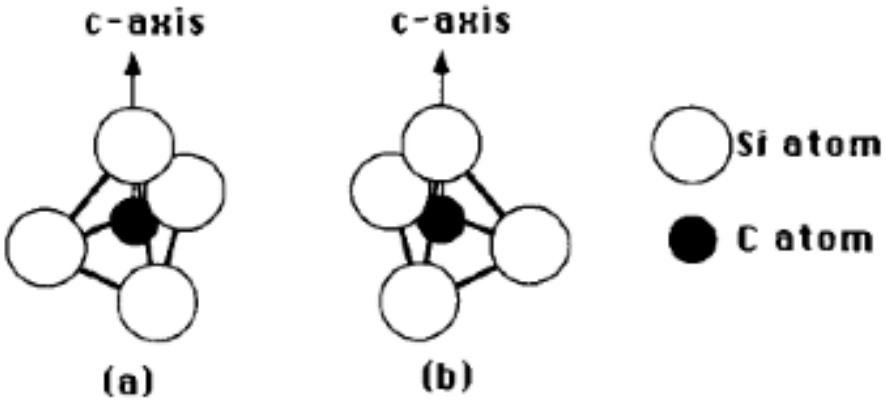

Figure II-33 a) SiC tetrahedron b) twinned variant [117]

The two variants are related to each other by a 180° rotation around the c-axis. These various polytype structures have layers of tetrahedral that stack to form frameworks in which all the tetrahedral have one apex out of the layer plane. These tetrahedra are linked at the corners to achieve four-fold coordination. Both cubic and hexagonal polytypes are found in SiC, they can be: intermixed, wide range ordered, larger period, stacked and disordered from heavy faulting.[119] The polytype conversion is thought to occur during various sintering stages of the SiC powders.[120,121] It is well known that in this conversion process stacking faults are easily generated and that the stacking faults accompany partial dislocations.[121] The common high temperature polytype has a hexagonal unit cell and a six layer repeat in the c-direction (perpendicular to the layers). This is shown in Figure II-34, in which the most common SiC polytypes are presented.

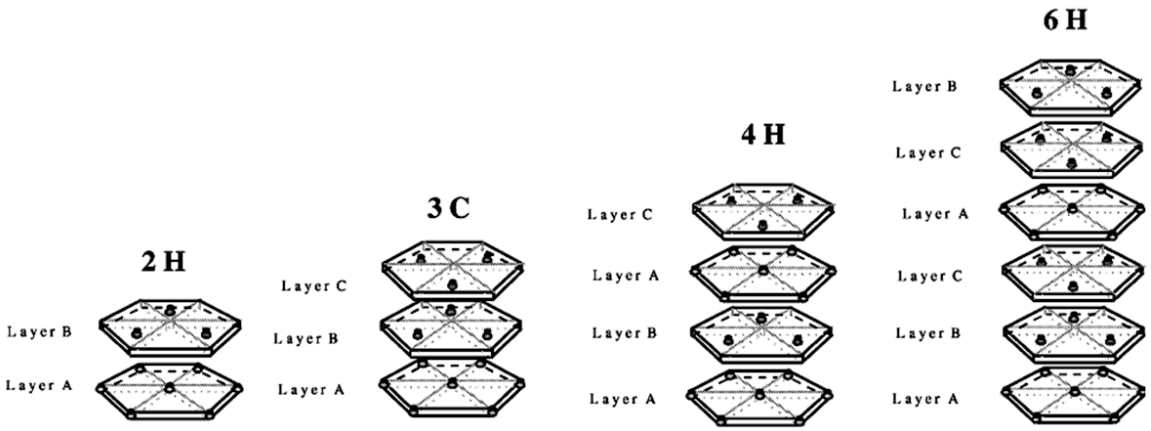

Figure II-34 Common SiC Polytypes [122]

The notation of the letters and numbers are indicative of how many repeating layers are found in the specific crystal structure. Therefore, 6H SiC refers to 6 being the number of layers in the repeat along the stacking direction together with the Bravais lattice type of the resultant

hexagonal crystal structure (H), whereas 3C refers to 3 repeating layers of the (C) cubic crystal structure and rhombedral is denoted with R. Although there are a large number of known polytypes of SiC, very few of these polytypes are considered to be thermodynamically stable with 2H 3C, 15R and 6H being known to occur with the greatest frequency.[119] The stacking sequences of these most common polytypes are given by: [119]

- 3C ABCABC –(∞)
- 6H ABCB'A'C'A (33),
- 4H ABA'C'A (22)
- 15R ABCB'A'BCAC'B'CABA'C'A $(32)_3$

While there are an infinite possible number of stacking variations, the structures of even the longest-period polytypes may be considered as sequences of one or more of the smaller-period units. In general, it is understood that β-SiC refers to the 3C structure and α-SiC refers to everything else including both rhombohedral and hexagonal crystal structures. X-ray diffraction (XRD) can be used to determine polytypes of SiC in addition to TEM and more recently Raman Scattering and Nuclear Magnetic Resonance Spectroscopy (NMR) have also been used as characterization tools.

A considerable amount of work has been conducted to understand the stability of these basic SiC polytype structures. In all of the cases, the resultant polytypes were observed to be dependent upon the rate of growth and the temperature. The following diagrams are suggested stability diagrams for the presence of SiC polytypes based on temperature Figure II-35:

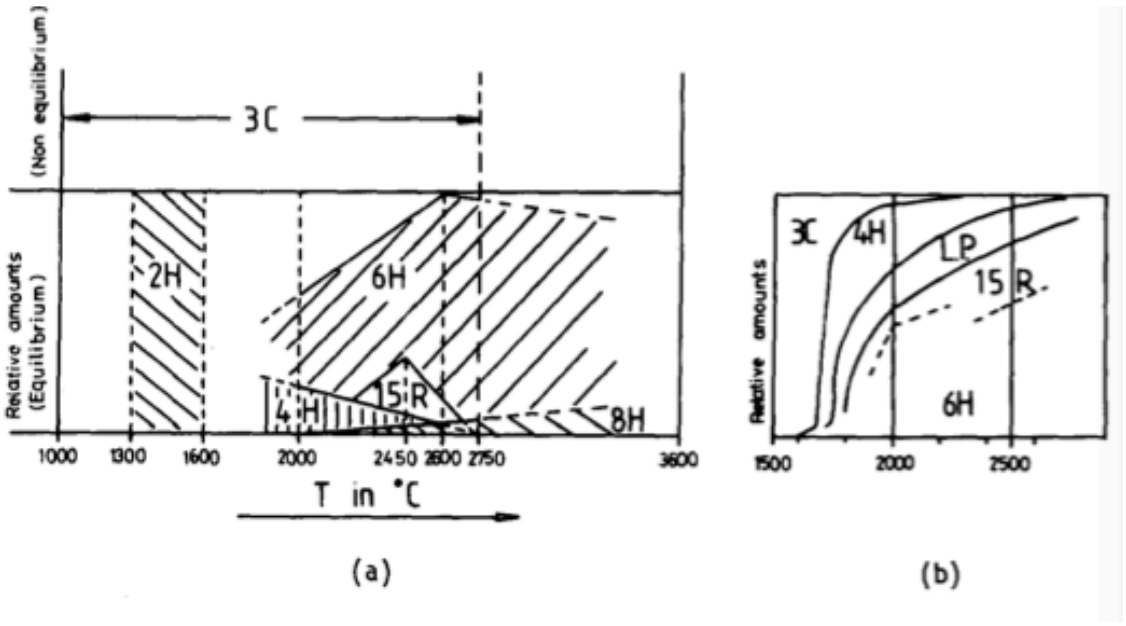

Figure II-35 Thermal Stability of Silicon Carbide Polytypes[119]

It can also be appreciated that minute quantities of impurities and non-stoichiometry have a substantial effect on stabilizing specific polytypes.[119] The elements that have been studied that are of considerable interest in the development of SiC are located in groups III and V, i.e. the electron acceptors; aluminium, boron, etc. and donors; nitrogen and phosphorous. Aluminum was first noted to stabilize the 4H structure [123] with boron having been shown to generate the same effect. Specifically boron may substitute on the carbon sublattice or may occupy either the carbon or the silicon site (or both), in order to minimize the total free energy of the system.[124] It is well appreciated that boron functioning as an impurity atom stabilizes the 4H SiC polytype.[125] It has been demonstrated that the more common small period polytypes are stabilized by

impurity atoms. Non-stoichiometry also plays a role in dictating the resultant polytype where the appearance of excess Si is shown to contribute to the growth of the 3C phase and oppositely the addition of carbon is shown to promote hexagonality (4H in particular).[125] Although, polytypic stability in SiC has been studied for many years no single existing theory can satisfactorily explain all of the observations given for polytypism in SiC.[126]

Existing theories can be divided into two categories; those involving kinetics and growth and those considering a thermodynamic basis. The growth theories are typically variations of spiral growth occurring around screw dislocations, where the repeat of the polytype is determined by the step height of spiral growth.[119] The differences of internal energies in the SiC polytypes were expected to be relatively small. However, bond length and band gap measurements imply that it is not negligible. The 2H polytype is found to have the largest band gap (largest binding energy) and measurements of the lattice parameters sugest it is the most dense with 3C being the most open structure (although it can be appreciated that these differences are relatively small).[119] While 3C seems to be the least stable polytype, it is observed in the initial stages of growth over a large range of temperatures. This is possibly due to its high degree of symmetry and low energy surfaces, which could potentially result in relative ease of nucleation and rapid growth in all directions.[127] The high symmetry of the 3C polytype possibly explains why the 3C SiC polytype is shown to occur over a wide temperature range. [119] It can be appreciated that although the 3C SiC polytype is present in a large temperature range it is an unnecessary intermediary phase in the 2H→6H transformation. That being said, the β-SiC (3C SiC) transformation to α-SiC hexagonal phase (4H, 6H, 15R, etc…) is the most common transformation in SiC. With the 3C→6H transition being observed more frequently than other polytypic transformations.[119]

Therefore, it can be argued that 3C has perhaps an increased stability or its occurrence is controlled through kinetic growth mechanisms.

Chapter III Research Scope

One of the strategies in the development of radiation damage resistant materials has focused on increasing recombination of Frenkel pairs in order to prevent deleterious microstructural evolution. This has proven difficult to accomplish until recent observations with the success of nanostructured materials (either nanoengineered oxides dispersed in ferritic steels or nanolayered materials).[48,49] It appears that the nanospaced and nanostructured interfaces present in these new materials offer exceptional stability under irradiation that other materials lack. Materials containing nanospaced interfaces appear to mitigate radiation damage by enhancing local recombination of defects at the engineered interfaces.[83,84] Several studies have shown the beneficial role of these nanostructures in nuclear environments for oxides. [91,92,93,94] Significant advances in nuclear energy technology could be achieved by realizing such nanostructures in material systems with higher temperature capabilities and more inherent radiation resistance i.e. SiC. This is the overall goal of this research.

This research will investigate the thermal and mechanical stability of the nanodomains and nanostructures in the Si-C materials. The stability of the nano-domains and the nanostructure will be carefully evaluated. Materials with a representative range of nanodomains and carbon nanostructures will be heat treated as a function of time and temperature in inert environment up to temperatures as high as 2000 $^{\circ}$C. This is being done to develop a relationship between nanostructure and the mechanical properties of the materials.

For a few selected compositions and processing conditions, high-density bulk samples for testing will be made by hot-pressing. The goal is to systematically determine the effect of the nanostructures on these properties over a broad range of the newly developed nanostructures.

As demonstrated in the swelling of the SiC under radiation and high temperatures, it is important to determine the stability of the nanostructure under irradiation and its suitability of storing inert gas fission products. Experimental techniques will be carried out at the Pacific Northwest National Laboratory (PNNL) and colleagues at Purdue University will conduct computational simulation research. Energetic ion irradiation will be used to produce displacement damage to simulate the radiation environment in PDC SiC. The effect of ion irradiation on the nanostructure, carbon domain, and microstructre will be evaluated. Samples will be irradiated at doses up to a few dpa and then examined for damage accumulation and property changes. TEM will be used to quantify the damage accumulation and thermal stability after irradiation and will then be compared to the as-fabricated stability. These irradiation-induced nanostructural changes will be correlated with processing conditions, such as processing time and temperature.

In summary, in this study the PDC route will be used to:

a) Investigate the effect of precursor chemistry (Si:C ratio and boron doping) on the nanostructure and properties
b) Investigate the effect of nanostructure (amorphous or nano-crystalline) on the properties.
c) Investigate the effect of crosslinking pathway on the nanostructure and properties.
d) Develop processing protocols to make dense and porous SiC based materials.

Chapter IV Experimental

IV.1 Materials Selection

IV.1.1 Preceramic Polymer

This research involves the processing and characterization of silicon carbide ceramics from the polymer derived ceramic processing route. Therefore, it is necessary to utilize a precursor from the polycarbosilane family in order to achieve SiC materials. Starfires ® allylhydridopolycarbosilane preceramic polymer (SMP-10) Figure IV-1, was chosen due to its ability to maintain a stoichiometric Si:C ratio following pyrolysis, as well as its commercial availability.

Figure IV-1 SMP-10 Molecular Structure

IV.1.2 Crosslinking agents

It is well known that the addition of crosslinking agents such as dicumyl peroxide Figure IV-2 lowers the crosslinking temperature of the polymer due to free radical initiation.

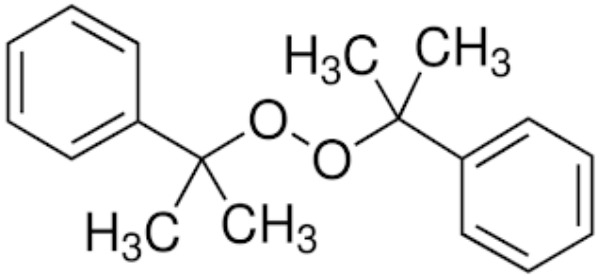

Figure IV-2 Dicumyl peroxide (crosslinking agent)

The addition of crosslinking agents also has the added benefit of increasing the degree of crosslinking and thus resulting in less mass loss during pyrolysis.

IV.1.3 Excess carbon from divinylbenzene

Divinylbenzene, a high carbon content polymer, Figure IV-3, was used to increase the carbon content of the ceramic.

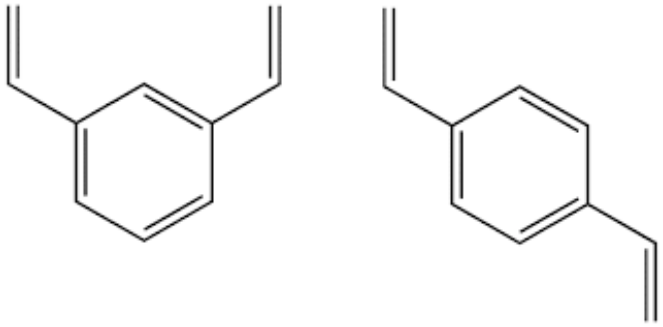

Figure IV-3 Divinylbenzene (DVB)

IV.1.4 Decaborane for dense & porous SiC

In order to densify SiC it is necessary to utilize a sintering additive. Boron is a well known sintering additive for SiC. Boron has the added advantage that it leads to enhanced densification without the formation of a liquid phase. In this research, boron in the form of decaborane (Figure IV-4) was utilized as a sintering additive.

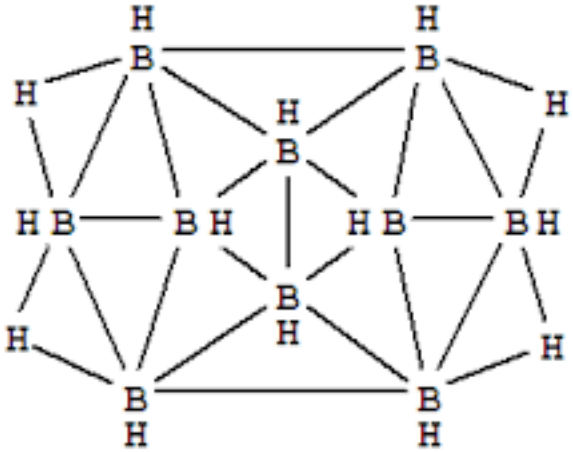

Figure IV-4 Caged structure of decaborane

The direct incorporation of sintering aids to the molecular architecture of the polymer precursor had not been previously explored. Therefore, it was important to consider alternative possibilities; as such amorphous boron was added to a separate set of polymer derived SiC powders following pyrolysis to assure the densification of the material. It can also be noted that decaborane also functioned as a foaming modifier in the development of porous SiC monoliths.

IV.1.5 Porous SiC

Three different methods of preparing porous silicon carbide were explored: foaming with azodicarbonamide, sacrificial burnout of PMMA beads and catalyst assisted with the platinum crosslinking catalyst; Platinum(0)-1,3-divinyl-1,1,3,3-tetramethyldisiloxane.

Azodicarbonamide a nitrogen based compound, Figure IV-5, decomposes at ~200 °C releasing gases to allow for foaming of the polymeric precursor

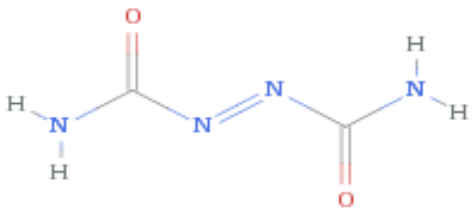

Figure IV-5 Azodicarbonamide molecular structure

Poly (methyl metharcrylate) (PMMA) (*Figure IV-6*) was utilized as a sacrificial filler to introduce porosity to an already crosslinked system.

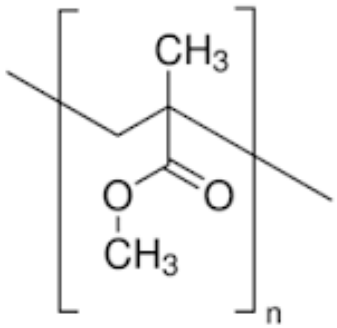

Figure IV-6 Poly (methyl methacrylate) (PMMA)

The catalyst Platinum(0)-1,3-divinyl-1,1,3,3-tetramethyldisiloxane, Figure IV-7, allows for the rapid crosslinking of polymers at room temperature. It was utilized in the generation of porosity due to the rapid off-gasing of hydrogen during curing.

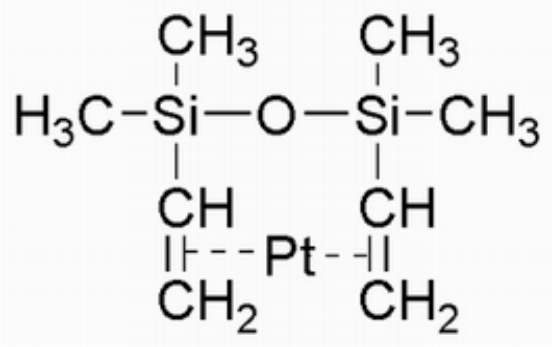

Figure IV-7 Platinum Catalyst

IV.2 General Processing Studies

IV.2.1 Crosslinking Experiments

It is understood that crosslinking the preceramic polymers has a substantial effect on the final ceramic yield. In order to establish crosslinking protocols, various additives as well as thermal treatments of allylhydridopolycarbosilane preceramic polymer (SMP-10) were explored. This was done in order to explore processing parameters with a goal of reducing mass loss during pyrolysis. The following approaches were investigated:

- Thermally crosslinking of SMP-10 using a rate of a heating rate of 5 °C /min to 350°C or 400°C in a gettered argon atmosphere.

- Decaborane was added in 0-5 wt% to the SMP-10 liquid precursor in a nitrogen glovebox. The complex was then sonicated for 2 hours followed by thermal crosslinking at 400°C in a tube furnace using a 5 wt% H_2 in Argon atmosphere for two hours.
- Divinylbenzene was added in 0-5 wt% to the SMP-10 liquid precursor in a nitrogen glovebox. The complex was then sonicated for 2 hours followed by thermal crosslinking at 400°C in a tube furnace using a 5 wt% H_2 in Argon atmosphere for two hours.
- Dicumyl peroxide was added in 0-5 wt% to the liquid SMP-10 precursor in a nitrogen glovebox. The samples were then sonicated for 2 hours followed by thermal crosslinking at 400°C using a using a 5 wt% H_2 in Argon atmosphere for two hours.

The crosslinked powders from the SMP-10 precursors (modified with C & B, as well as unmodified) were prepared using the following procedure.

SMP-10 (either with or without C and B modifications) was placed in the furnace for crosslinking by heating at 2°C/min to 200°C holding for 1 hour and then heated at 2°C/min to 400°C for 2 hours under gettered argon the thermal profile is shown Figure IV-8.

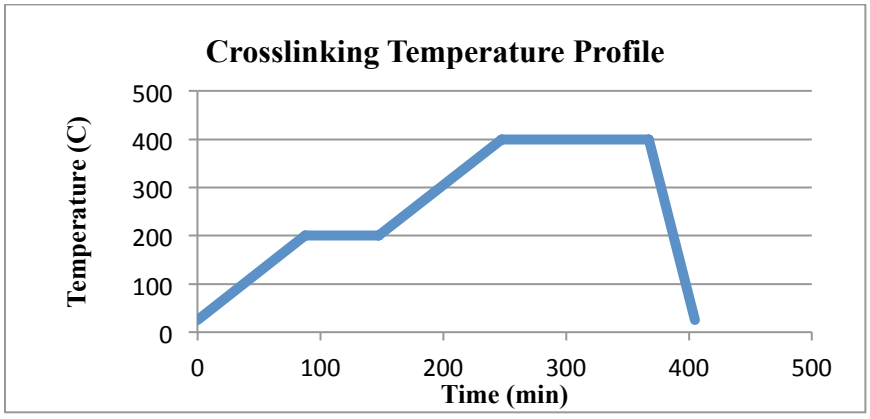

Figure IV-8 Thermal profile for crosslinking of SMP-10

IV.2.2 Milling the Crosslinked Powders

Once the crosslinked material (modified or otherwise) was removed from the furnace, it was placed in a polypropylene Nalgene™ vial containing YSZ 5mm media balls (4:1 ball:charge wt. ratio) and sealed under nitrogen atmosphere for high energy ball milling for 60 minutes. For milling, the Spex Mill shown in in Figure IV-9 was used (Spex Mixer/Mill 8000M Spex SamplePrep, Metuchen, NJ, USA).

Figure IV-9 Spex Mill 8000

The samples were then removed and opened in air to be transferred to an inert tube furnace in a graphite paper lined crucible for pyrolysis in 5% H_2 in Argon atmosphere.

* It should be noted that the milled crosslinked precursors were observed to be slightly pyrophoric when exposed to air directly after ball milling. This was most likely due to a chemical reaction from the increased vibrational energy from the Spex Mill with the oxygen

from the air. As a result, after Spex milling, the powders were opened in an inert (nitrogen) glovebox.

IV.2.3 Pyrolysis of the Crosslinked Material

The milled crosslinked materials (modified or otherwise) were removed from the Spex Mill and opened in an inert glovebox to be transferred to the furnace in a graphite lined (Graphoil) crucible. The temperature was increased at a rate of 10 °C/min to 400 °C, held for 5 minutes and then 5° C/min to 600 °C, held for 1 hour followed by a final heat treatment to 800 °C at 5 °C/min and held for two hours in gettered argon. The powders were then cooled to10°C/min to room temperature. The temperature profile is shown in Figure IV-10.

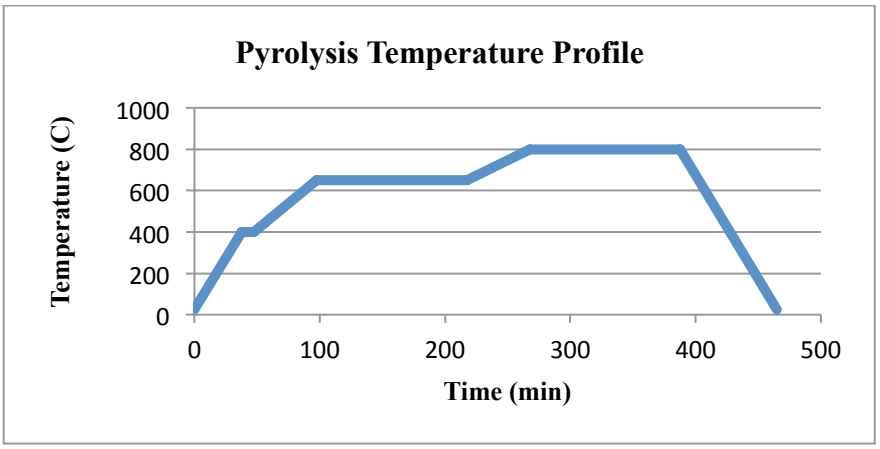

Figure IV-10 Pyrolysis temperature profile for fully pyrolyzed powders to be hot pressed

IV.2.4 Addition of free carbon into SiC

Excess carbon was added directly to the liquid SMP-10 preceramic polymer through the addition of divinylbenzene (DVB) in the range of 0-5 wt% in a nitrogen glovebox. The SMP-10 sample with DVB was sonicated for 2 hours in a glass vial sealed under nitrogen atmosphere. The various Si:C samples were then crosslinked at 400°C for two hours in a tube furnace using 5 wt% H_2 in Argon atmosphere, followed by pyrolysis holding at 600°C for 1 hour and 800°C for two hours in a tube furnace using a 5 wt% H_2 in Argon atmosphere.

IV.2.5 Decaborane addition to SMP-10 Precursor

Boron was added to SMP-10 by adding 1 wt% Decaborane to the liquid polymer in an inert glove box. The boron modified SMP-10 was sonicated for 2 hours in a glass vial sealed under nitrogen atmosphere. The boron doped SMP-10 was thermally crosslinked up to 400°C under 5 wt% H_2 in Argon atmosphere for two hours.

IV.3 Processing Fully Dense PDC SiC

The fully dense SiC ceramics were made from the amorphous SiC powders with and without excess carbon as well as with and without boron doping by hot pressing. The boron should serve as a sintering aid by reducing grain boundary energy between the grains. The excess carbon will serve to remove oxygen from the material during sintering and was also intended to provide

nanostructured carbon precipitates. The emphasis is obtaining a fully crystalline nanostructure. The hot pressing work was completed under the International Center for Materials Science Research (ICMR) Grant sponsored by the National Science Foundation (NSF). This work was done in Professor Pavol Sajgalik's group at the Institute of Inorganic Chemistry, Slovak Academy of Sciences, Bratislava, Slovakia.

Powders containing varying weight percent of carbon, both with and without boron (sintering aid) were prepared in adequate quantities to study the radiation properties of polymer derived SiBC (SMP-10 with decaborane modifications) and SiC (with amorphous boron) powders. The samples containing excess carbon in the SMP-10 precursor were prepared through molecular modifications with DVB in 0, 1 & 5 wt%. After DVB addition, the samples were crosslinked under 5% H_2 in Argon atmosphere to 400° C for two hours. The crosslinked samples were then milled using a Spex mill to obtain fine powders. After milling the crosslinked samples to a fine powder they were pyrolyzed to 800°C for two hours.

IV.3.1 Amorphous Boron Addition to Amorphous Polymer Derived SiC

SMP-10 was thermally crosslinked to 400°C under 5 wt% H_2 in Argon atmosphere for two hours. Once removed from the furnace the crosslinked polymer was placed in a polypropylene Nalgene™ vial for high energy ball milling (Spex Mixer/Mill 8000M Spex SamplePrep, Metuchen, NJ, USA) in the Spex Mill for 60 minutes.

The samples were then removed and opened in air to be transferred to an inert tube furnace for pyrolysis in 5% H_2 in Argon atmosphere. The temperature was increased at a rate of 10 °C/min to 400 °C, held for 5 minutes and then 5° C/min to 600 °C, held for 1 hour followed by a final ramp to 800 °C at 5 °C/min and held for two hours. The powders were then cooled at 10°C/min to room temperature.

Amorphous boron in the amount of 1 wt% was added to the pyrolyzed amorphous SiC powders followed by attrition milling to very fine particle size as discussed in the following section.

IV.3.2 Attrition Milling Amorphous Polymer Derived SiC Powders

In order for the samples to achieve high density by hot pressing, it is necessary to mill the powders to a very fine particle size. All the powders were milled using an attrition mill (Szegvari Attritor). This was done using 750 grams of 5 mm SiC milling media and a Si_3N_4 attritor arm in a 750 mL Teflon lined vessel. The samples were all milled for 2 hours at 400 rpm in the presence of 200 mL of hexane. All the samples were then removed and placed in a 1000 mL round bottom flask and placed in a rotovap (Heidolph laborata) at 40°C at a pressure of 335 mbar to remove all of the hexane from the finely milled powder. The pressure from the rotovap was slowly decreased as more of the hexane was removed from the sample. After much of the hexane had been removed from the sample it was then placed in a Vacucell BMT vacuum oven, heated to 80°C under a pressure of ~200 mbar and left overnight to fully evaporate off the hexane. The sample was then sieved for 15 minutes at a time with 20-second intervals until all of the powder went first through a 125 μm sieve containing about fifteen 5 mm SiC media balls followed by the 71 μm sieve also containing about fifteen 5 mm SiC media

balls and into the final collection pan. The following sample compositions shown in Table IV-1 were milled to submicron particle size using the procedure described above. Furthermore, one additional sample was prepared in the same manner, only with 1 wt% amorphous boron powder added to pyrolyzed powders consisting of 1 wt% excess C in amorphous SiC in the attritor.

Table IV-1 SiC/SiBC Powders Prepared for Hot Pressing

Sample ID	%DVB	Decaborane
0SiC	0	0 wt%
1SiC	1	0 wt%
3SiC	3	0 wt%
5SiC	5	0 wt%
0SiBC	0	1 wt%
1SiBC	1	1 wt%
3SiBC	3	1 wt%
5SiBC	5	1 wt%

The attrition milling of the SiC and SiBC amorphous materials was accomplished at the Institute of Inorganic Chemistry Slovak Academy of Sciences through the support of the International Center for Materials Research (ICMR) Grant sponsored by the National Science Foundation (NSF).

IV.3.3 Hot Pressing Amorphous Polymer Derived SiC

The amorphous submicron SiC powders were hot pressed to a temperature of 2050 °C and a pressure of 30 MPa in a 30 mm graphite die in the presence of gettered argon. The hot pressing

was conducted at the Technology University in Vienna (done in partial sponsorship of the ICMR NSF Grant). The temperature/pressure regime that was used to hot press the powders is shown Figure IV-11. The samples were heated at 10°C/min to 1800°C; then at 5°C/min to 2050°C and held for 60 minutes. The samples were cooled at 5°C/min to 1500°C and the cooling rate was then increased to 10°C/min to room temperature. The pressure was applied at 1800°C and released after holding at the final temperature of 2050°C for 60 minutes.

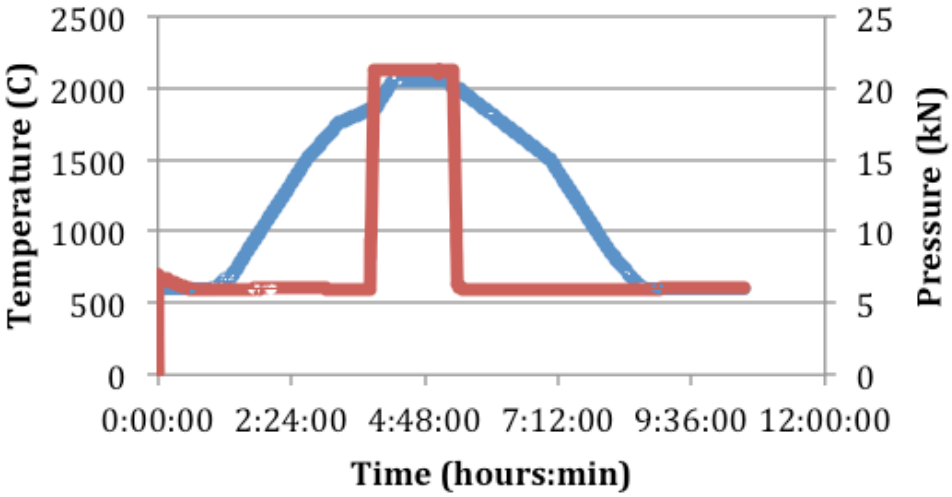

Figure IV-11 Temperature Pressure Regime During Hot Pressing

The Table IV-2, indicates all the samples that were hot pressed using the above temperature/pressure regime.

Table IV-2 SiC and SiBC Samples Hot pressed

Sample
0SiBC
1SiBC
3SiC
5SiBC (2 samples)
5SiC

IV.4Hot Pressing Partially Pyrolyzed Powders

In addition to the hot pressing of the fully pyrolzed powders, hot pressing was also conducted on partially pyrolyzed samples. 1 wt% decaborane was added to SMP-10 in a nitrogen glove box and sealed in a glass vial. The modified SMP-10 sample was placed in a ultrasonic bath for 2 hours. The sample was then placed in the furnace using the temperature profile shown in Figure IV-12, under 5%H_2 in Argon atmosphere for thermal crosslinking at 400°C for two hours.

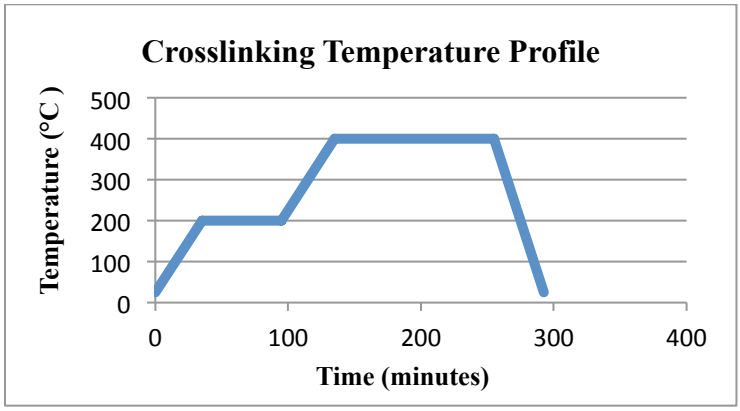

Figure IV-12 Crosslinking Temperature Profile

Once removed from the furnace, the crosslinked polymer was placed in a 60 mL polypropylene Nalgene® vial containing YSZ 5mm media balls (4:1 ball:charge wt. ratio). The vial was sealed under argon atmosphere and high-energy ball milled using the milling procedure. The sample was then removed from the Spex Mill and opened in an inert glovebox and transferred to the furnace in a graphite lined crucible for pyrolysis at 650 °C for two hours. The temperature profile is shown in Figure IV-13.

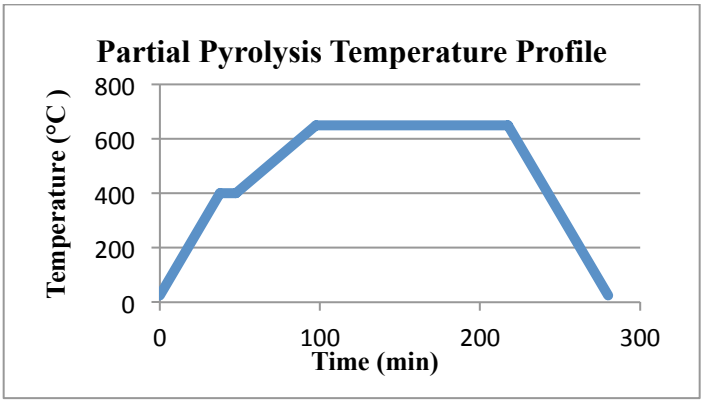

Figure IV-13 Partial pyrolysis temperature profile

The partially pyrolyzed sample was then taken out of the furnace and placed in an inert glovebox and transferred to a polypropylene Nalgene® vial and milled utilizing the procedure stated above.

The sample was placed in a 10 mm diameter high strength graphite die while in an inert glovebox and then hot pressed at 1550°C, using the thermal profile show in Figure IV-14

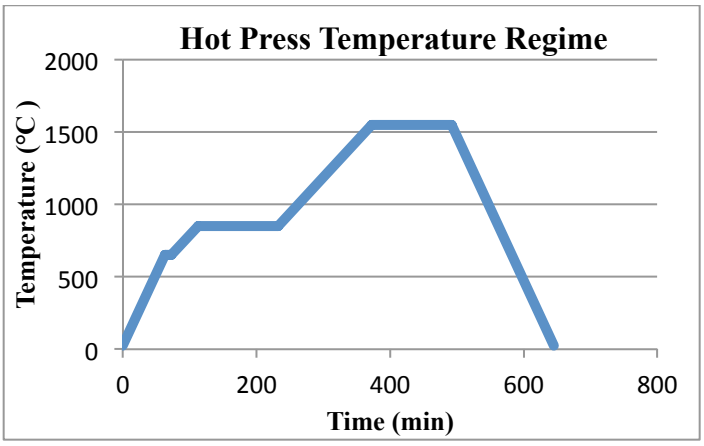

Figure IV-14 Hot press temperature profile

The pressure was slowly ramped up to 20 MPa alongside with temperature, such that it reached the full pressure of 20 MPa as it was fully pyrolyzed at 800°C. It was held at 20 MPa until the sintering temperature of 1550°C was complete and then was slowly released during cool down.

IV.5 Vacuum Processing PDC SiC

As an alternative to hot pressing, several approaches were investigated to make relatively dense samples. 1 wt % dicumyl peroxide (dp) was placed in SMP-10 polymer and dispersed by ultrasonicating for 2 hours under flowing argon. A glass petri dish was then lubricated with dow corning vacuum grease and the SMP-10/dp mixture was poured inside. This was done to reduce the tensile forces between the polymer during crosslinking and the glass dish. The glass petri dish containing the SMP-10/dp was placed in a vacuum desiccator to remove all of the bubbles

from the polymer. The sample was then placed into the tube furnace purged 6 times with argon and left under vacuum at ~-457 torr. The ramp rate was 1°C/min, held at 200°C for 1 hour and then heated again at 1°C/min to 400°C held for 2 hours, followed by cooling at 3°C/min to 25°C. The thermal profile is shown in Figure IV-15.

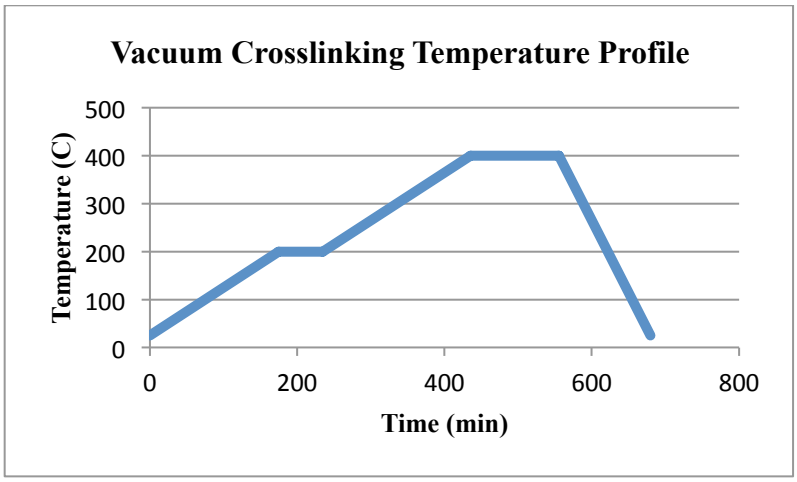

Figure IV-15 Vacuum Crosslinking Temperature Profile

They crosslinked polymer was pyrolyzed in a graphite lined crucible at 800°C for 2 hours under ~-457 torr of vacuum Figure IV-16.

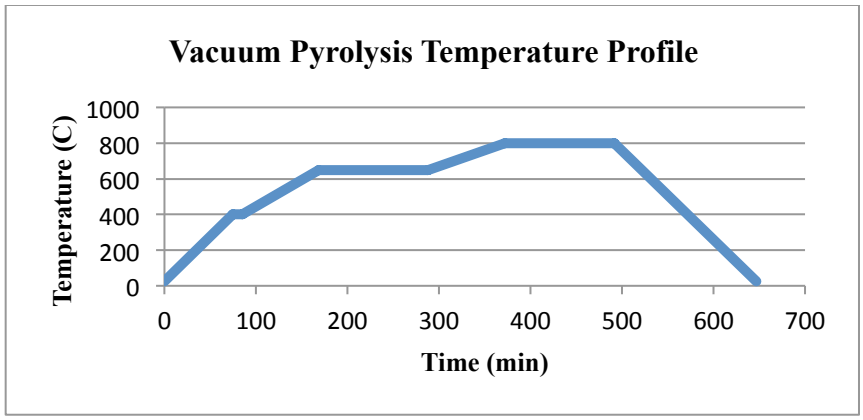

Figure IV-16 Vacuum Pyrolysis Temperature Profile

IV.6 Electron Beam Curing of SMP-10 Followed by one step pyrolysis

Another approach to make dense samples was electron beam curing, followed by pyrolysis. Electron beam curing of the SMP-10 polymer was accomplished using Boeing facilities. The polymer was placed in a tin dish, covered with an aluminum bar used to scatter the electron beam. The sample was then vacuum bagged using a typical composite style layup with vacuum ports to remove any off-gasing occurring during the electron beam curing. The samples were then dosed with a total of 15 Mrad at the Boeing Radiation Effects Laboratory. The crosslinked samples then underwent a one step pyrolysis profile as shown in

Figure IV-17. The samples were then heated to 1700 °C in a high temperature vacuum furnace to crystallize the amorphous SiC.

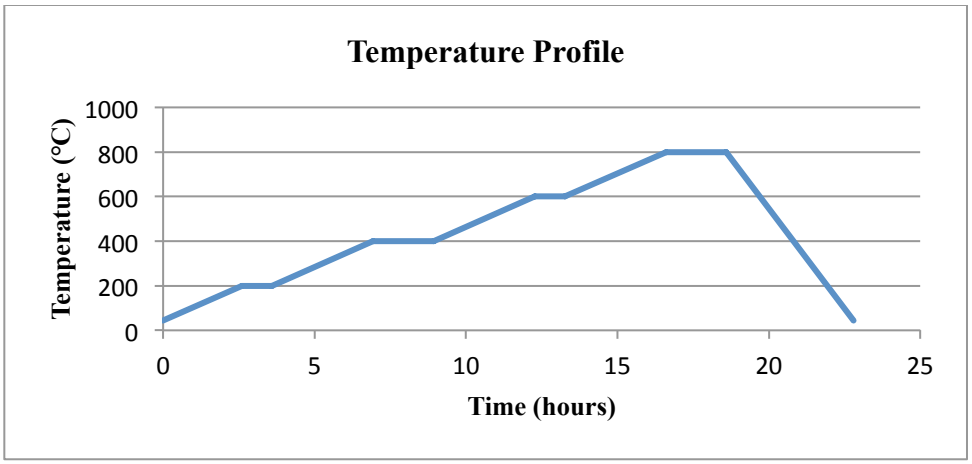

Figure IV-17 One step pyrolysis profile of post e-beam cured SMP-10

IV.7 SMP-10 as a Binder for Milled Crosslinked SMP-10 Powders

For this investigation 1 weight % decaborane was added via the hydroboration reaction to SMP-10 (B-SMP-10) to dope the sample with boron for use as a sintering aid. The sample was compared to SMP-10 without boron doping in the generation of dense samples. The samples were crosslinked at 400°C for two hours in gettered argon. These samples were subsequently placed in a zirconia vial while in an inert glove box and milled in the high energy ball mill. The B-SMP-10 and the SMP-10 milled samples were then separately mixed with liquid B-SMP-10 and liquid SMP-10 preceramic polymer respectively. As little as possible of the liquid precursor was added to each of the powders to bind the crosslinked powders into a hand formable shape. The B-SMP-10 sample was exposed to thermal heat treatment up to 1400°C and the SMP-10 to 1500 °C for two hours under gettered argon.

IV.8 Matrix studies for SiC

These studies were undertaken to explore the possibility of using the SMP-10 polycarbosilane as a matrix for SiC/SiC composites. The focus was on prevention of self-foaming of the SMP-10 during the crosslinking phase such that a decreased amount of pores formed during curing and final pyrolysis. Therefore, emphasis was placed on the rate of curing and additives to suppress foaming during crosslinking. The temperature profile that was used in this research is shown in Figure IV-18:

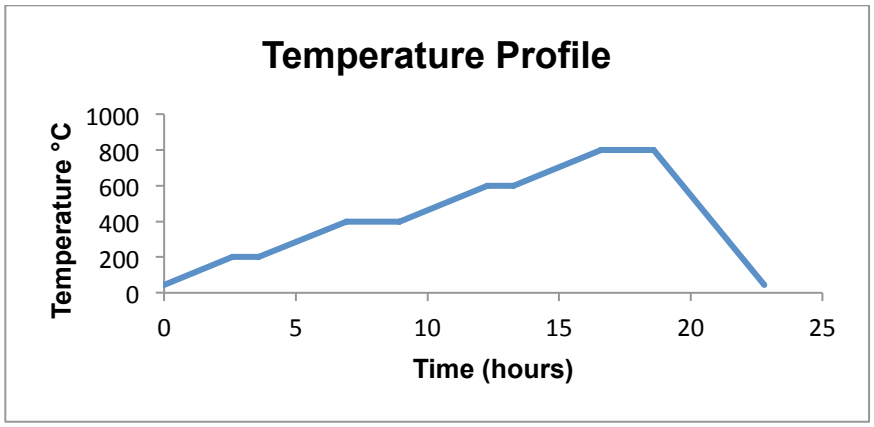

Figure IV-18 Heating profile for matrix studies

In these studies, 1wt% dicumyl peroxide (dp) was added to SMP-10 polymer and dispersed by ultrasonicating for 2 hours sealed in a vial sealed in the presence of argon. Decaborane was also incorporated into the SMP-10 to increase ceramic yield as well as to add boron its potential in increasing diffusivity of mass during crystallization temperatures. A glass petri dish was then lubricated with dow corning vacuum grease and the SMP-10/dp (both with and without

decaborane) mixture was poured inside the glass crucible. This was done to reduce the tensile forces between polymer during crosslinking and the glass dish.

IV.9 Processing Studies for Porous Monoliths

This section will discuss the various techniques that have been explored in this work in order to make porous SiC from SMP-10. These methods include: a sacrificial burnout method, foaming with azodicarbonamide and rapid crosslinking with a Pt catalyst. The major focus was on the use of azodicarbonamide as a foaming agent. This foaming method was studied in more depth than either the sacrificial burnout or the self-foaming of SMP-10 using a Pt catalyst. The most critical element of the foaming study is control over how the sample is cured as it transforms from the liquid polymeric state to the crosslinked solid state.

IV.9.1 Sacrificial Burnout Method

This method utilized Polymethylmethacrylate beads in the production of porous pellets. These pellets are prepared by first partially crosslinking SMP-10 by heating in gettered argon to 300°C for two hours. The partially crosslinked polymer was then pulverized and then mixed with PMMA beads. A 70/30 mix of SMP:10 to PMMA was used with a 50:50 mixture of 9 μm and 50 μm sized beads).

This sample was then placed into a ½ " die, insulated and placed in a warm press. The die was loaded at a rate of 10,000 lb. f/min to 0.5 lb. f and heated at a rate of 20 ˚F/min to 350 ˚F for 2 hours. After removal of the sample from the die it was pyrolyzed at 1450°C under gettered Argon for burnout of the PMMA beads and additionally to partially sinter the material. Ultimately this method was abandoned for this research due to PMMA being notorious for leaving behind excess carbon after burnout. This method was also inappropriate due to the increased exposure to air during the warm press treatment, which would potentially lead to contamination of the material.

IV.9.2 Foaming with Pt Catalyst

The method explores the use of exploiting the foaming capability of a catalyst in the rapid crosslinking of the SMP-10 precursor. The catalyst Platinum(0)-1,3-divinyl-1,1,3,3-tetramethyldisiloxane complex solution was used to initiate the crosslinking of the polymer chains. The sample was prepared by placing 1 wt % of the Pt complex solution in the SMP-10 polymer in an inert glovebox and sealed under the Nitrogen environment. The sealed vial was then removed and ultrasonicated for an hour at room temperature. This allowed the formation of a foamed gel, which was then placed in a tube furnace under gettered argon to 400°C to be fully crosslinked, followed by pyrolysis also in gettered argon at 900 °C.

IV.9.3 Foaming with Azodicarbonamide & Modifier

Foaming with azodicarbonamide (ADA), a nitrogen based compound, is a common method in generating a porous polymeric structure. Utilizing this method in preceramic polymers is a novel method for the development of porous SiC for nuclear applications. This method controllably introduces pores into the system that are unattainable through traditional ceramic processing routes. When heat-treated, the decomposition of the ADA leaves behind a porous structure. The ADA was added to SMP-10 in weight percentages of 0, 1, 3, and 5 wt. %. The mixtures were sealed in a N_2 glovebox and placed in an ultrasonic bath for 2 hours. As known from the literature, ADA thermally decomposes completely at 200°C releasing nitrogen gas.

The following processing parameters have been explored for the formation of foamed SiC (with and without decaborane and DVB) structures using azodicarbonamide.

- Determination of optimal holding temperature during foaming
- Determination of optimal ramp rate for foaming
- Dispersing of ADA
- ADA concentration in foamed SiBC
- Decaborane in foamed SiBC
- Divinylbenzene addition for samples containing excess carbon in foamed SiBC

IV.9.3.1 Dispersing of ADA

ADA dispersion was accomplished in two different methods first by adding 1 wt% ADA to the SMP-10 precursor and followed either by stirring or ultrasonication. Stirring took place within a N_2 pure glovebox for ~24 hours until the ADA appeared to be evenly dispersed. Dispersion through ultrasonication was carried out by adding 1 wt% ADA to the SMP-10 in a N_2 pure glovebox, sealed in a vial, and placed in an ultrasonic bath for 2 hours of ultrasonication.

The viscosity of the SMP-10 precursor while foaming was also considered to be a possible factor and was thus controlled. Samples with the addition of a 1:5 wt. ratio (Hexane:SMP-10) followed by the addition of 1 wt% ADA in SMP-10 were investigated. This was done to determine the role of viscosity in the foaming properites of SMP-10. The hexane was employed to further increase the separation of ADA particles in the SMP-10 through a non-oxide solvent. The remainder of the ADA foaming parameters below all use a 1:5 ratio of Hexane:SMP-10 and ultrasonication for two hours while sealed within a N_2 pure glovebox. This method resulted in the most uniform and reproducible foams.

IV.9.3.2 Foaming hold temperature

ADA decomposes at 200 °C releasing nitrogen in the process causing foaming. Therefore a 200°C hold temperature is typical for foaming with ADA is used. In this study, the hold time was

vixed at 2 hours to ensure complete ADA decomposition. The hold temperature was varied in order to explore its effect on the foam morphology. The ADA was dispersed as noted above by the addition of 1 wt% ADA in SMP-10, with a 1:5 Hexane:SMP-10 ratio, followed by ultrasonication for two hours. The sample was then placed in the furnace and the foaming temperature was varied (200, 250, 300°C) and held for two hours at a time under gettered argon. The holding temperature of 300°C for two hours was used for the remaining of the foaming studies followed by a pyrolysis temperature of 900 ° C. The hold temperature of 300°C was used because the foams had the most uniform and reproducible porosity.

IV.9.3.3 Heating Rate

The foaming rates are precursor dependent, with the majority of the literature utilizing solid precursors in the development of porous monoliths. Because this research utilizes a liquid precursor, a variety of heating rates were explored for the foaming process. A mixture of ultrasonicated SMP-10 with Hexane (1:5 Hexane:SMP-10 wt. ratio) and 1 wt. % ADA was heated at 1, 2, 3, 5, 10 , and 20 °C/min to 300 ˚C in gettered argon Figure IV-19. The ramp rate of 10°C/min was used for the remainder of the studies since it achieved the best results.

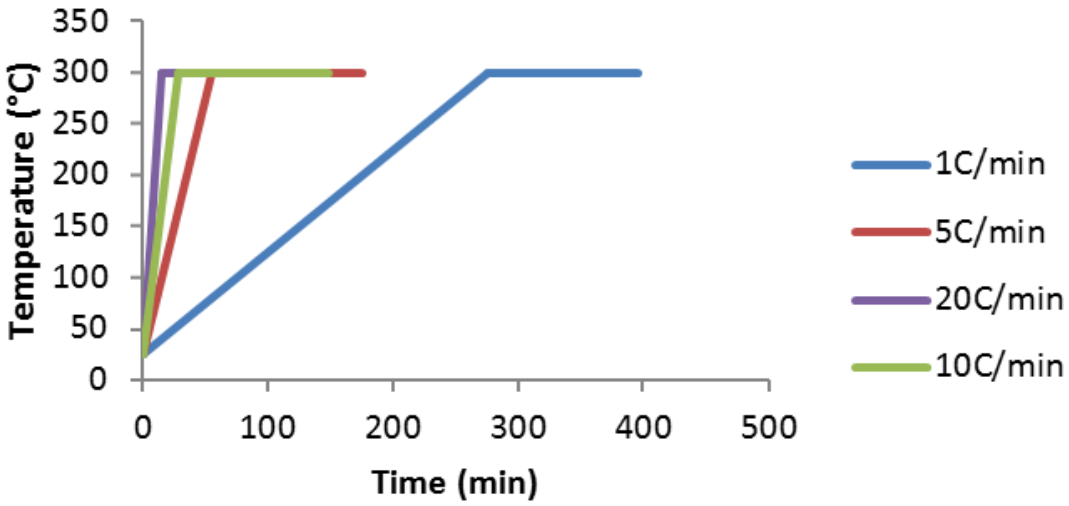

Figure IV-19 Heating rate for foaming

IV.9.3.4 Foaming Modification through a Hydroboration Reaction of SMP-10

The foaming modifier (decaborane) was found to be necessary because large pores were forming in the center of the monolith from coalescence of gas bubbles during curing in the absence of a foam modifier. The effect of a foaming modifier in its functionality with ADA and SMP-10 was therefore rigorously explored in this work. The samples here were designed to understand the effects of the foaming modifier (decaborane) on the pore formation of the foamed SiC. This was accomplished through the addition of various amounts of decaborane (0, 0.25, 0.5, 1.5 wt %) added to 1 wt % ADA in a 1:5, Hexane:SMP-10 wt. ratio mix. The samples were then ultrasonicated for 2 hours and transferred to a tube furnace with a ramp rate of 10 °C/min and a holding temperature of 300 °C and finally pyrolyzed to 900°C under gettered argon.

IV.9.3.5 ADA Concentration in Foamed SiC

In this study we investigated the effect of various concentrations of ADA (0.1, 0.3, 3 & 5 wt% ADA) on the direct foaming of SMP-10. This was accomplished through utilizing the above said parameters of adding 1 wt% decaborane foaming modifier and the various wt% of ADA to the 1:5, hexane:SMP-10 mix, followed by ultrasonication, then utilizing a heating rate of 10° C/min and holding temperature of 300 ° C in gettered argon for 2 hours. The samples were then pyrolyzed to 900°C in gettered argon. This investigation was conducted to explore the effect of ADA concentration on pore morphology and pore density.

IV.9.3.6 Effects of Excess Carbon on Foamed SiC

A final modification of the SMP-10 precursor was with excess carbon in the form of divinylbenzene. These samples were prepared to determine the effects of precursor stoichiometry (specifically C/Si) as well as the possibility of adding excess carbon in the form of graphene interfaces. The quantity of DVB used allowed for fine tuning of the free carbon introduced into the system. This additionally allowed the possibility to understand the effect of other additives on the pore morphology of the system. In this method excess carbon was introduced into the samples using divinylbenzene (DVB) a high carbon content polymer. Various concentrations of DVB (0, 5 & 10 wt %) were added to the mixture containing 1 wt% decaborane foaming modifier in a 1:5, hexane:SMP-10. The sample was then ultrasonicated for 2 hours followed by placement in a tube furnace utilizing a heating rate of 10° C/min and holding temperature of

300° C under gettered argon for 2 hours. The samples were then pyrolyzed to 900°C also in gettered argon.

IV.10 Experimental Techniques

A broad range of experimental techniques was used in this study and is summarized in this section.

IV.10.1 Thermal Gravimetric Analysis (TGA)

Thermo gravimetric analysis (TGA) (STA 409C, Netzsch, Selb, Germany) was used for determining the mass loss of the various polymeric systems (SMP-10 w/: DVB, dicumyl peroxide, decaborane). These experiments were significant in understanding the role of additives and mass loss and designing appropriate temperature regimes for pyrolysis of both the powders and porous monoliths. The gases used for these experiments were either argon or a 5 wt% hydrogen in argon mixture.

IV.10.2 X-Ray Diffraction

The crystallographic phases of polymer derived SiC ceramics was investigated using X-Ray Diffration (XRD (Bruker D8 FOCUS, Bruker AXS Inc., Madison, WI, USA). Specifically, the amorphous to crystalline transition in powders with increased pyrolysis temperatures was studied. In addition, the crystalline phases present after hot pressing the SiBC and SiC (with amorphous boron as a sintering additive) sintered pellets were considered. A Cu-Kα source with a 40kV accelerating voltage and 40mA was used for all samples. The phase identification a scanning range of 10 to 90˚ 2θ at a step size of 0.02˚ 2θ and a dwell time of 1 second/step was utilized.

IV.10.3 Raman Spectroscopy

Pyrolyzed powders heat treated at various temperatures under gettered argon were studied for their for Raman active modes. The Raman Spectroscopy was performed at the Nanotech User Facility (NTUF) located at the Universtiy of Washington using the Renishaw Raman Microscopy, Renishaw Inc., Hoffman Estates, Il, USA. A 512 nm laser excitation source was used to cover a scan range of 3200 – 100 cm^{-1}.

IV.10.4 Scanning Electron Microscopy (SEM)

An FEI Sirion SEM located in the NTUF was used to observe microstructural features of dense SiC with varing polytypes. The samples were cross-section with a low speed diamond saw and mounted in an epoxy resin. The samples were then ground with diamond bonded pads (70, 15 and 6 μm) and then polished on polishing pads with 3, 1, and 0.1 μm diamond suspensions for a final finish before observation using SEM.

IV.10.5 ^{29}Si MAS-NMR & ^{11}B MAS-NMR

XRD analysis did not effectively separate the SiC polytypes due to overlapping α SiC and β SiC peaks. Therefore, ^{29}Si MAS NMR which is an ideal method to effectively separate out the 3C and the 6H SiC phases was conducted using the 750 MHz Radiological NMR Bokan. ^{11}B MAS NMR was also conducted to develop an understanding of the boron phases in the samples.

^{29}Si and ^{11}B direct polarization experiments were conducted on a Varian/Agilent VNMRs system operating at 14.1 Tesla and utilizing a 4.0 mm HXY probe in DR mode tuned to 119.145084 and 192.429301 MHz respectively. A calibrated $\pi/3$ pulse of 3 us, a recycle delay of 3600 s, a spinning speed of 16 kHz, and a constant 20^{O}C temperature was used to collect between 4 and 8 transients within a spectral window of 200 kHz for the ^{29}Si spectra. A calibrated $\pi/20$ pulse of 0.7 us, a recycle delay of 5 s, a spinning speed of 16 kHz, and a constant 20^{O}C temperature were used to collect 8192 transients within a spectral window of 100 kHz for the ^{11}B spectra. Time domain free induction decays were apodized with 400 Hz of Lorentzian broadening after zero filling to 16384 points, with subsequent referencing to TMS at 0 ppm for ^{29}Si. The ^{11}B generated

time domain free induction decays were apodized with 50 or 200 Hz of Lorentzian broadening for samples exhibiting high levels of crystallinity or amorphous character, respectively. Spectra were referenced to solid boric acid at 16.6 ppm (referenced to 1 M boric acid at 19.6 ppm).

IV.10.6 Nano-SIMS

The Environmental Molecular Science Laboratory (EMSL) at the Pacific Northwest National Laboratory (PNNL) houses an ion microprobe that extends high spatial resolution secondary ion mass spectrometry (NanoSIMS) analysis to extremely small areas (down to 50 nm), while maintaining high sensitivity at high mass resolution. NanoSIMS was utilized because it has the ability to measure the Si, C, B and O ions in parallel, allowing image superimposition for determination of locations of the elements within the bulk sample. This was otherwise impossible as B is a lightweight, low energy element that cannot be observed using energy dispersive spectroscopy.

IV.10.7 Atomic Force Microscopy

Preliminary ion accelerator experiments were performed at EMSL to determine the effects of processing and microstructure on stability after exposure. The swelling of the material due to point defect accumulation was explored using the Asylum MFP-3D AFM at EMSL. Compositions of the exact same stoichiometries (1 wt% excess C and 1 wt% B in SiC) but using

two different methods of boron incorporation (added molecularly to the precursor vs. added to the powder) were compared in their ability to mitigate radiation damage from ion bombardment.

IV.10.8 Experimental Studies on Radiation Effects

In order to effectively design the ion implantation experiments using ion accelerator facilities at the EMSL at PNNL, the stopping range of ions in matter (SRIM) as well as transport of ions in matter (TRIM) simulations were necessary. The SRIM & TRIM simulations were utilized to determine the depth of ion penetration as well as the amount of recoils that could be experienced by SiC given various parameters. The experimental parameters were based on varying the type of ion, energy and angle assuming fully dense SiC. The limits of the accelerator and length of the experiment were also taken into consideration with the TRIM simulations. Since, time is a factor that must be considered gold ions were used for implantation due to their success in generating a good beam as well as their ability to induce more damage in a shorter time frame. 5MeV was the energy used in these simulations for the same logic as using gold ions, to induce more damage at greater depths in a shorter period of time.

Chapter V Results & Discussion

V.1 Effect of Crosslinking Temperature on Ceramic Yield

The SMP-10 polymer was crosslinked to 350°C and 400°C, these crosslinked polymers were converted to an amorphous ceramic by heating in an argon environment. The mass loss was monitored continuously in a thermogravimetric analyzer and the results of this study are shown in Figure V-1.

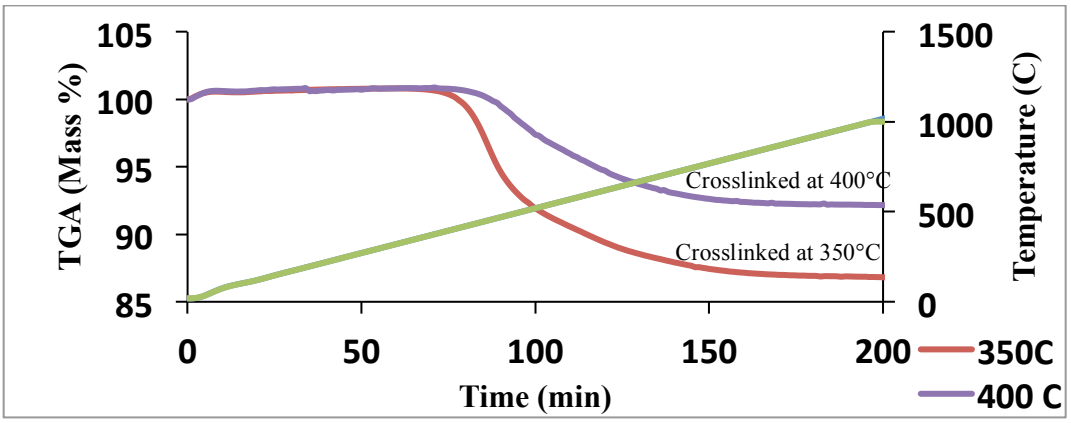

Figure V-1 Effect of crosslinking temperature on the ceramic yield during pyrolysis

Figure V-1 clearly shows that the onset of mass loss starts earlier and there is a larger mass loss with lower crosslinking temperature. The final ceramic yield is 86% and 92% for the 350 °C and the 400°C crosslinked samples respectively. For the sample with the higher crosslinking temperature, the mass loss is complete at about 800°C. This was the justification to use 800°C as the final pyrolysis temperature throughout additional processing of the SMP-10 precursor for the entirety of this work. The pyrolysis at this temperature was necessary in order to assure that all oligomers and monomers that did not crosslink with the large polymeric polycarbosilane chains

and were released during pyrolysis. The higher crosslinking temperature results in a higher degree of crosslinking and is important in getting the maximum ceramic yield.

The fully pyrolyzed SMP-10 (now amorphous SiC) as observed using XRD is shown to crystallize to β-SiC (3C) upon further heat treatment of the amorphous SiC materials. The XRD pattern reveals that following pyrolysis to 1000°C the sample is an amorphous SiC. Whereas upon heat treatment to 1600°C in gettered argon for 2 hours the ceramic appears as crystalline SiC as shown in Figure V-2.

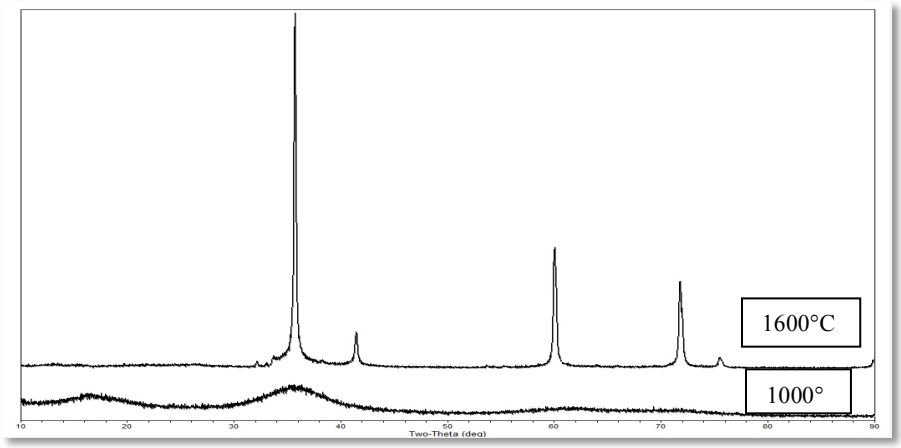

Figure V-2 XRD of PDC SiC amorphous to crystalline transition

The 1000°C heat-treated sample is amorphous typical phase with evidence of initial crystallization. The 1600°C samples is clearly crystalline β-SiC with no other phases present at this stage. This is consistent with literature in which this is a typical temperature regime for the formation of the 3C SiC polytype. These results are also consistent with the data sheets provided by Starfire Polymers for the SMP-10 precursor.

V.2 Stability of Boron Doped SMP-10

The SMP-10 precursors were doped with decaborane in order to explore how adding a sintering aid directly to the precursor could influence densification and phase stability. This was accomplished through a hydroboration reaction of SMP-10 with decaborane. It was observed that a reaction with air occurred after milling the crosslinked powders making the boron-doped samples pyrophoric from the milling process in the presence of oxygen. This was evident when opening the milling vial to air and the sample immediately releasing heat due to a hydroboration oxidation reaction. After the boron doped sample was cooled down it was placed in the furnace for pyrolysis to 1300°C and 1500°C under gettered argon for two hours. It is evident from the XRD graphs (Figure V-3 & Figure V-4) that these decaborane modified samples introduced substantial amount of oxygen due to exposure to air after the milling process. These boron-doped samples were compared with SMP-10 alone processed under the same conditions. From Figure V-3 & Figure V-4, it is clear that SMP-10 without decaborane had significantly lower amounts of oxygen.

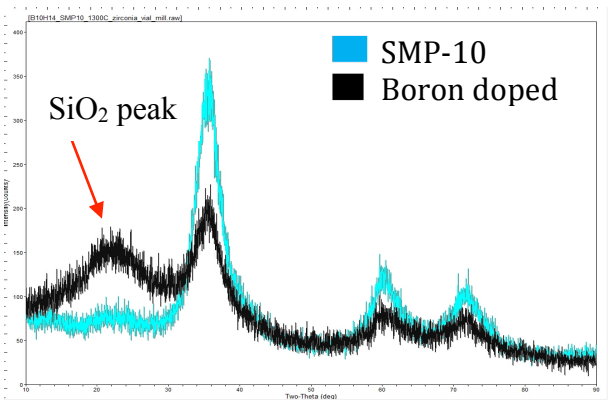

Figure V-3 SMP-10 vs. B-SMP-10, 1300°C

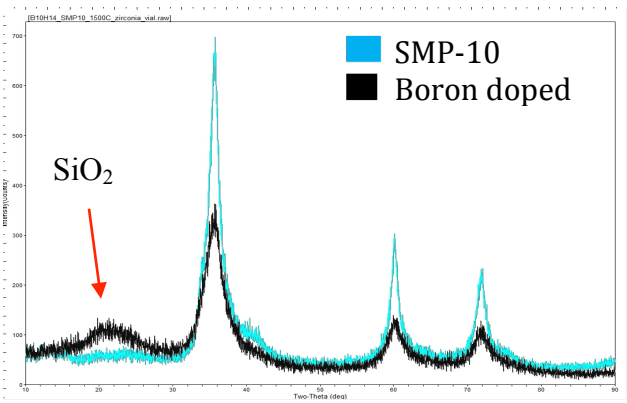

Figure V-4 SMP-10 vs. B-SMP-10, 1500°C

This oxidation evidence is indicated in the XRD graphs (Figure V-3 & Figure V-4) due to the presence of a SiO_2 peak in the boron doped sample when compared to the SMP-10 only sample exposed to the same conditions. It can also be noted that the boron doped SMP-10 remains significantly more amorphous than un-doped SMP-10. Hydroboration oxidation reactions are important in organic chemistry because boron allows the addition to the least substituted bond (anti-Markovnikov rule), as opposed to introducing oxygen to the most substituted bond (Markovnikov rule). It is likely that ball milling the sample in a zirconia vial in air allowed enough thermal energy for oxidation of the boron to occur.

It is important to note that the observed SiO_2 peak is eliminated when handling the milled powders in an inert glove box after milling rather than exposing to air. This is evident from the figures shown below for the boron doped SMP-10 sample and also the SMP-10 sample alone (Figure V-5 and Figure V-6)

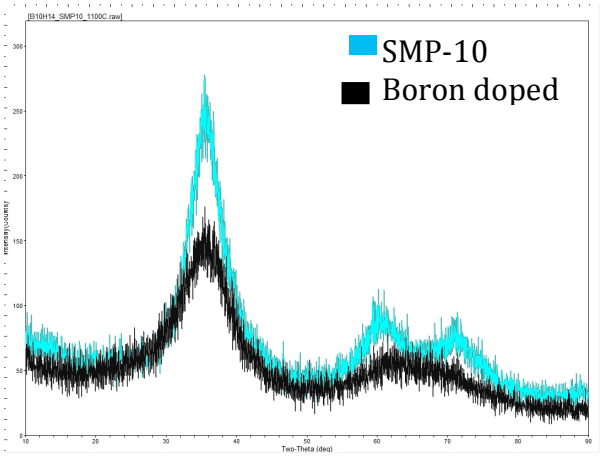

Figure V-5 SMP-10 vs. B-SMP-10, 1100°C

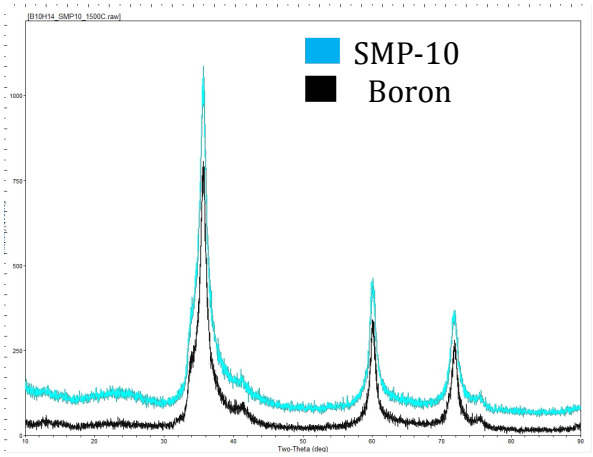

Figure V-6 SMP-10 vs. B-SMP-10, 1500°C

Additionally, it can be noted in (Figure V-5 and Figure V-6) at lower temperatures the boron doped sample impedes crystallization as opposed to SMP-10 alone. This is likely due to boron providing a barrier to nucleation of the crystals similar to the observation of SiBCN.[96]

V.3 Evolution of the Free Carbon Phase

This part of the study is to determine the evolution of the free carbon phase with various temperatures through Raman Spectroscopy. Raman spectra from samples with 60:40 SMP-10:DVB mixtures heat treated at 800°C, 1100°C and 1500°C were obtained. As shown in Figure V-7 the d and g (disordered and graphite respectively) peaks become more resolved with increasing temperature. This is important when understanding the evolution of an ordered carbon phase within the ceramic network.

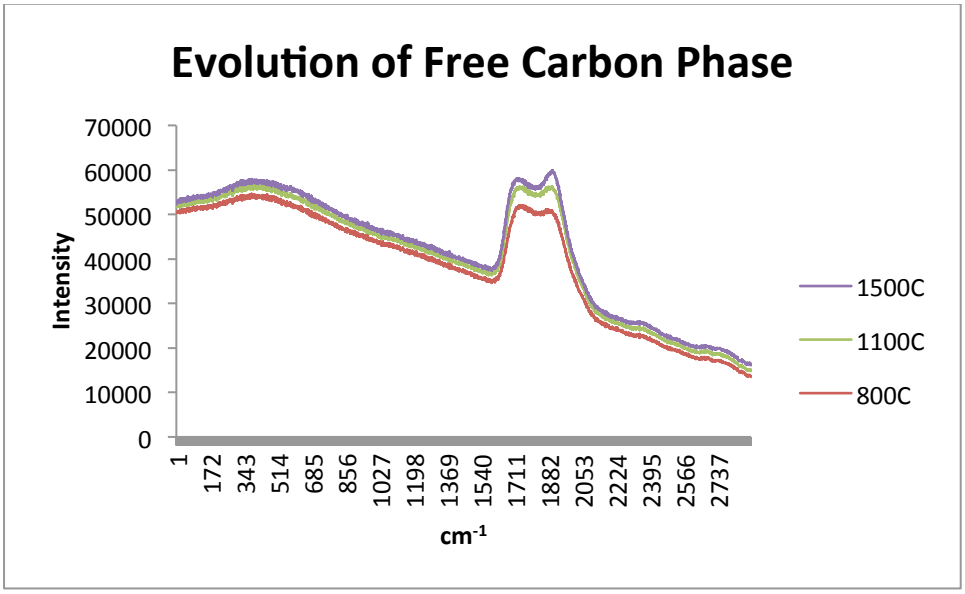

Figure V-7 Evolution of free carbon phase with increasing temperatures

At 800° C the peaks are very broad and essentially un-resolvable indicating a completely disordered graphite phase. Further increasing the temperatures allows for a more ordered graphite peak as can be observed from the sample heated to 1500 °C. These results indicate that increasing the heat treatment temperature allows for ordering of the carbon phase within the system. It should be noted that the excess carbon content in these samples was relatively high and it will be important to study the effects of temperature with lower weight percent of DVB added to SMP-10.

V.4 Effect of additives and mass loss

In this work various additives were used to manipulate the SMP-10 precursor (e.g. addition of sintering aids, rapid crosslinking, incorporation of carbon). Therefore, it was important to understand their effects on the ceramic yield following pyrolysis. Through TGA analysis the full process from crosslinking to final pyrolysis was analyzed. It was important to have a very slow crosslinking rate to avoid any foaming of the material during curing of the preceramic polymer in the TGA. Through this one step pyrolysis profile process, it can be observed that the SMP-10 alone (without any additives) has the lowest ceramic yield at only 68% whereas inclusion of dicumyl peroxide for crosslinking assistance increases the ceramic yield to 81% and decaborane increased the yield to 78% as shown in Figure V-8.

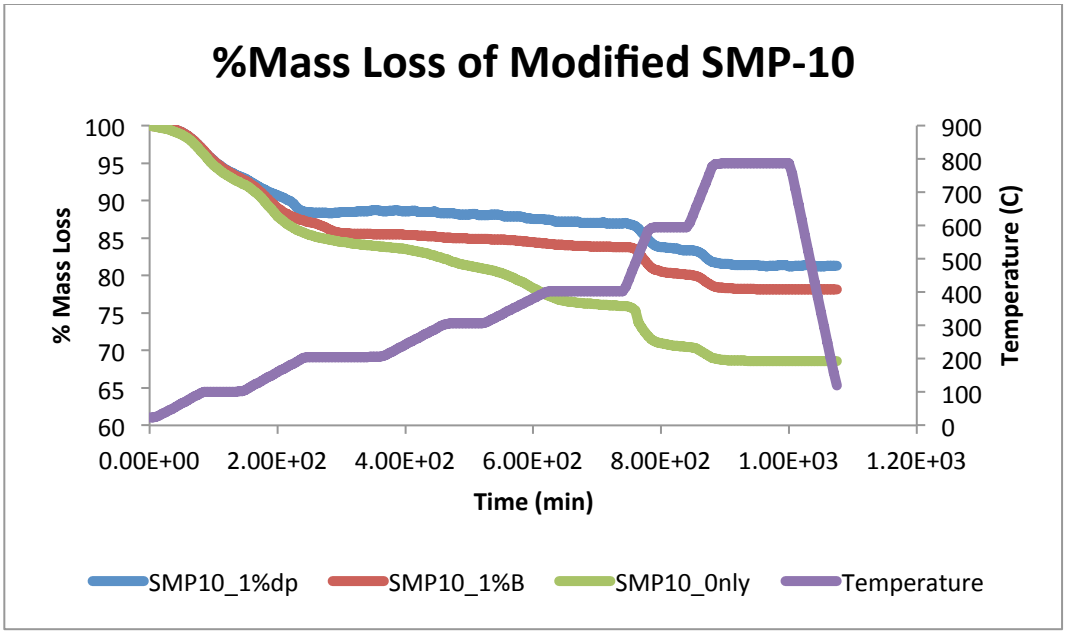

Figure V-8 Effect of additives on mass loss during pyrolysis of SMP-10

V.5 Engineering Porosity in Polymer Derived SiC Ceramics

V.5.1 Foaming with Pt Catalyst

This method explored the use of a catalyst for rapid crosslinking of the SMP-10 precursor. This was explored due to the ability to foam the SMP-10 at room temperature and the possibility to manipulate the resultant structure during foaming. The Platinum(0)-1,3-divinyl-1,1,3,3-tetramethyldisiloxane complex solution foamed the SMP-10 such that a gel was formed. This allowed the ability to develop a complex shape prior to final curing of at 400°C. This processing route has not been further characterized in this study due to lack of controllable parameters.

V.5.2 Foaming with Azodicarbonamide

The decomposition of ADA occurs during leading to release of gases and thus leaving behind a porous structure within its medium. The successful processing of foamed ceramics is a delicate balance between gas release due to decomposition of ADA and the increase in viscosity of the polymer due to crosslinking. Figure V-9 schematically shows the crosslinks increasing density within the polymer that leads to curing of the thermoset SMP-10 polymeric system.

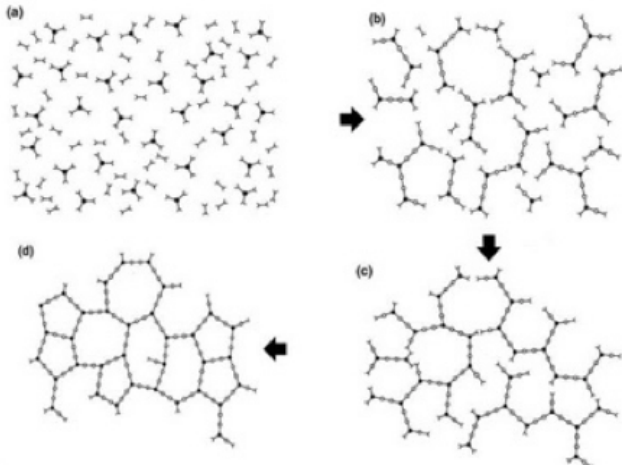

Figure V-9 Increasing crosslinks within the chains

As shown below in the thermogravimetric analysis (TGA) (Figure V-10) the ADA releases gases at 200°C.

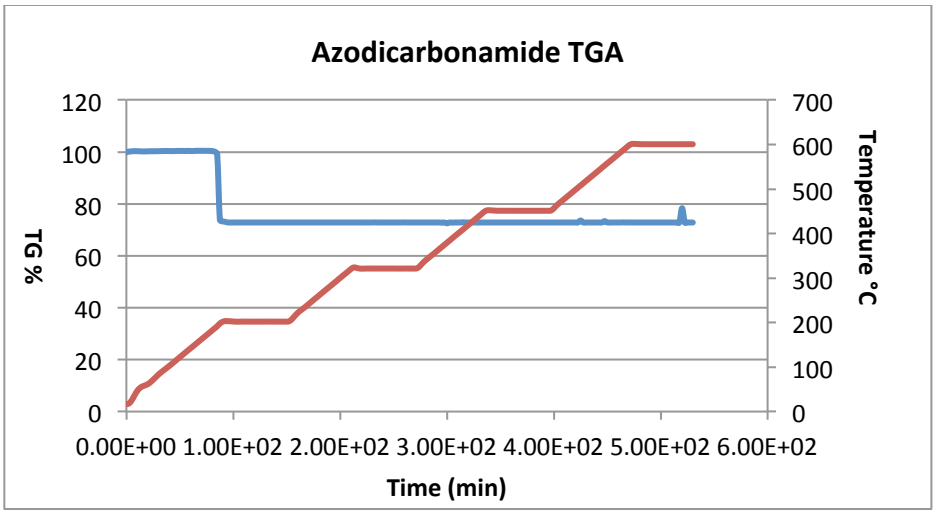

Figure V-10 Thermogravimetric analysis of ADA

After the ADA is evenly dispersed in the SMP-10 through ultrasonication, the sample is then placed in the furnace at a ramp rate of 10°C/min to 250°C in Ar and held for 2 hours releasing the gases from the ADA and crosslinking the polymer to form a porous structure.

The samples are then ramped at the same rate to 400°C to fully crosslink the material. A uniform distribution of pores was obtained as opposed to the graded porosity that was produced initially with the sample in which ADA was dispersed by stirring instead of ultrasonication. The samples were then pyrolyzed to 800 and 1100°C in Ar Figure V-11 and Figure V-12 show the pore structure and the open porosity.

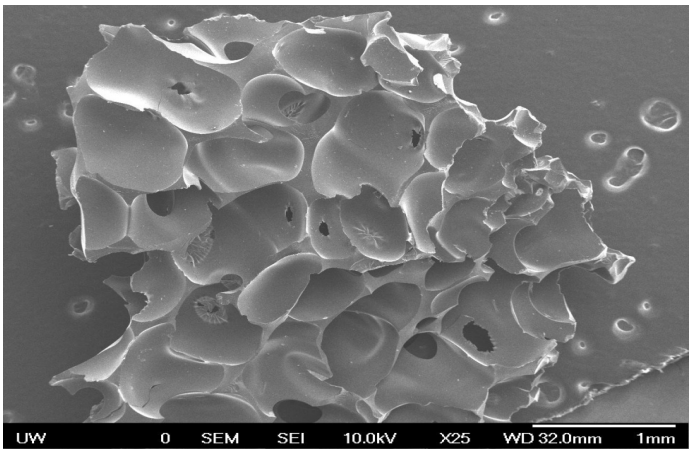

Figure V-11 ADA Foaming 1100°C

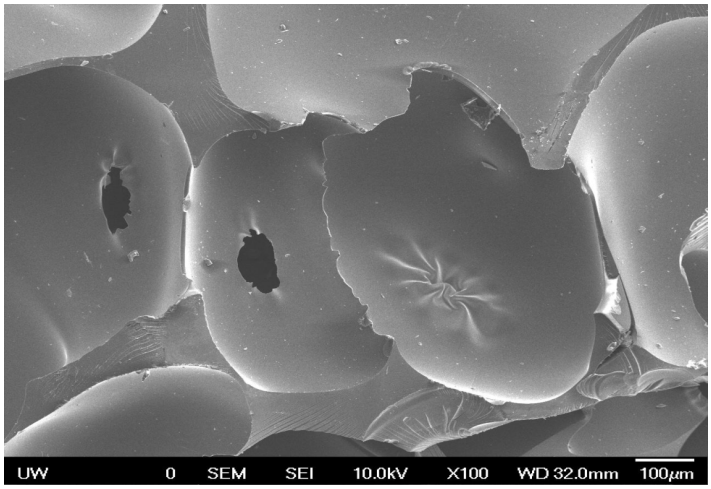

Figure V-12 SEM showing open porosity 1100°C

The density of the samples was measured using the Archimedes method. The samples with higher ADA content floated in water and isopropyl alcohol was carefully used in order to obtain values for the suspended mass of the samples. Table V-1 shows the density as a function of wt% of ADA dispersed in the SMP-10

Table V-1 Effect of ADA on the bulk density of the SiC foam

Wt% ADA	Density (% TD)
0	40
1	34
3	25.4
5	22.4

It appears that by increasing the concentration of ADA in the SMP-10 leads to a decrease in density of the porous monolith.

V.5.2.1 Dispersing of ADA & Functionality of the Foaming Modifier

The approach of dispersing the ADA through mixing was initially pursued in this work, however a graded porous structure was obtained due to uneven dispersion of the ADA. Recalling from the experimental section, various parameters were explored in order to obtain ideal foaming properties. One key requirement was obtaining an ideal dispersion as seen in Figure V-13

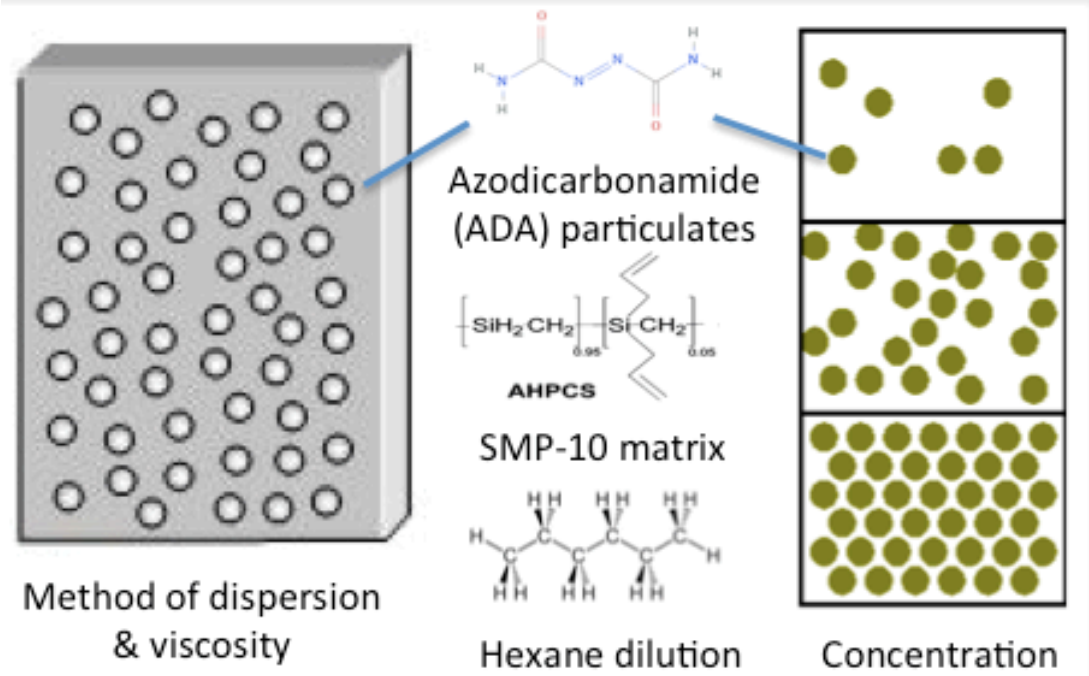

Figure V-13 Dispersion of foaming agent in polymeric precursor

In lieu of stirring, ultrasonication was investigated as an alternative method to evenly disperse the ADA with a goal of making uniform porous structures. In utilizing this method of dispersal, a uniform distribution of pores was obtained as well as the processing time of dispersing the ADA was significantly decreased (2 hours as opposed to the 24 hours needed for stirring the ADA into the liquid polymer). The method of stirring was abandoned and ultrasonication was used for the remainder of the study. However, it can be noted that if the sample is left without agitation for a period of time, than the ADA will slowly begin to settle and thus can leave behind a gradient porous structure.

In all samples in which the ADA was dispersed by ultrasonication a uniform distribution of pores was obtained. However there was the new issue of the presence of deleterious gaps (or large pores) within the foamed structure. It was therefore important to determine if a foaming/crosslinking modifier existed that had the ability to alter the curing mechanism during the release of gases during ADA decomposition. A variety of potential modifiers shown in Figure V-14 were investigated.

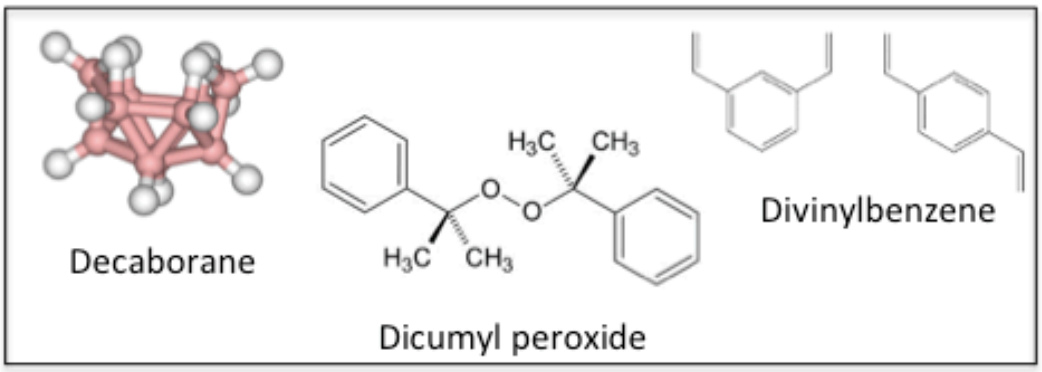

Figure V-14 Additives that alter the crosslinking and thus function as a foaming modifier

Decaborane was employed as a foaming modifier in order to prevent structures with deleterious gaps that compromise the integrity of the sample as shown in Figure V-15 and Figure V-16.

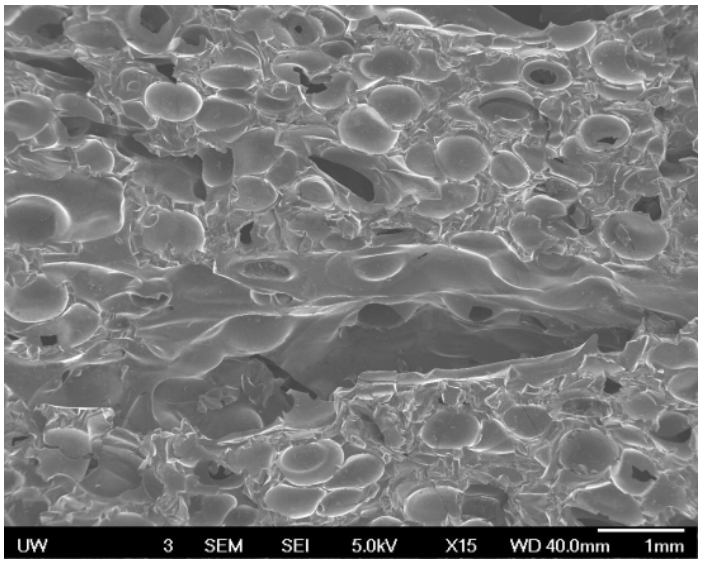

Figure V-15 SEM, 1wt% ADA in SMP-10 showing large pores within the foam

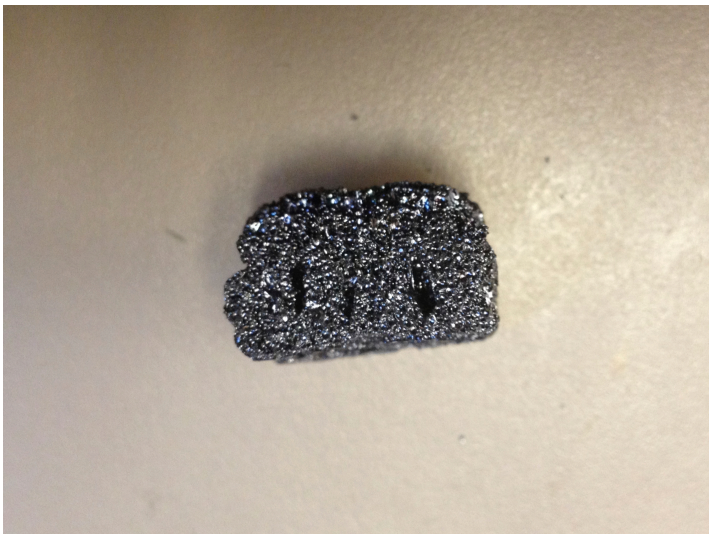

Figure V-16 Foaming with ADA alone and the presence of gaps within

Decaborane employs a hydroboration reaction that acts according to anti-Markovnikovs rules, which allows the introduction of boron to the least substituted side of the C=C. The two figures, Figure V-17 and Figure V-18 show the foams that are formed when utilizing decaborane by itself

(without the presence of ADA as a foaming agent). It can be noted that it clearly shows its own distinct form of foaming from the hydroboration reaction of SMP-10 with decaborane in Figure V-17 and Figure V-18.

Figure V-17 1 wt% decaborane in SMP-10

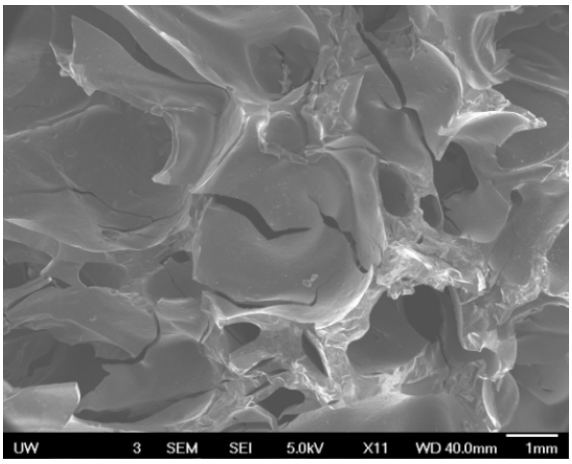

Figure V-18 1 wt % decaborane in SMP-10 (SEM).

Without azodicarbonamide, decaborane is not an ideal foaming agent and thus decaborane is only being considered as a modifier rather than the foaming agent in this study. As shown in

Figure V-19 and Figure V-20 the addition of decaborane (1 wt%) with ADA (1wt%) yields a uniform distribution of pores without the presence of deleterious gaps and uneven porosity.

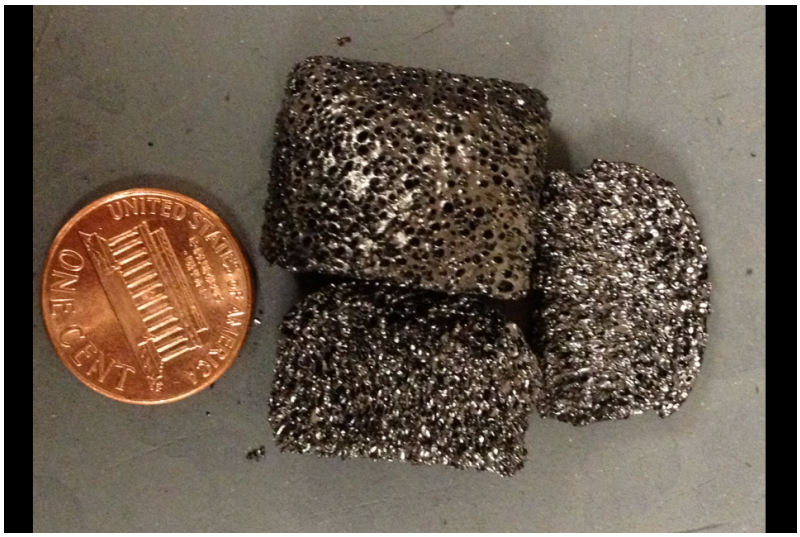

Figure V-19 SMP-10 & 1wt% ADA & 1 wt% decaborane, pyrolyzed (900°C)

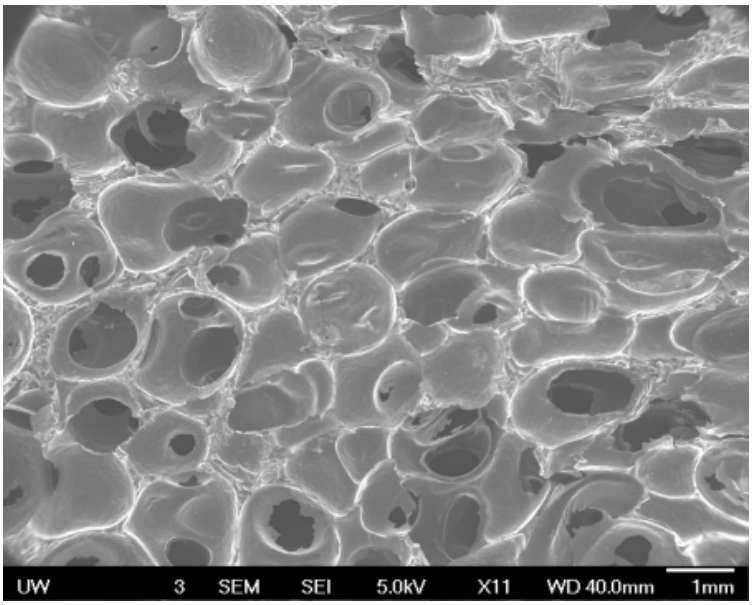

Figure V-20 SMP-10 & 1 wt% ADA + 1 wt% decaborane, pyrolyzed (900°C)

The presence of decaborane allows for more uniform curing when heated and thus removes the deleterious gaps that form in samples without decaborane. In samples without decaborane there is uneven curing of the sample where the outside is curing faster than the inside. This is leading to the coalescence of bubbles in the center of the monolith. Effectively there could be a variety of potential crosslinking/foaming modifiers, which allow more uniform curing of the polymer. Now that processing protocols have been determined for this system, to generate uniform porosity, control over pore morphology is further explored by varying selected processing parameters.

V.5.2.2 Foaming hold temperature

The TGA data of ADA shown in the literature as well as the TGA data generated of ADA in our lab, shown in Figure V-1 indicates that ADA decomposes at 200 °C releasing nitrogen gas. It is therefore common in the literature for the temperature of 200°C to be used as the holding temperature for the foaming of polymer derived ceramics with ADA. We therefore utilized 200°C as a start for foaming SMP-10 and holding for two hours to allow all off gasing to take place. However, at this temperature the sample tended to trap gases causing explosions in the monolith leaving behind many pieces. A series of experiments at different holding temperatures were conducted and it was found that holding at 300°C resulted in the most ideal foamed samples. This was noted as there was a monolithic form and there was absence of an uneven distribution of pores with this holding temperature.

V.5.2.3 Effect of Heating Rate

A slow heating rate was initially investigated for the production of foamed SiC. However, a slow heating rate was not viable due to many instances in which the sample burst into many pieces following crosslinking. The likely cause of this was from gases being trapped within the crosslinked sample leading to catastrophic failure. It was also evident that there was settling of the ADA particles with time, which was also problematic to obtain uniformity within the monolith structure. The ramp rate was varied using 1,2,3,5,10,20 °C/min and also putting in the sample in a preheated furnace at forming temperature. It can be noted that at very high ramp rates (20°C/min to directly inserting the sample at temperature) the sample outgased aggressively and left behind a directional structure with most of the prosity near the top, intermingled with regular open porosity as shown in Figure V-21 and Figure V-22 below

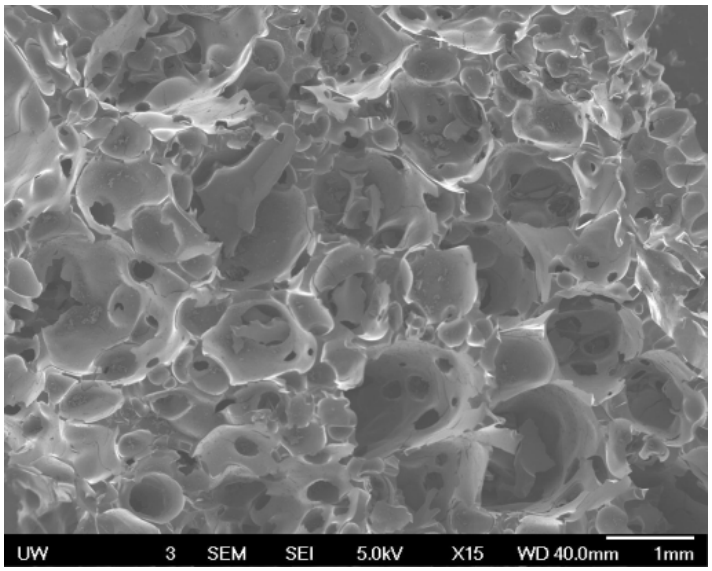

Figure V-21 SEM of foamed SMP-10 at 20°C/min

Figure V-22 Monolith of foamed SMP-10 20°C/min (view facing down from the top)

Samples foamed at all the heating rates and it was determined that a rate of 10°C/min was optimal for foaming SMP-10 with ADA. The optimal foaming temperature was 300°C with a hold temperature of 2 hours. These samples had the most uniform porosity as shown in Figure V-23 and Figure V-24.

Figure V-23 Foamed SiC Monolith

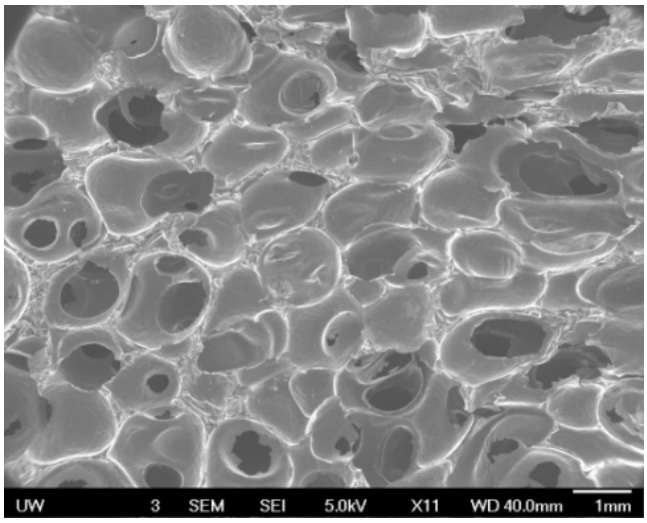

Figure V-24 Higher magnification of foamed sample

This was graded by determining what rate gave the most uniform distribution of pores within the monolithic structure.

V.5.2.4 Effect of ADA Concentration on Foam Microstructure

For this part of the study the concentration of ADA was varied (0.1, 0.3, 3 & 5 wt% ADA) and its effect on the foamed microstructure was explored. A system of SMP-10 with 1 wt% decaborane foaming modifier was used. All samples were heat treated at 10°C/min to 300°C. The following SEM images; Figure V-25, Figure V-26, Figure V-27 and Figure V-28 show the changes in pore morphology and pore density as a function of ADA concentration.

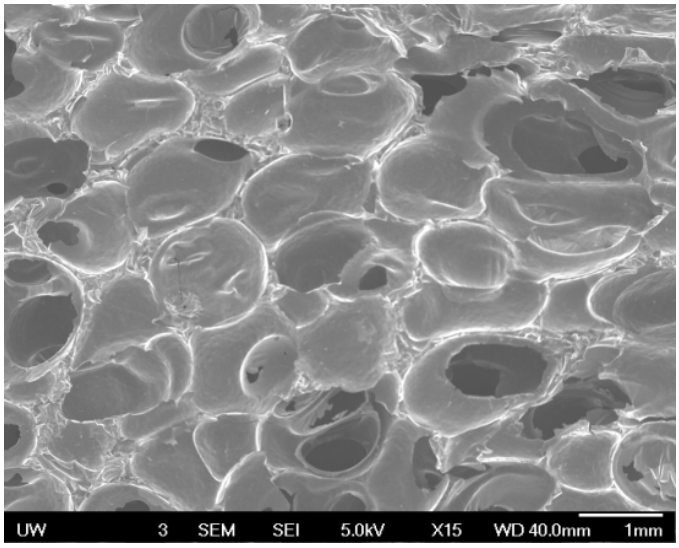

Figure V-25 Foamed ceramic microstructure from SMP-10 at 10°C/min to 300°C with 0.1 wt% ADA, 1 wt% B

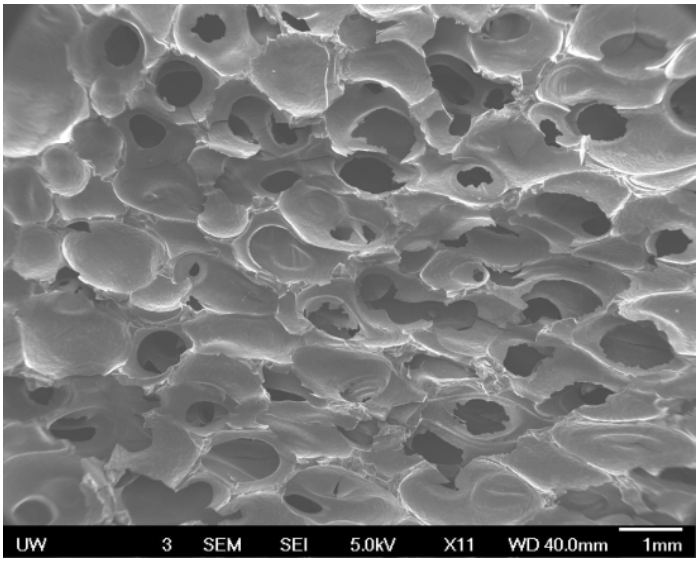

Figure V-26 Foamed ceramic microstructure from SMP-10 at 10°C/min to 300°C with 0.3 wt% ADA, 1 wt% decaborane

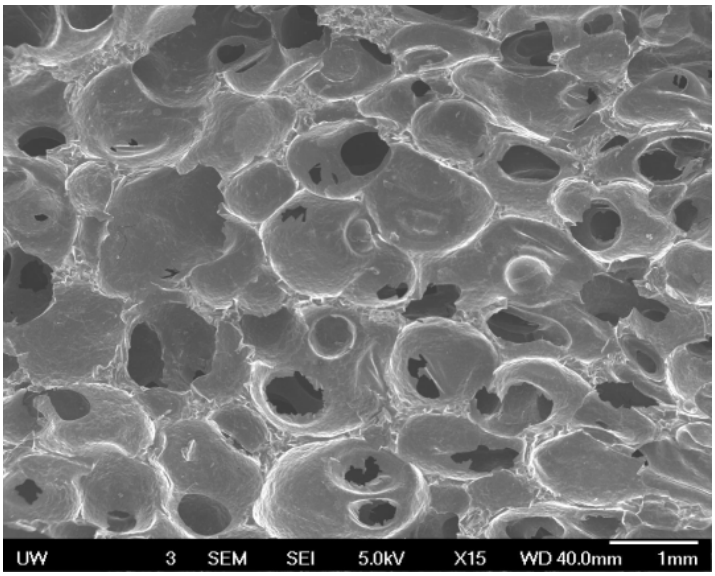

Figure V-27 Foamed ceramic microstructure from SMP-10 at 10°C/min to 300°C with 3wt% ADA, 1 wt% decaborane

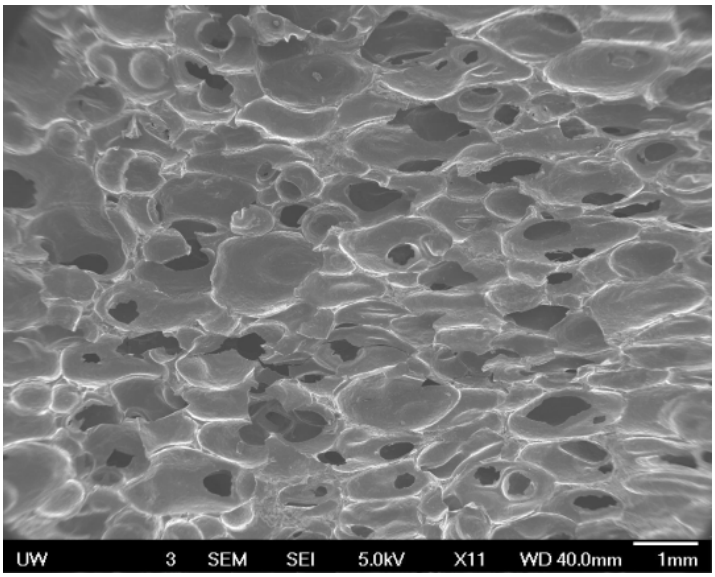

Figure V-28 Foamed ceramic microstructure from SMP-10 at 10°C/min to 300°C with 5 wt% ADA, 1 wt% decaborane

It can be noted that as the ADA concentration increases there is a decrease in pore size and pore morphology transitions from spherical to ellipsoidal. The number density of pores also increases with increasing ADA content. *Table V-2* quantifies the volume fraction of porosity and shows it increases with increasing concentration of ADA leads to an increase in total porosity of the sample.

Table V-2 Concentration of ADA and Total Porosity

Wt% ADA	% Porosity
0	60
1	66
3	74.6
5	77.6

V.5.2.5 Effect of Foaming Modifier Concentrations on SMP-10 Foam Structure

These samples were designed to understand the effect of the foaming modifier (decaborane concentration) on the pore morphology and porosity of the foamed SiC. Figure V-29, Figure V-30, Figure V-31 and Figure V-32 show the effect of various amounts of decaborane (0, 0.25, 0.5, 1.5 wt % decaborane) added to samples with 1 wt % ADA in SMP-10 foamed at 300°C (heating rate of 10°C/min) by curing and pyrolzed at 900°C.

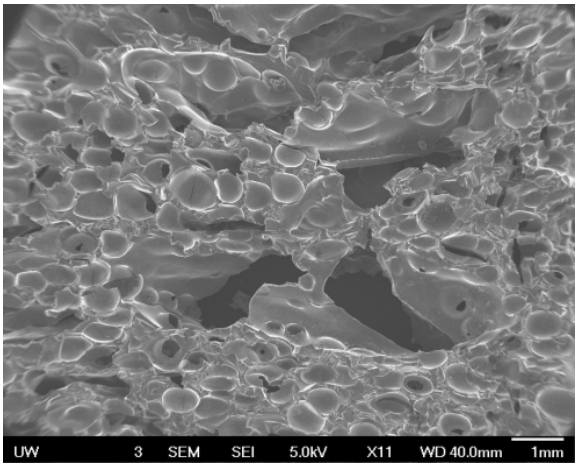

Figure V-29 0 Foamed ceramic microstructure from SMP-10 with 1 wt% ADA and 0 wt% decaborane foamed at 300 °C wt% with a heating rate of 10 °C/min

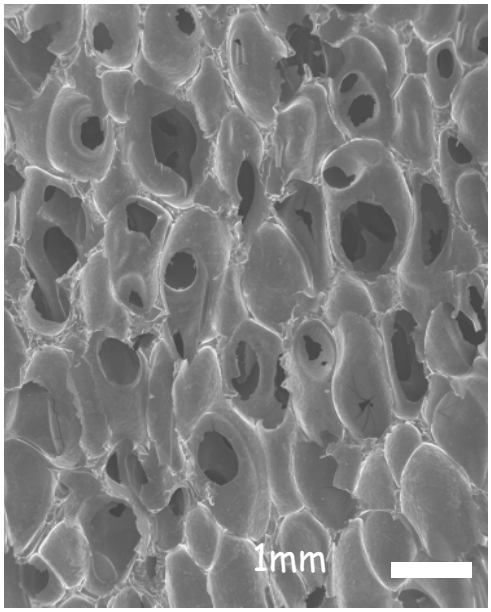

Figure V-30 Foamed ceramic microstructure from SMP-10 with 1 wt% ADA and 0.25 wt% decaborane foamed at 300 °C wt% with a heating rate of 10 °C/min

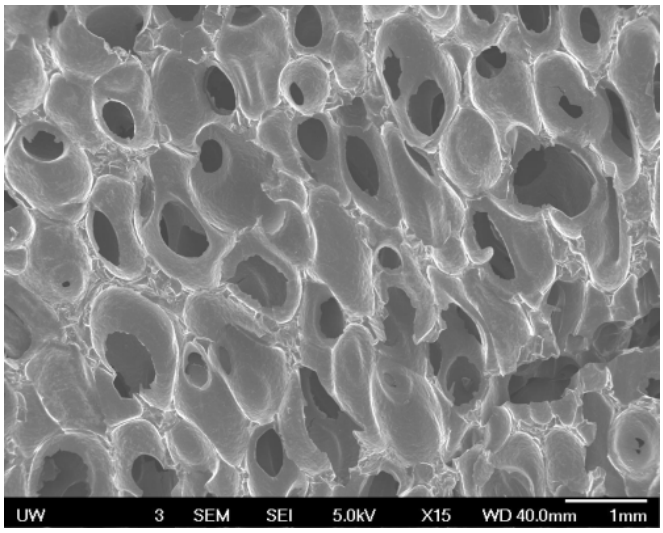

Figure V-31 Foamed ceramic microstructure from SMP-10 with 1 wt% ADA and 0.5 wt% decaborane foamed at 300 °C wt% with a heating rate of 10 °C/min

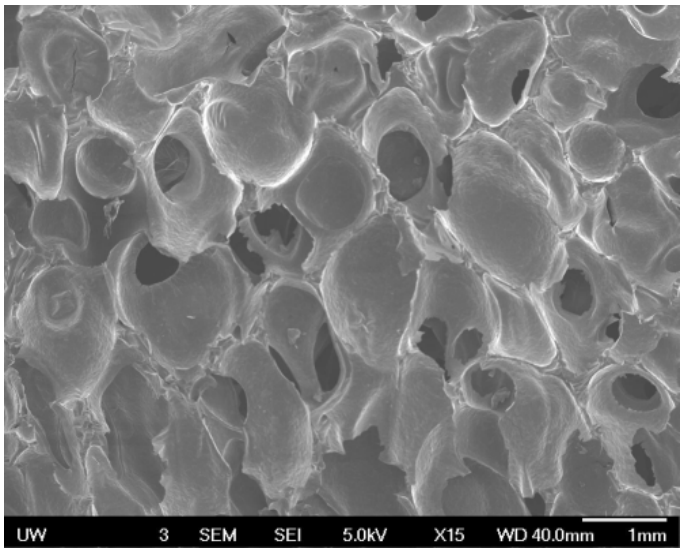

Figure V-32 Foamed ceramic microstructure from SMP-10 with 1 wt% ADA and 1.5 wt% decaborane foamed at 300 °C wt% with a heating rate of 10 °C/min

From the above images it can be clearly seen that the increase in foaming modifier leads to an increase in pore size and also a change in pore morphology. This investigation has provided a

detailed observation of the effect of the composition and processing parameters on pore size, shape and total porosity.

V.5.2.6 Effects of Excess Carbon on Foamed SiC Microstructures

Since DVB can also function as a foaming modifier an investigation was conducted to investigate the effect of DVB on porous microstructures. Various concentrations of DVB (0, 5 & 10 wt %) were studied and the resultant microstructures are shown in Figure V-33, Figure V-34 and Figure V-35.

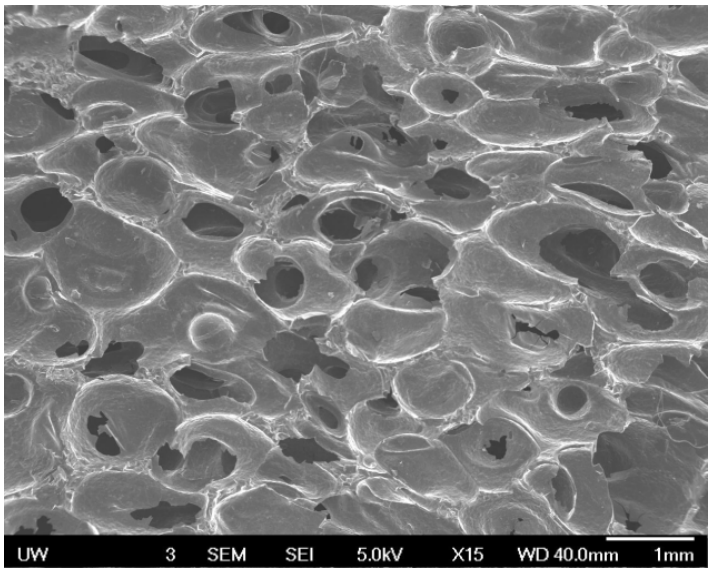

Figure V-33 Foamed ceramic microstructures from SMP-10 with 0 wt% ADA, 1 wt% decaborane and 0 wt% DVB (foamed at at 300 °C wt% with a heating rate of 10 °C/min)

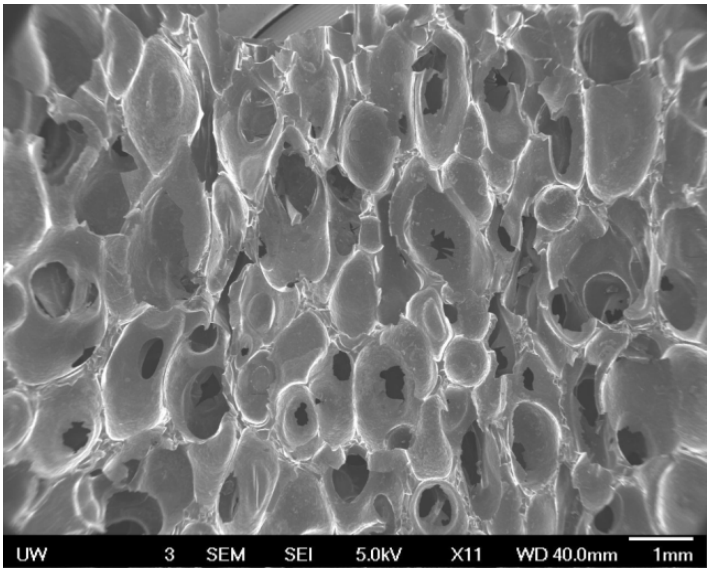

Figure V-34 Foamed ceramic microstructures from SMP-10 with 5 wt% ADA, 1 wt% decaborane and 1 wt% DVB (foamed at at 300 °C wt% with a heating rate of 10 °C/min)

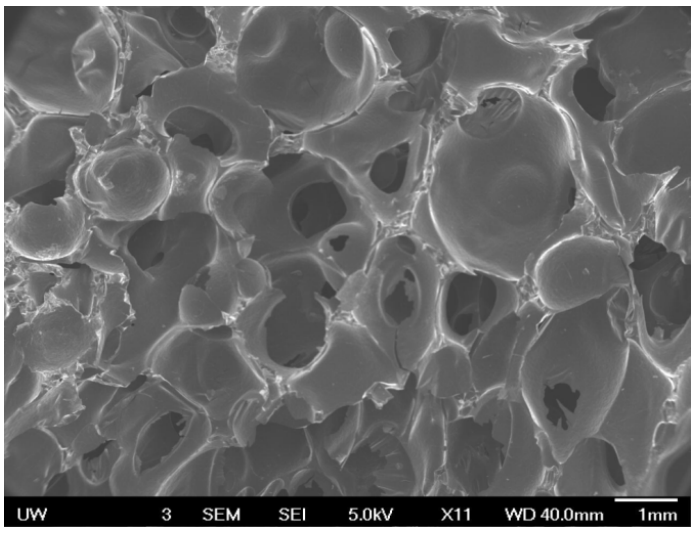

Figure V-35 Foamed ceramic microstructures from SMP-10 with 10 wt% ADA, 1 wt% decaborane and 1 wt% DVB (foamed at at 300 °C wt% with a heating rate of 10 °C/min)

The morphology remains fairly constant until the amount of DVB is 10 % DVB. The 10 % DVB clearly displays a significant increase in pore size compared to samples with lower

concentrations of DVB. In this research the wt% of DVB was limited to 5 wt % and so the morphology for the amount of DVB was not investigated further.

V.6 Densification of PDC SiC

V.6.1 Effects of Carbon and Boron on Hot Pressed PDC SiC

In this research, a graphene nanodomain was introduced into the SiC system through molecular modifications of the preceramic polymer utilizing divinylbenzene (DVB) (as previously mentioned). Additionally, the SMP-10 polymer was modified with decaborane to explore its functionality as a sintering additive during the sintering process. The various steps previously discussed were used to make dense samples as show in Figure V-36 and samples hot pressed are shown in Table V-3 Sample types that

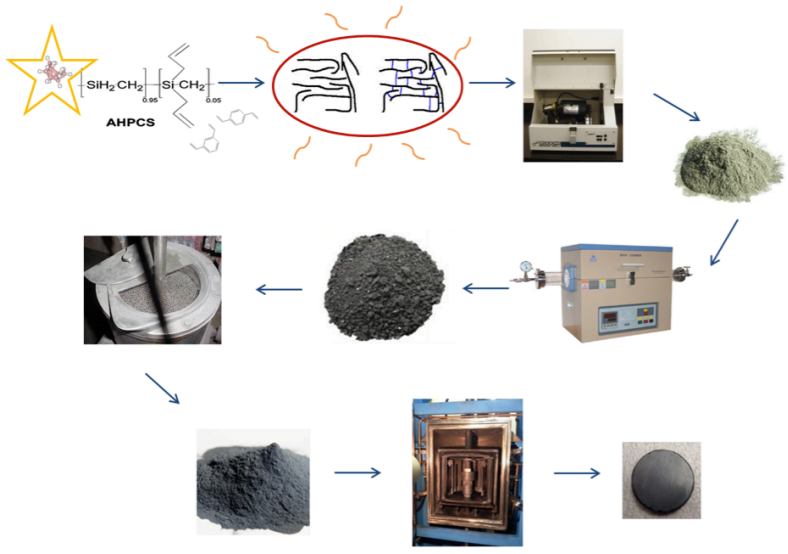

Figure V-36 Hot pressing procedure for decaborane modified SMP-10 (A molecular approach)

Table V-3 Sample types that hot pressed

Sample	Divinylbenzene	Decaborane	Amorphous B
Varying C, 1%B	X	X	
Varying C	X		
1% C, 1% B	X		X

The graphitic regions in this material have been explored using Raman spectroscopy Figure V-37. The G band indicates the presence of ordered graphitic regions, whereas the D band represents lack of lattice symmetry. Furthermore, turbostratic regions can also be seen from TEM analysis, which is indicative of graphitic basal planes that have been slipped out of alignment as shown in Figure V-38.

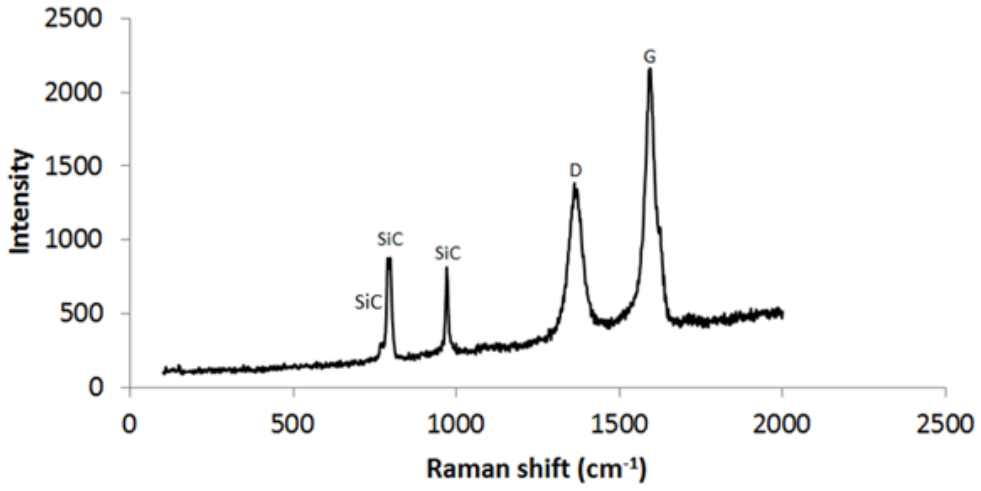

Figure V-37. Ordered carbon domains within an SiBC system consisting of 1 wt% decaborane and 5 wt% DVB hot pressed at 2050°C.

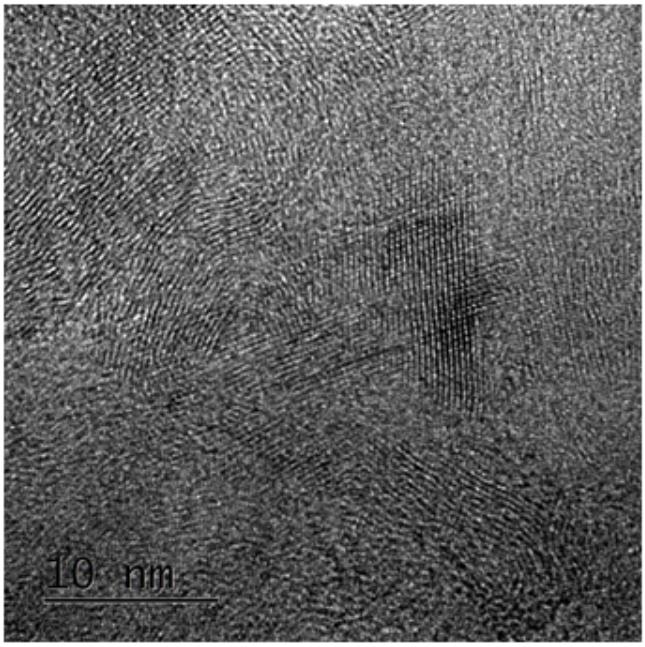

Figure V-38 Turbostratic regions in an SiBC system consisting of 1 wt% decaborane and 5 wt% DVB hot pressed at 2050°C as evidenced through TEM

XRD analysis of the SiC PDCs heat-treated at different temperatures indicated that the 3C phase is the first polytype that forms during the amorphous to crystalline transition.

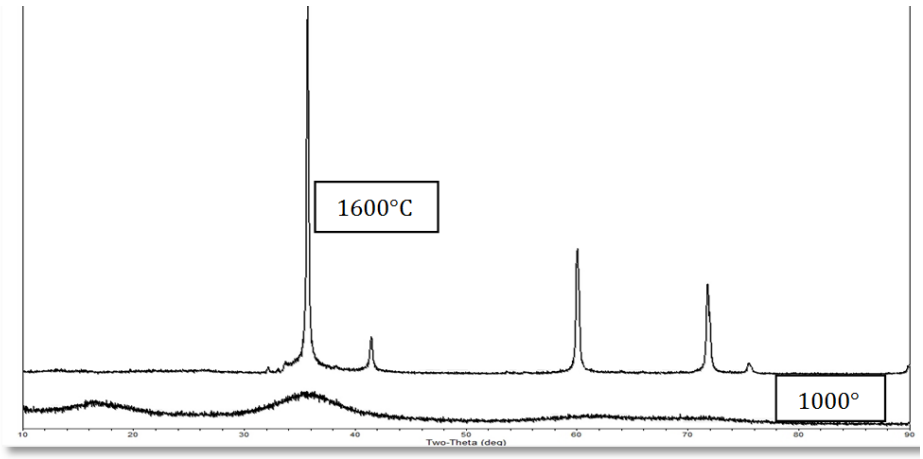

Figure V-39 Amorphous to Crystalline transition and the presence of cubic SiC upon crystallization of the various SMP-10 powders (modified or otherwise) heat treated at 1600°C

Through characterization of the hot pressed SiC ceramics the 6H phase along with the 3C polytype is observed in the XRD (Figure V-40). The 3C polytype overlaps entirely with the peaks in the 6H phase, therefore additional characterization of the material is necessary to determine adequate ratios of the two phases present in these samples.

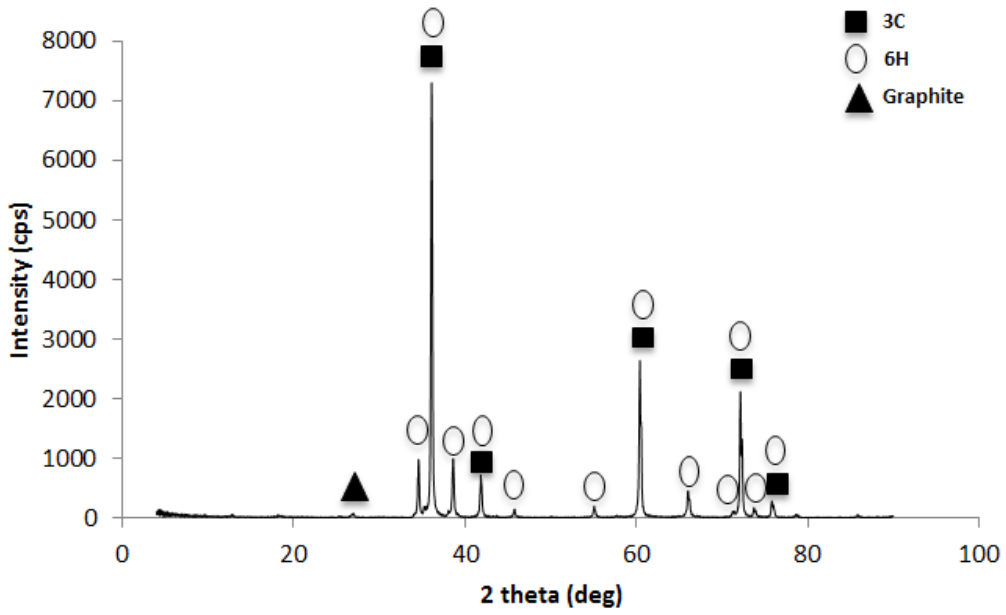

Figure V-40 3C and 6H polytypes present in all precursor modified samples (or SMP-10 alone) hot pressed to 2050°C

As shown in the XRD in Figure V-39 with respect to Figure V-40 it is understood that the 6H polytype forms at the expense of the 3C polytype.

From SEM, the appearance of elongated needle-like grains representative of abnormal grain growth are observed in the hot pressed SiC sample with the decaborane modified SMP-10 polymeric precursor. The elongated grains are indicative of a hexagonal polytype, more

specifically 6H (determined from XRD analysis). It can be seen that with increasing concentration of carbon there is an increasing concentration of the 6H phase (Figure V-41). This is suggestive that the graphite nanodomains within the material are dictating the resultant polytype.

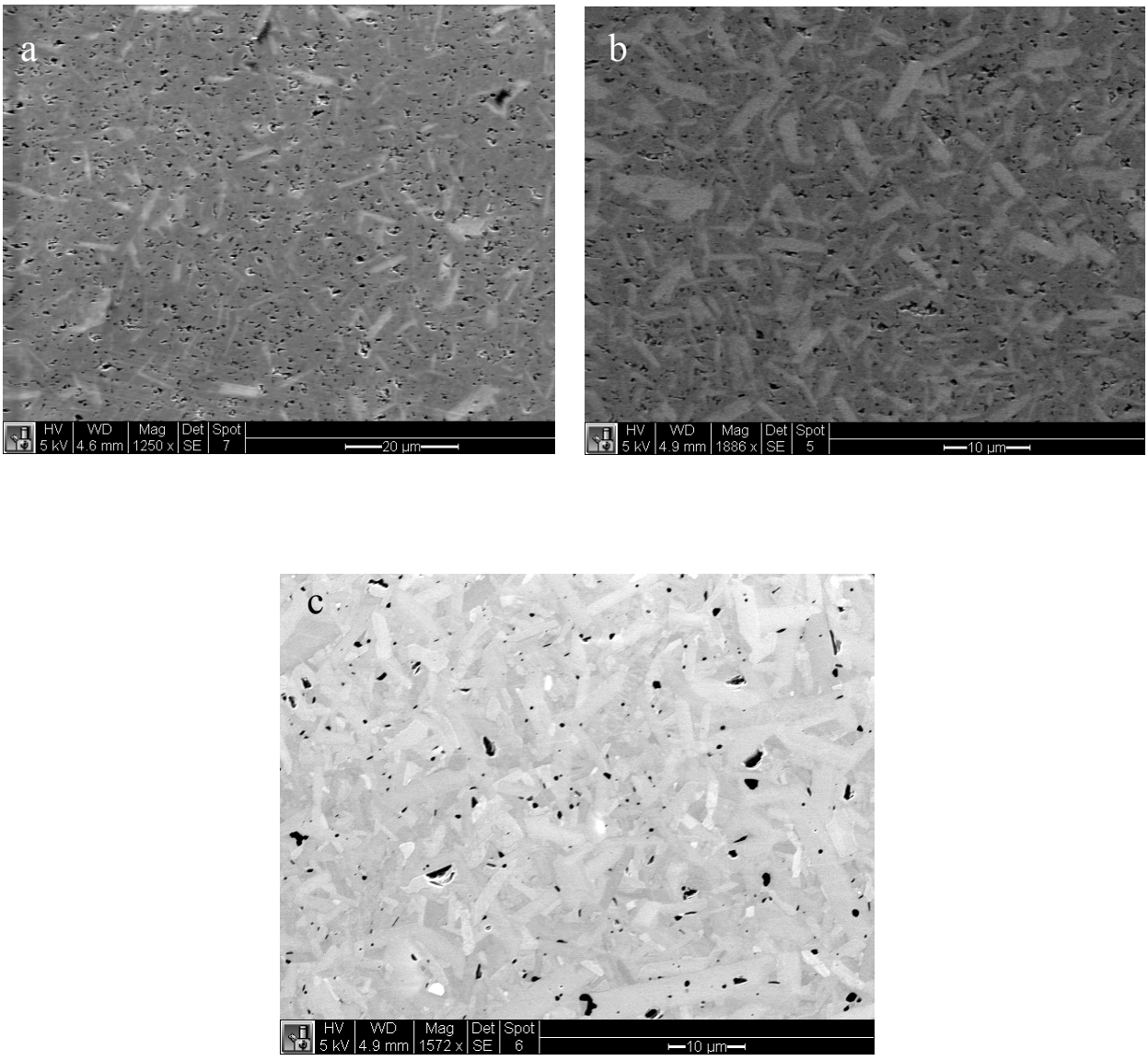

Figure V-41 Microstructural evolution of SiC with 1 wt% decaborane added to the precursor and excess carbon added in the form of DVB at 0, 1 and 5 wt% excess: a) 0SiBC, b) 1SiBC c) 5SiBC in which all samples were hot pressed at 2050°C

The evolution of the 6H polytype with increasing carbon concentration can be further investigated through ^{29}Si MAS NMR. Using ^{29}Si MAS NMR, the polytypes present in the SiC samples can be effectively separated. Here it can be seen that with increasing carbon concentration the 6H phase is stabilized at the expense of the 3C phase as shown in Figure V-42.

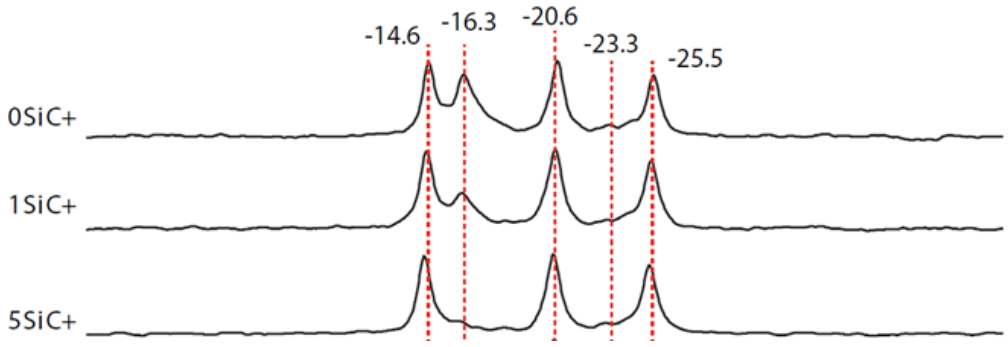

^{29}Si Chemical Shift

	6H	3C	4H
A	-13.9		
B	-19.9		
C	-24.6		-23
		-16.1 or -18.3	

Figure V-42 ^{29}Si MAS NMR of carbon 0SiBC, 1SiBC and 5SiBC hot pressed at 2050°C

It can be appreciated that although boron is present in this system, the manner in which boron was introduced in this processing route did not dictate the resultant polytypes. This can be seen in the XRD in *Figure V-43*, indicating that either with or without boron the same phases are present in the polymer derived SiC.

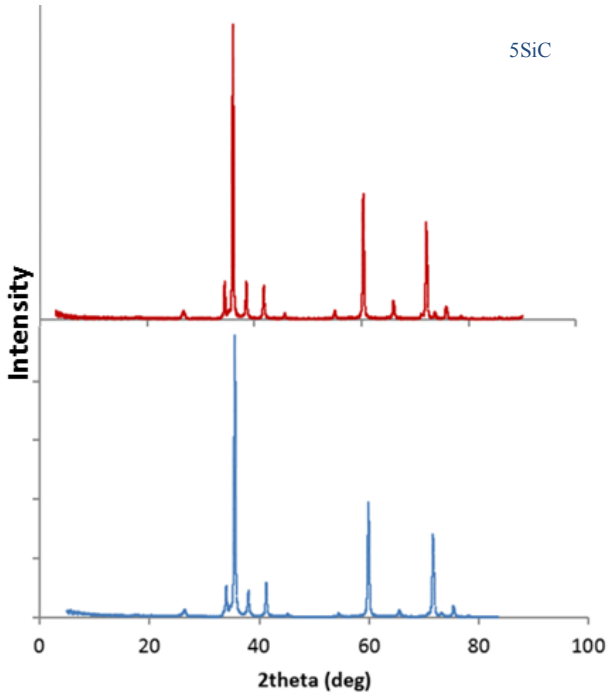

Figure V-43 XRD of 5 wt% excess C w & w/o boron

Although, the polytypes are the same, boron serves the important role of a sintering aid. This is shown in Figure V-44 where boron is shown to significantly enhance densification. The measured Archimedes densities further verifying this are plotted in Figure V-45.

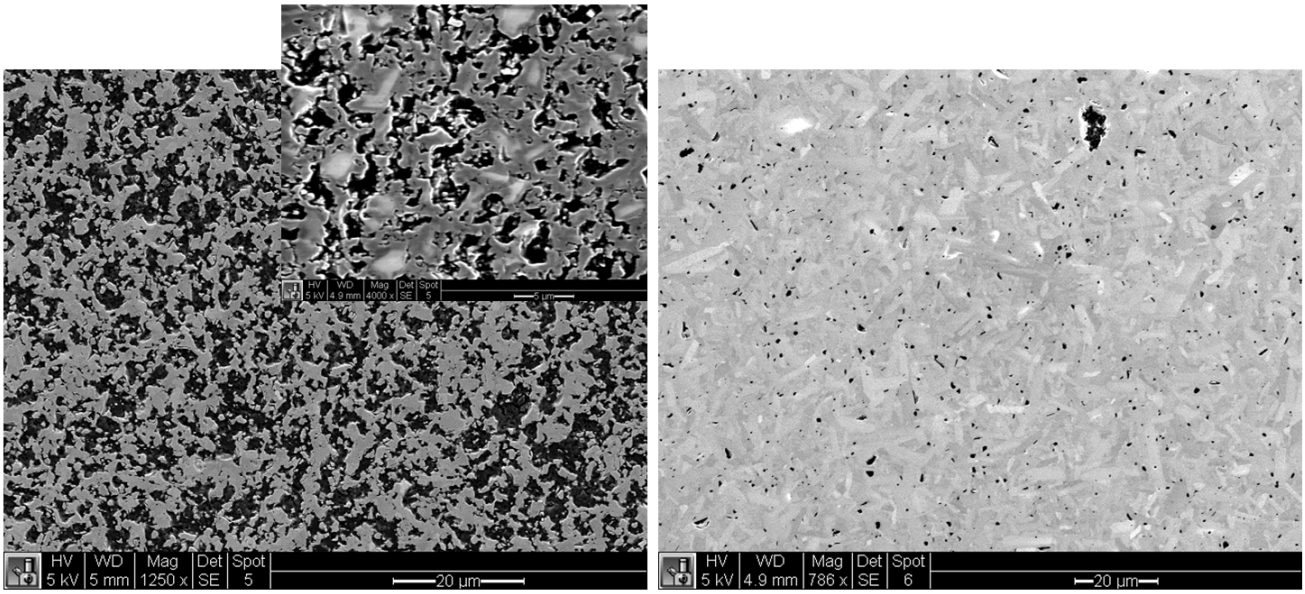

Figure V-44 Effect of boron sintering aid on the microstructure of hot pressed SiC with 5 wt% C in SiC (left figure, no boron) and 5 wt % C, 1 wt% B (right figure)

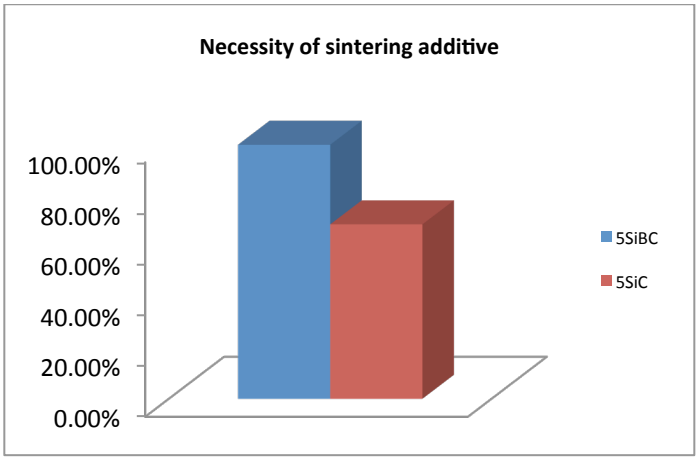

Figure V-45 Effect of boron on Archimedes density of hot pressed SiC with 5 wt % C

Although use of boron as a sintering aid is not a new phenomenon, the method in which boron was introduced in this study was novel. In the literature, it is noted that when amorphous boron is milled in with SiC powders the impurity of the amorphous boron influences the SiC polytypes present. It has been documented that this method of boron addition promotes the stabilization of the 4H polytype[128]. Whereas, in this study boron modification to the preceramic polymer did not appear to dictate the resultant polytype, nor did it result in the evolution of the 4H polytype. It did however allow for the densification of SiC, which was not possible without the use of a sintering additive.

The addition of amorphous boron to the submicron amorphous polymer derived silicon carbide samples were also explored to compare with both literature and with modified polymer approach of this study. This was accomplished using the procedure schematically shown in as in Figure V-46 and described in more detail in IV.3.2.

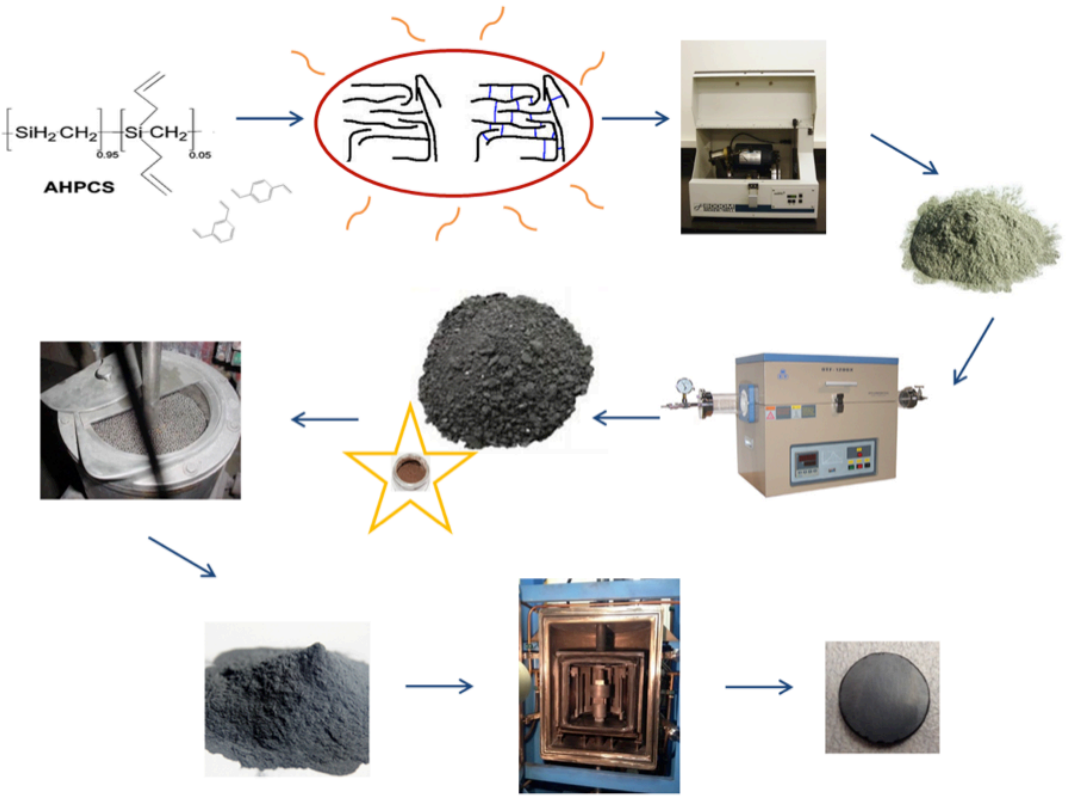

Figure V-46 Boron added to the pyrolyzed amorphous SiC powders (more traditional ceramic processing approach)

These studies revealed the presence of the 4H polytype as has been reported in the literature when boron (either in the form of boron carbide or amorphous boron) was added as a sintering aid to SiC using the powder approach (Figure V-47). When utilizing the same composition, with boron modifications to the polymer, we observe 6H and 3C SiC (the same phases present without boron modifications).

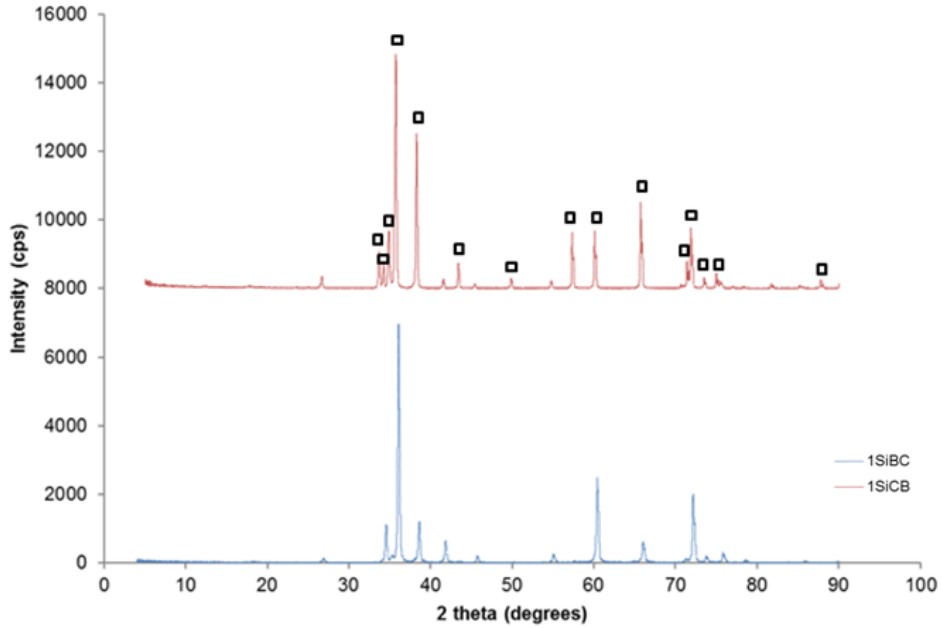

Figure V-47 Polymeric modifications (bottom blue) vs. powder modification w/ boron (top red)

Through SEM analysis we observe very large elongated grains of 4H SiC when amorphous boron powder is added to the amorphous SiC PDC powders (Figure V-48). There is clearly a significant difference of the resultant microstructure depending on how and when boron is added to the system. When boron is added molecularly (of the same composition) within the system it is composed of two phases; a 3C matrix embedded within the 6H elongated grains (Figure V-48).

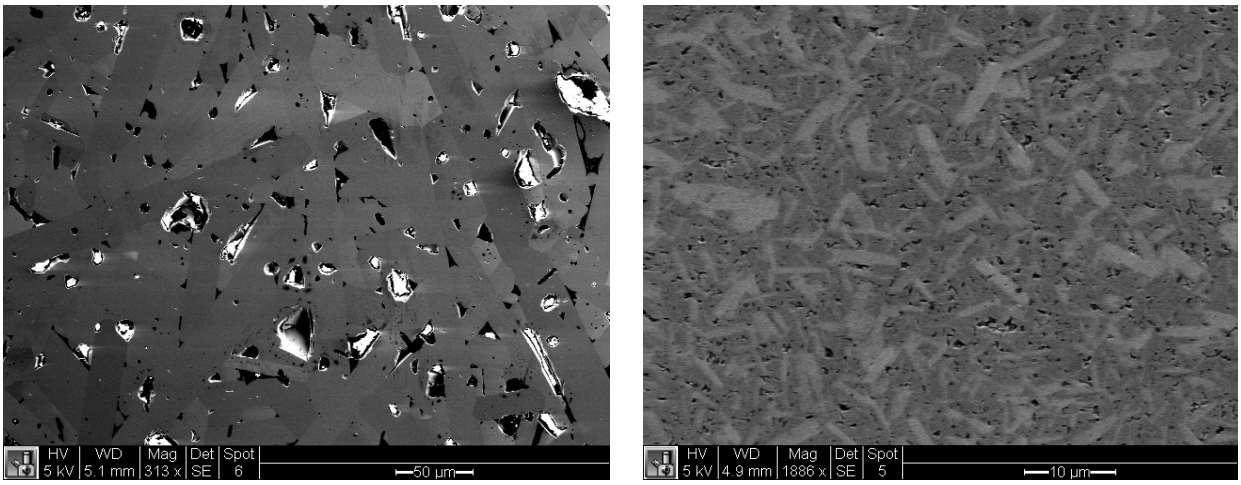

Figure V-48 Amorphous boron in 4H SiC (left), Polymer modifications w/ B (3C & 6H) (right)

Using them EMSL facilities at PNNL, Time of Flight Secondary Ion Mass Spectrometry (ToF SIMS) was used to observe the distribution of boron in the densified SiC samples. In the molecularly modified precursors, we can see that the boron is finely dispersed, however when boron was introduced to the amorphous SiC powders the boron is located predominantly on the grain boundaries and in large clusters Figure V-49.

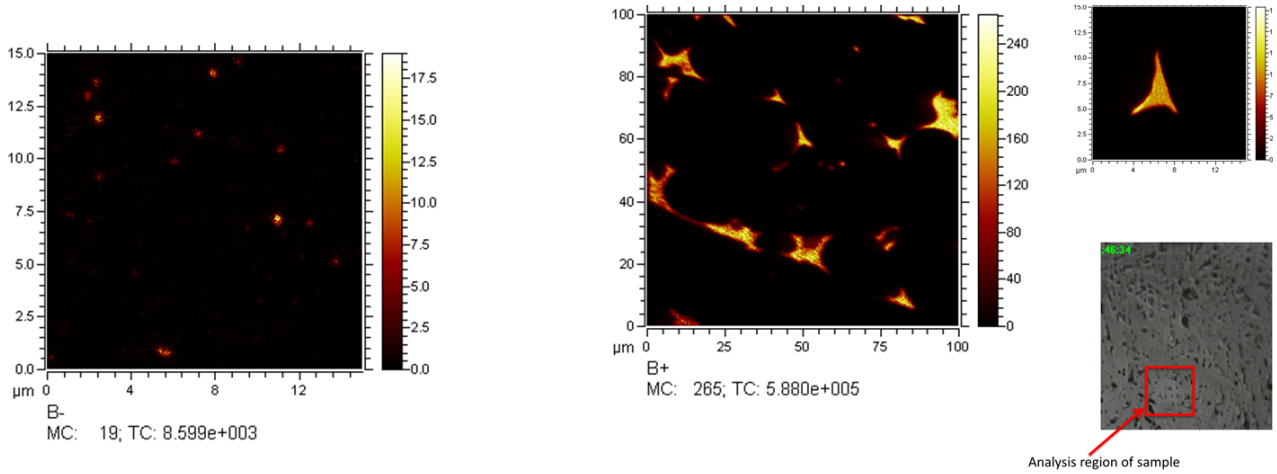

Figure V-49 boron distribution in densified samples from modified polymers and powders (left and right respectively)

Although the use of ToF SIMS gave indications of the boron distribution, it did not give clear resolutions of the surrounding elements that made up the system, as it is unable to explore multiple ions at once. Therefore, the usage of the Nano-SIMS at EMSL facilities was explored to give further details of the location of the elements within the material.

Using Nano-SIMS the elements most closely associated with boron and their locations relative to the microstructure could be observed. The SiC in which amorphous boron was added to the powder displayed a strong association of boron with carbon and is suggestive that it is organized into a boron carbide phase represented by the magenta region in Figure V-50. The green region outside the boron carbide areas showed boron and silicon rich areas most likely indicative of the interface of the BC phase with the SiC.

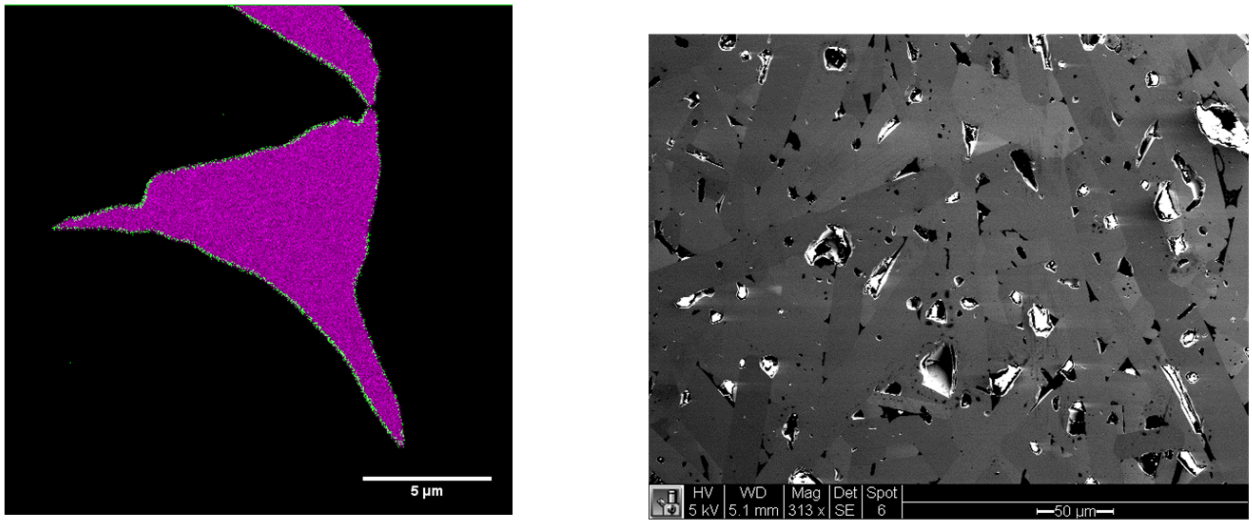

Figure V-50 Nano-SIMS showing regions w/ increased B concentration (left) and their association with Si & C in the microstructure (SEM right)

Using NanoSIMS to explore the regions of high boron concentration in samples in which boron was introduced to the polycarbosilane through a hydroboration reaction showed that boron is situated inside the SiC grains (as opposed to on the grain boundaries as is experienced when adding boron powder to SiC powder) Figure V-51.

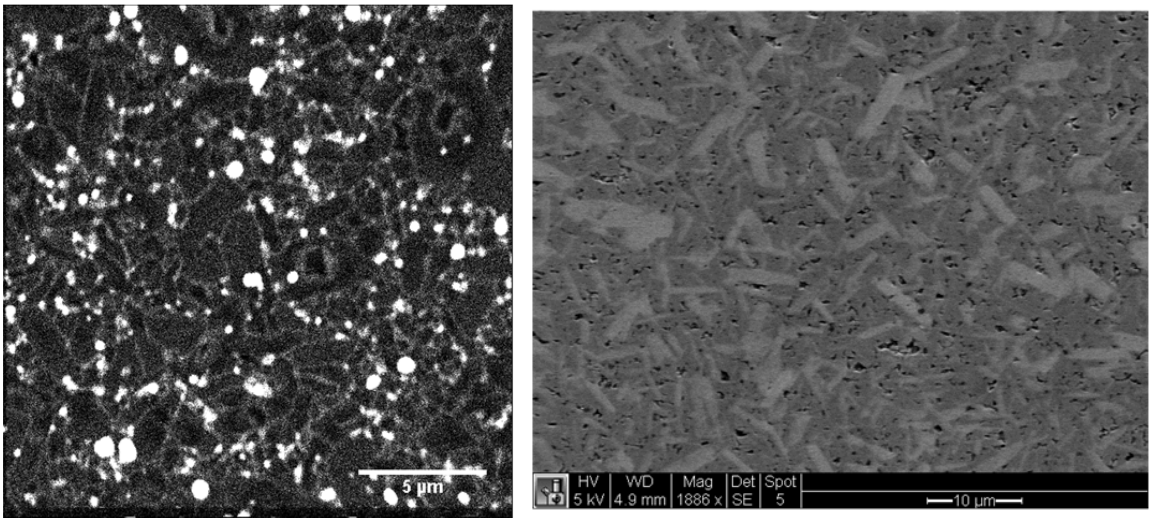

Figure V-51 NanoSIMS image (left) where the white areas are representative of boron located inside the grains in relation to the microstructure (right)

Due to the unique manner in which boron is situated in this material the diffusivity of species may vary considerably in comparison to more traditional routes of solid state sintering SiC with B addition. When further locating boron, carbon and silicon rich regions in the molecularly modified precursors, by using Nano SIMS, it can be observed that the boron again organizes with carbon suggesting the formation of a boron carbide structure (as represented by the magenta regions). Additionally the BC interface with SiC is represented by the white regions Figure V-52. The red regions are representative of carbon rich areas in the sample.

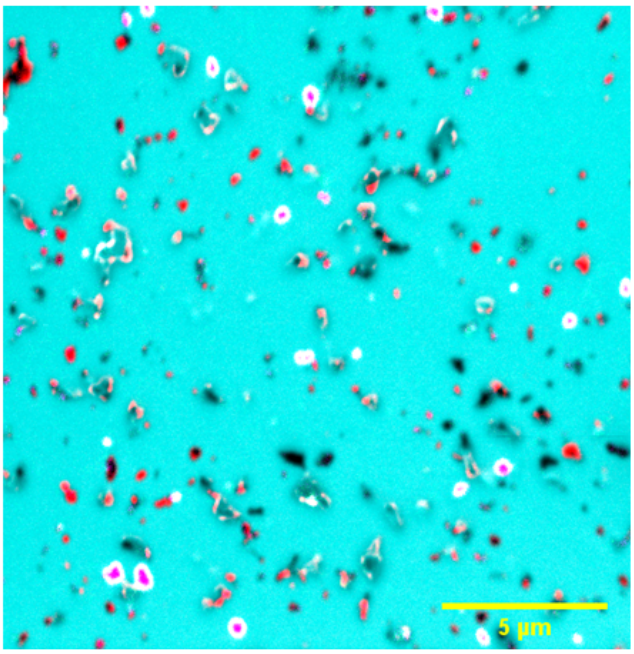

Figure V-52 Boron modified precursor, showing organization of B & C in the structure

NanoSIMS analysis of modified precursors with excess carbon from 1 & 5 wt % show variability in the size distribution of the boron and carbon clusters (Figure V-53). Here it can be observed that in the 1 wt% excess carbon in SiC the boron and carbon are more finely dispersed, whereas with increasing carbon concentration larger clusters domains within the system. Due to both compositions having the same amount of boron in the system this is perhaps indicative that diffusion is faster during sintering with increasing carbon concentration. Preliminary TEM results further confirm that there are larger clusters of both C and BC within the SiBC systems with higher C concentrations.

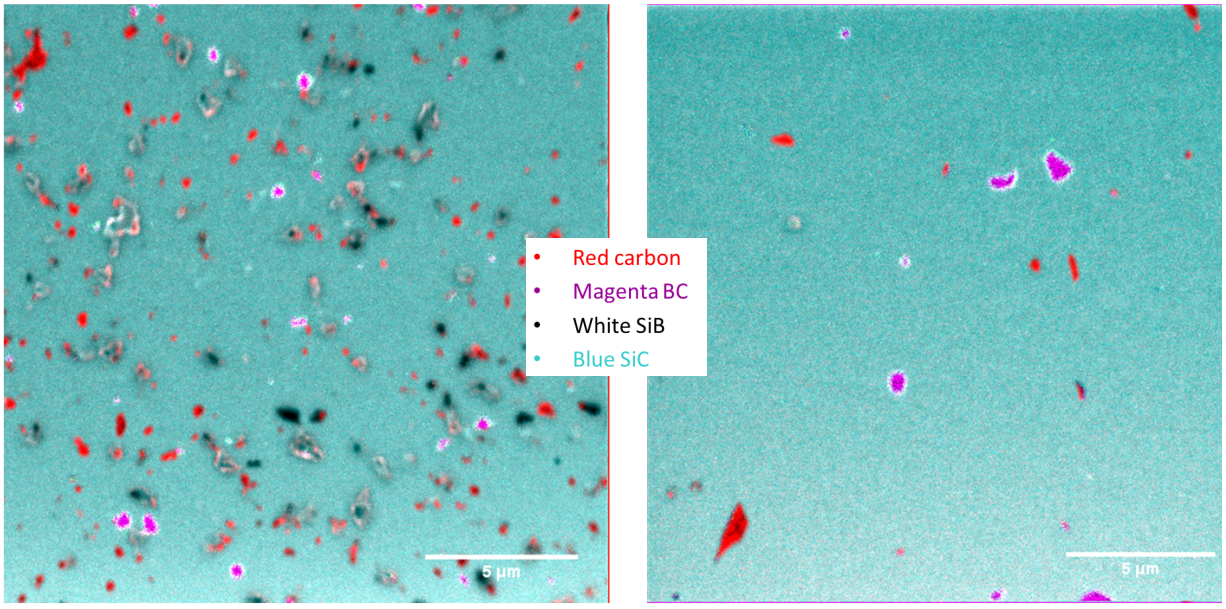

Figure V-53 B-doped SiC with 1 wt% excess carbon and 5 wt% excess carbon (right to left)

The larger clusters shown in the samples with 5 wt% excess carbon are potentially indicative that the rate of mass transport of the particles during sintering is increased. The Figure V-54 shows that the densities of the SiC samples are increased with increasing carbon concentration. In addition, preliminary TEM studies also shows the presence of larger clusters of boron and carbon with increasing carbon concentration.

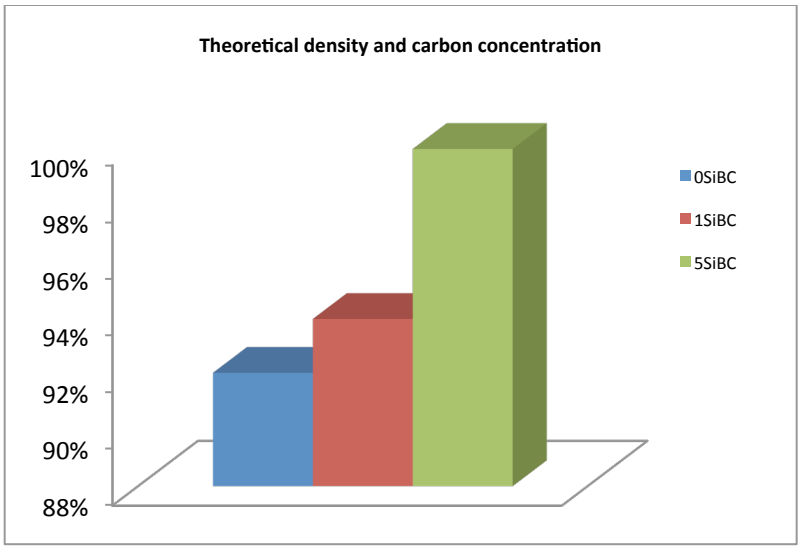

Figure V-54 Density increase with increasing carbon content in the hot pressed SiC with 1 wt% decaborane added to the precursor along with 0, 1, 5 wt% C (left to right respectively)

At PNNL, we have explored ^{11}B MAS NMR to determine the coordination chemistry of the boron in the matrix as well as TEM to observe locations and elements surrounding the boron. Here we observed the presence of distinct crystalline regions and also regions that are amorphous. The ^{11}B MAS NMR is shown in Figure V-55. The assignment of the crystalline peaks is still being analyzed, as this is a new material system. That being said, the elements most associated with the Nano-SIMS as well as the TEM results obtained are suggesting that boron is coordinating with carbon to form a boron carbide phase within the material.

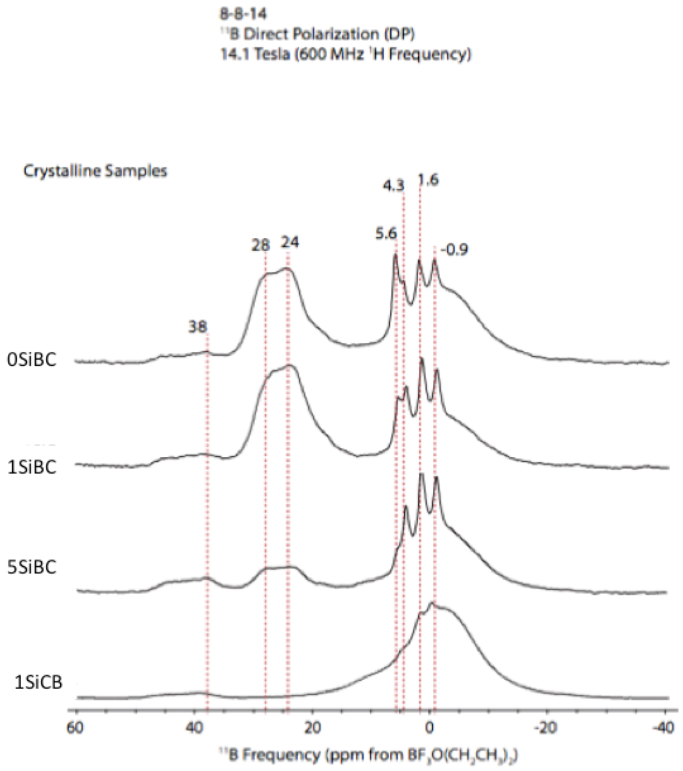

Figure V-55 ^{11}B MAS NMR of boron modified precursors and amorphous boron added to SiC powders with 0, 1 and 5 wt% excess carbon from top to bottom and 1SiCB representing 1 wt% amorphous boron powder added to amorphous SiC powder with 1wt% excess carbon.

Preliminary TEM results of the samples in which the polymeric phase was modified with boron, show that boron is located directly within the grains themselves (as opposed to being situated on the grain boundary). Additional TEM investigations are needed to correlate the observation from Nano SIMS, Raman and NMR. A summary of the effect of boron and excess C on the polytype and density of the hot pressed SiC is presented in Table V-4.

Table V-4 Summary of the density and polytypes associated with the hot pressed PDC SiC with C and boron additives

Sample	Bulk Density g/cm3	Theoretical Density	Polytype 1° & 2° (SEM/ NMR)
0 wt% C, 1 wt% Decaborane	2.96	92%	3C, 6H
1 wt% C, 1 wt% Decaborane	3.02	93.9%	3C, 6 H ~50:50
3 wt% C, 1 wt% Decaborane	2.78	86.6%	3C, 6H
3 wt% C, 1 wt% Decaborane	2.68	83%	3C, 6H
3 wt%C, 0 wt% B	1.95	61.3%	3C & 6H
3 wt%C, 0 wt% B	2.27	70.6%	3C & 6H
5 wt% C, 1 wt% Decaborane	3.205	99.9%	6H, 3C
5 wt% C, 1 wt% Decaborane	3.14	97.8%	6H, 3C
5 wt% C, 0 wt% B	2.20	68.6%	3C & 6H
1wt% C, 1 wt% amorphous B	NA	NA	4H & 6H

V.6.2 Hot Pressing Partially Pyrolyzed Powders

Initially hot pressing was conducted on partially crosslinked powders in an attempt to avoid complex milling processes. However, those samples experienced far too much offgasing during pyrolysis as well as lack of densification following hot pressing. Archimedes density measurements were done on these samples and it was determined that the density was 70% of the theoretical density of SiC. It can also be appreciated that these samples were only taken to 1500°C, which is not nearly the sintering temperature of SiC (2000°C). The resultant microstructure of these hot pressed powders is shown in the following Figure V-56 & Figure V-57

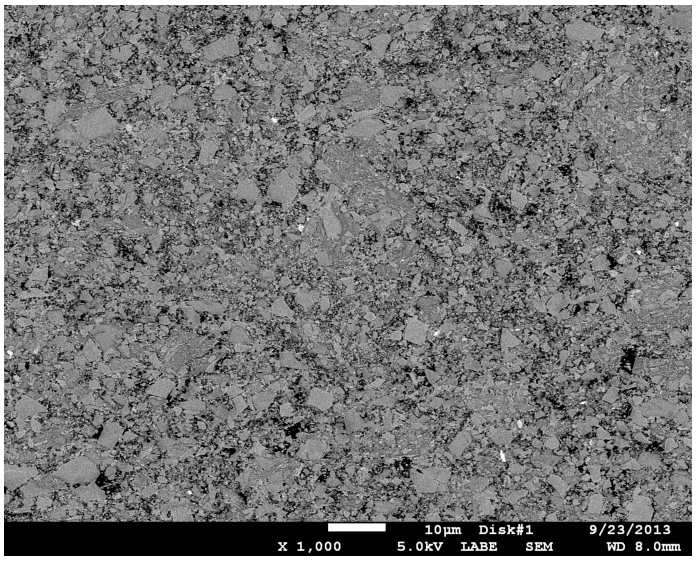

Figure V-56 Partially Pyrolyzed Hot Pressed Powders

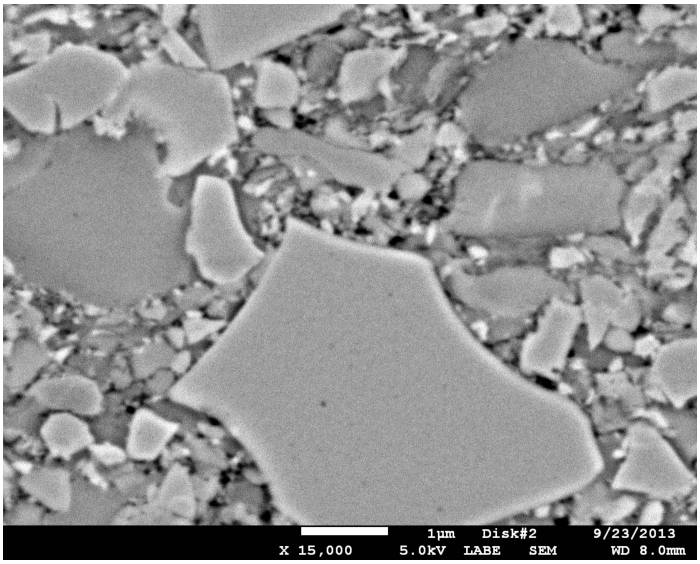

Figure V-57 Mixed Particle Sizes of the Hot Pressed Powders

It can be noted that the partially pyrolyzed powders were only milled in the Spex Mill for 30 minutes. After observation of the very different sized particles located in the SEM images

particle size analysis was performed on these samples. It was noted that in general the trend showed the majority of particles under 10 microns. However, there were still a decent amount of particles ~50 microns in size. From this preliminary study, it was concluded that the powders should be fully pyrolyzed and should be milled to a high degree.

V.6.3 Vacuum Processing for Dense Ceramics

The use of vacuum during thermal crosslinking of the samples was investigated. The idea is to remove gases as quickly as they were evolved to prevent foaming of the polymer and attempt to obtain a monolithic dense part. The SMP-10 preceramic polymer was initially poured directly into a glass petri dish. However, the resultant samples came out cracked from tensile forces between the crosslinking polymer and the glass dish. This was alleviated by placing dow corning vacuum grease to reduce the bonding between the dish and the curing polymer. The final crosslinked sample is cin one piece and has no apparent foaming or cracks as shown in Figure V-58 below

Figure V-58 Crosslinked SMP-10 under vacuum and at 400°C

Observing the cross section of the crosslinked SMP-10 under the microscope did show areas of porosity (Figure V-59).

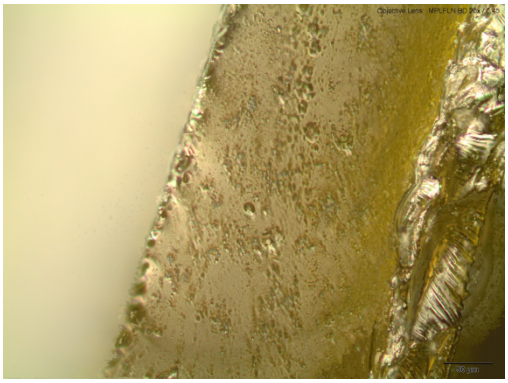

Figure V-59 Cross section of crosslinked polymer (w/o dp)

The crosslinked polymer was pyrolyzed in a graphite lined crucible to 800°C for 2 hours under ~-457 torr of vacuum. This sample did not crack during pyrolysis and was eventually sintered to 1700 °C again without any cracking. The sample however only densified to 68% of its

theoretical density of 3.21 cm^3/g. The cross section of the sample has many pores as shown in Figure V-60 and Figure V-61 below.

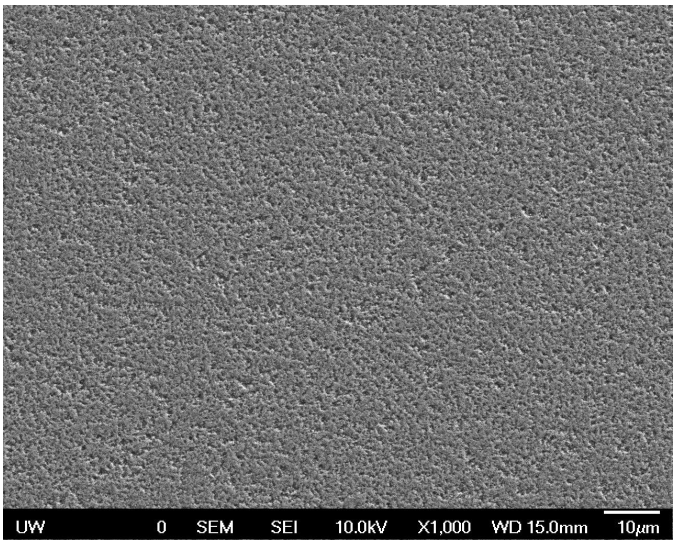

Figure V-60 SiC Cross section sintered to 1700C

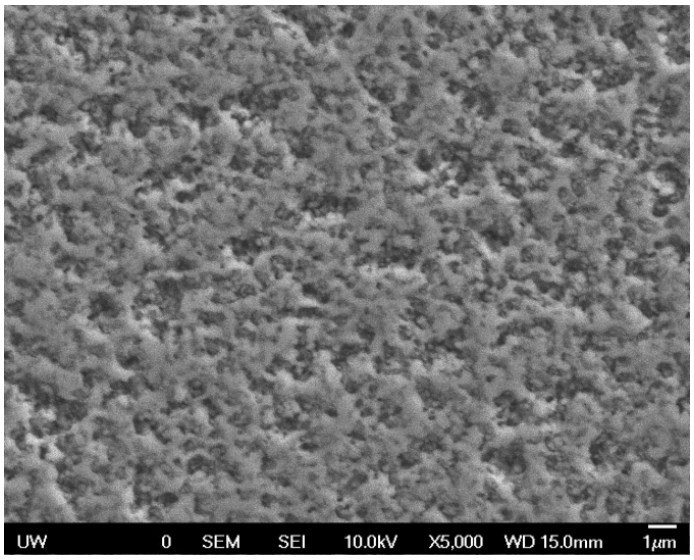

Figure V-61 SiC cross section sintered to 1700C

Figure V-62 below shows that the surface of material is essentially free of voids, whereas the central portion is porous. We conclude that the closing up of the surface during crosslinking left

no path for the gases evolved during pyrolysis to escape, resulting in porosity due to trapped gases.

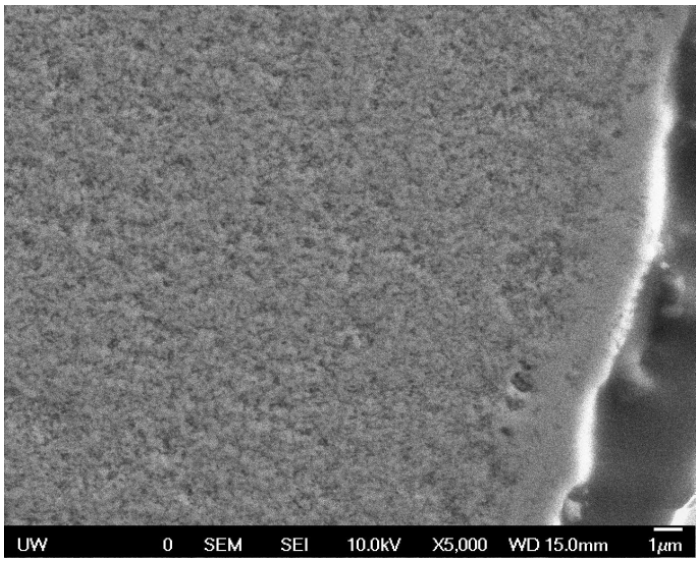

Figure V-62 Gradients of the inner vs surface

This is the most likely the reason why samples prepared in this manner had low density and why this processing method was abandoned in trying to achieve fully dense SiC. However, this may be a suitable procedure when trying to make thin samples. Table V-5 shows how density increases with increasing heat treatments and additionally confirming the SEM analysis that the porosity was all closed porosity vs open. The densities and open porosity were measured using the Archimedes method.

Table V-5 Archimedes method for determining density of vacuum processed samples

S*ample w/o dicumyl peroxide*	*Volume Open Pore*	*Bulk density*
X-link	0.0002	1.14
Pyrolyed	0.0002	1.81
Crystallized	0.0000	2.17

Although for this research, this method was not investigated further, there is potential in this approach. In the future samples with boron and sintered at higher temperatures should be investigated.

V.6.4 Electron Beam Curing of SMP-10 Followed by one step pyrolysis

Electron beam curing was explored due to its unique method of crosslinking the chains and its ability to generate samples with very low oxygen content in comparison to other methods. This is the method used in producing commercial SiC fibers. Therefore, this method was explored in determining the achievable densities of bulk ceramics compared to thermal curing

After the samples were cured using the radiation facilities at Boeing, they were sintered and crystallized at 1700°C in a high temperature vacuum furnace. As shown in Figure V-63, there are tunnels left over from pyrolysis representing paths of diffusion for the low molecular weight

oligomers that didn't crosslink. Figure V-64 represents the areas in between the tunnels revealing the presence of nanopores.

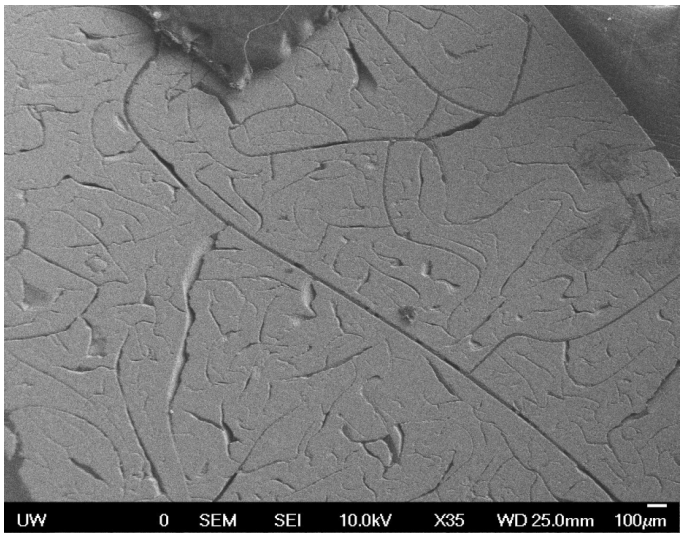

Figure V-63 Crystallized SiC depicting tunnels from pyrolysis

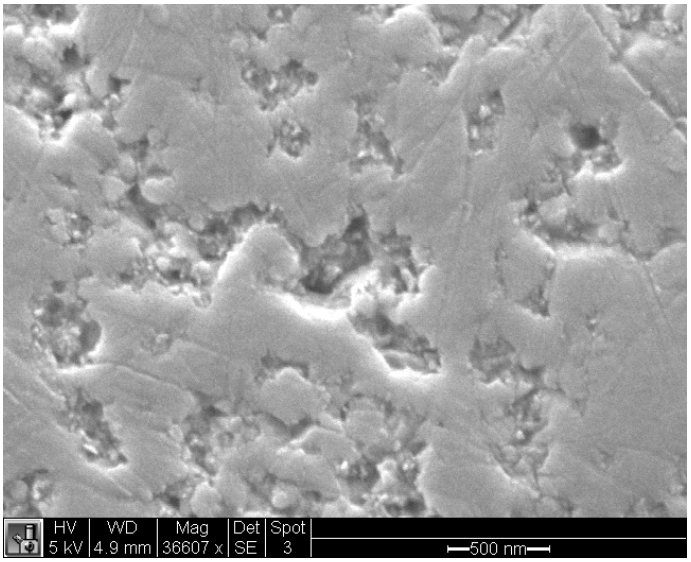

Figure V-64 SEM image depicting nanoporous region within the dense SiC

Table V-6 lists the densities of both the amorphous and the crystallized samples measured using the Archimedes method.

Table V-6 Comparison of density of amorphous & crystalline e-beam cured SMP-10

Sample	Bulk Density	Crystallized TD
SMP-10 (pyrolyzed 800°C)	1.97	62%
SMP-10 (Crystallized 1700°C)	2.46	77%

It can be pointed out that these samples were processed without pressure assisted sintering, no sintering aids with a maximum processing temperature of 1700°C (vs 2100°C the more appropriate temperature to achieve fully dense SiC samples). Considering the mild conditions, the densities are quite impressive. Due to the escape of gases during the pyrolysis this is not an ideal method in which to produce bulk dense SiC specimens. However, it is possibly worth exploring how decreasing the thickness of the sample may result in dense SiC for thin film samples.

V.6.5 Matrix studies

One of the promising nuclear applications of SiC is an SiC/SiC composite. Therefore, a study was undertaken to see if PDCs would be a viable route as a matrix in SiC/SiC composites. We have prepared samples to increase the carbon content by adding divinylbenzene (DVB) in quantities from 0-5 wt% in allylhydridopolycarbosilane (SMP-10) from Starfire Systems..

The rate of curing was the first step in achieving samples to represent the matrix. This was done such to prevent self-foaming of the SMP-10 during the crosslinking phase. All samples were held at 200°C followed by fully curing to 400°C under gettered argon atmosphere. The heating rate during crosslinking of the decaborane modified SMP-10 samples (5°C/min and 1°C/min) dictated the quality of the monolith (Figure V-65).

Figure V-65 Heating rate 5°C/min (left) and 1°C/min (right)

It is observed that a slow heating rate is needed to release the gases at a controlled rate in order to prevent trapping of the gases during curing of the sample. The same self-foaming of SMP-10 is observed when SMP-10 with dicumyl peroxide (or SMP-10 alone) is cured at faster rates. Figure V-66 shows that SMP-10 containing 1 wt% of dicumyl peroxide can be controllably cured without trapping gases when the heating rate is very slow. This was also performed under gettered Argon at the same curing temperature as noted above.

Figure V-66 Curing at 1°C/min (SMP-10 w/ 1 wt% dicumyl peroxide)

Having established the optimum curing schedule, samples with varying carbon content were prepared using a one step pyrolysis method in gettered argon to 800°C. The samples were then crystallized to 1500°C and density measurements (using the Archimedes method) were taken before and after devitrification. The density of the samples pyrolyzed at 800 and 1500°C were 69 and 73% of the theoretical amount for SiC, respectively. SEM imaging of the 1 wt% excess carbon shows tunnels leftover from hydrocarbon evolution during pyrolysis at both 800 and 1500°C in Figure V-67 below.

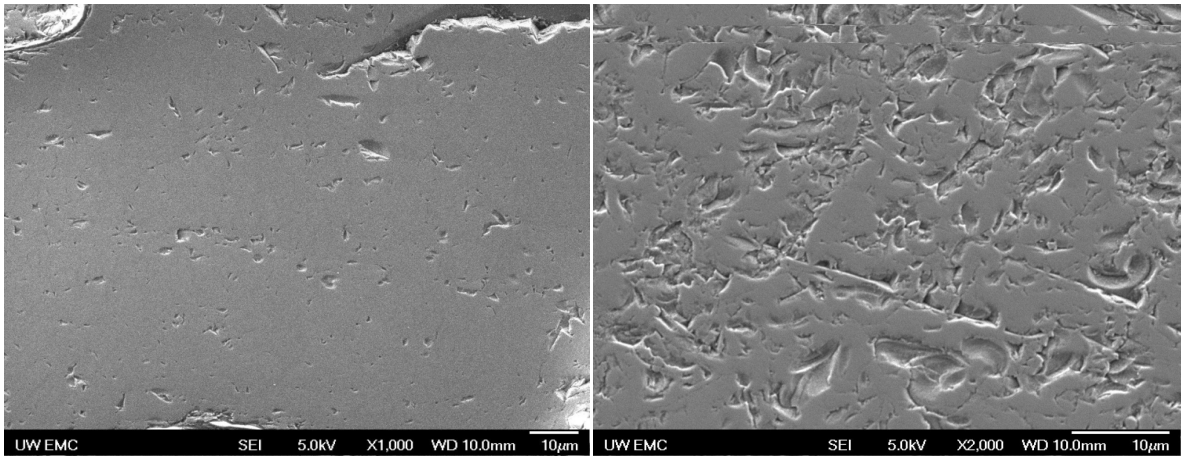

Figure V-67 Pyrolysis of SMP-10 at 800°C at 1500°C (L to R)

V.6.6 SMP-10 as a binder for milled crosslinked SMP-10 powders

The amorphous/partially nanocrystalline samples of B-SMP-10 and SMP-10 achieved 74% and 66% of the theoretical density respectively of fully crystalline SiC through this procedure. It can be appreciated that boron either functioned as a sintering aid in this investigation, or there was less mass loss due to the modification of the sample. The density was shown to increase the B-SMP-10 sample by 8% at even lower sintering temperatures than SMP-10. The experiments could be further investigated with addition of decaborane to the SMP-10 precursor. However, the focus of the thesis was on developing powders for hot pressing so this method was not further pursued.

V.7 Stopping Range of Ions in Matter and Transport of Ions in Matter Simulations

Initially various ions were explored in simulating the damage in SiC with energies of 2MeV as well as 5MeV. While He damage in the neutron environment is a well known problem, it is not practical to simulate the He damage in the neutron environment from ions due to the time required to induce damage. Due to time constraints, Au ions were employed in order to generate damage to the SiC in a reasonable time period to understand the reactivity of the developed SiC samples with ion bombardment. The damage induced by Au ions with energies of 2MeV (Figure V-68) and 5 MeV (Figure V-69) was simulated.

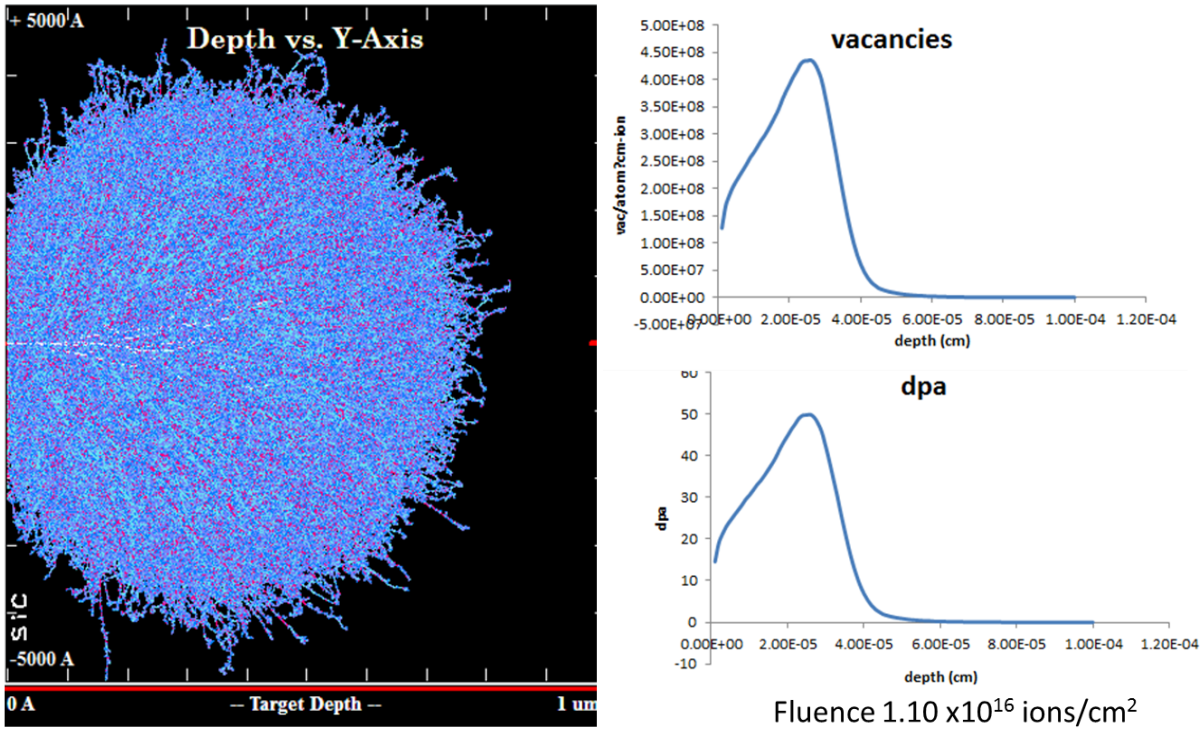

Figure V-68 Simulation of damage from 2MeV Au implantation in SiC

Based on simulations, for the experiments we opted to use 5MeV in order to induce more damage at greater depths in a shorter period of time.

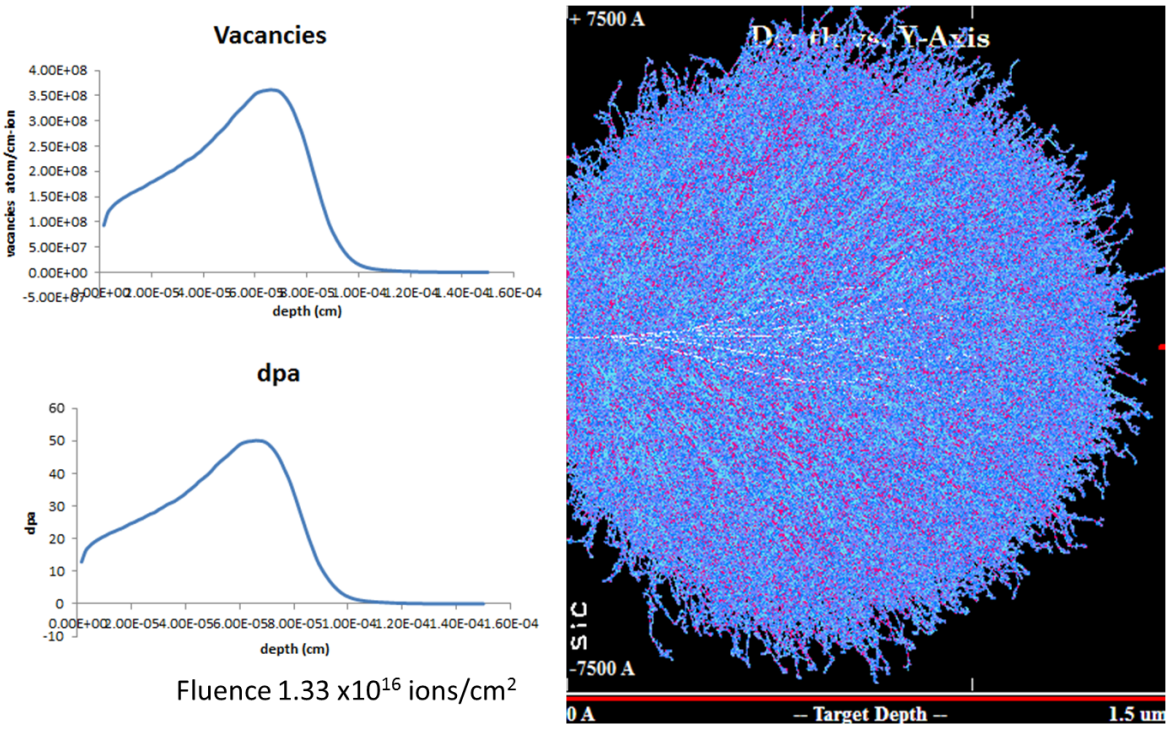

Figure V-69 Simulation of damage from 5 MeV Au implantation in SiC

The implantation was done at 600°C and the dpa at the surface was 20 and 2 dpa for the 2 sets of samples. The samples included 3 samples in which boron was added at the molecular level and excess carbon in the amounts of 0, 1 & 5 wt%. In this set we also included the one sample in which boron was introduced as powder. Additionally, we masked off a region such that a portion of the sample did not experience any ion irradiation damage. Furthermore, we additionally implanted ions for a short period of time at cryogenic temperatures so that we had low temperature irradiation damage for easy identification of irradiated regions.

V.8 Step Height Swelling from Irradiated SiC with Au ions

The change in step height from point defect induced swelling between the masked and un-masked regions for samples in which boron was added as a powder Figure V-70 and in which boron was added at the molecular level Figure V-71.

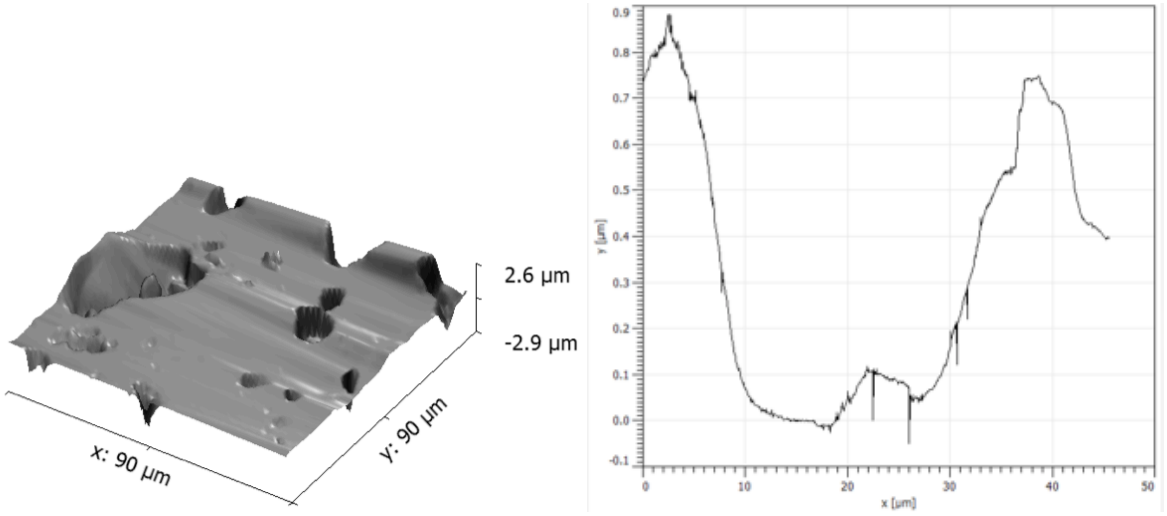

Figure V-70 SiC with amorphous boron step height changes of irradiated regions

It can be observed in Figure V-70that when processing the ceramics using more traditional routes the step height change is ~1 µm. However, when utilizing the SMP-10 modified system (where boron was introduced to the molecular architecture of the polymer) a step height change of only 0.2 µm was observed in Figure V-71. It is clear from the results that samples with molecularly added boron are significantly more resistant to point defect swelling than their traditionally processed counterparts.

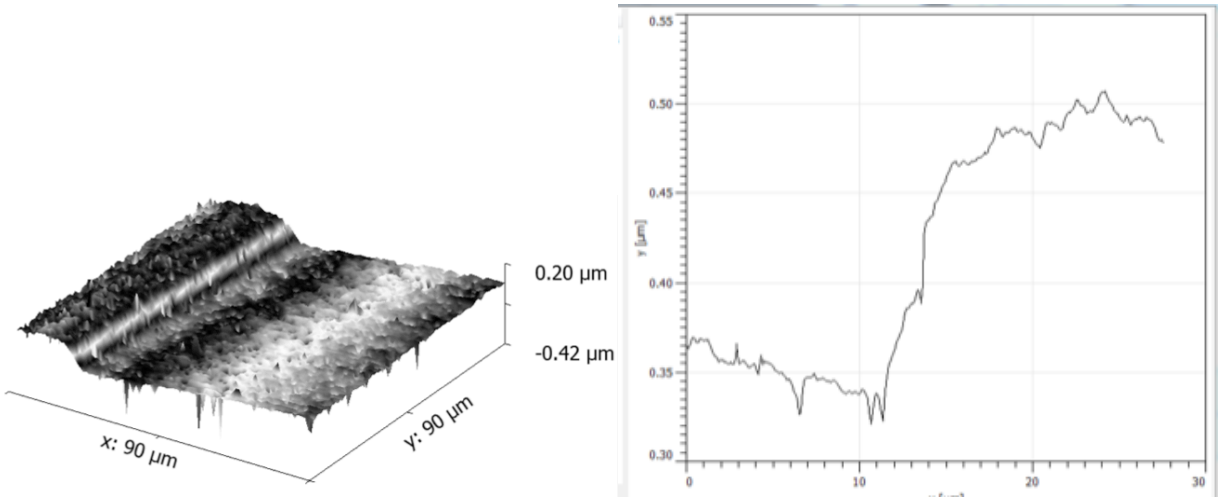

Figure V-71 Molecular modified precursors step height changes from ion irradiation

In summary, compositions of the exact same stoichiometries (1 wt% excess C and 1 wt% B in SiC) but varying methods of boron incorporation (added molecularly to the precursor vs. added to the powder) were compared in their ability to mitigate radiation damage from ion bombardment. It was observed that boron added at the molecular level demonstrated an increased ability in mitigating radiation defects as evidenced by significantly reduced step height changes associated with point defect swelling between masked and un-masked regions. The interaction of the ions with the two different methods of processing is indication that the method in which SiC is processed does play a role in the radiation properties of the material. In order to better establish how the ions damaged the material it is necessary to do TEM analysis. While, TEM analysis was not possible during the course of the Ph.D., it will be completed under the East Asia and Pacific Summer Institute Fellowship sponsored by the National Science Foundation during Summer 2015. The details of the work to be completed are outlined in the future work portion of this dissertation.

Chapter VI Summary and Conclusion

VI.1 Controlled Pore Morphology in Polymer Derived Silicon Carbide Foams

A variety of methods were utilized to develop porous SiC, with the ADA foaming route being the choice processing method in this research. The ADA foaming route allowed for a uniform distribution of pores to be obtained, as well as control over the pore size and morphology as can be seen in Figure VI-1.

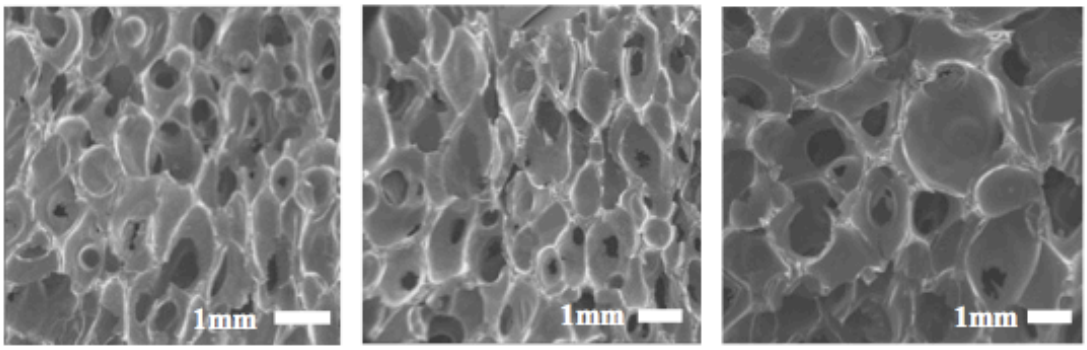

Figure VI-1 0,0.5 & 1 wt% decaborane in 1wt% ADA respectively (left to right)

This was possible through manipulation of the following processing parameters:

- Determination of optimal holding temperature during foaming
- Determination of optimal ramp rate for foaming
- Dispersing of ADA
- ADA concentration in foamed SiBC
- Decaborane in foamed SiBC
- Divinylbenzene addition for samples containing excess carbon in foamed SiBC

VI.2 Polytypic Stability of Polymer Derived Silicon Carbide Ceramics

A variety of processing methods were explored in the generation of dense PDC SiC. The hot pressing route of boron and carbon modified SMP-10 precursors was the primary investigation of this work. This method was used to due the ability to achieve nearly fully dense SiC as shown in Table VI-1.

Table VI-1 Overview of SiC and SiBC observations

Sample	Bulk Density g/cm3	Theoretical Density	Polytype 1° & 2° (SEM/ NMR)
0 wt% C, 1 wt% Decaborane	2.96	92%	3C, 6H
1 wt% C, 1 wt% Decaborane	3.02	93.9%	3C, 6 H ~50:50
3 wt% C, 1 wt% Decaborane	2.78	86.6%	3C, 6H
3 wt% C, 1 wt% Decaborane	2.68	83%	3C, 6H
3 wt%C, 0 wt% B	1.95	61.3%	3C & 6H
3 wt%C, 0 wt% B	2.27	70.6%	3C & 6H
5 wt% C, 1 wt% Decaborane	3.205	99.9%	6H, 3C
5 wt% C, 1 wt% Decaborane	3.14	97.8%	6H, 3C
5 wt% C, 0 wt% B	2.20	68.6%	3C & 6H
1wt% C, 1 wt% amorphous B	NA	NA	4H & 6H

This is a novel processing method in which the SiC polytypes and microstructures are controlled through molecular modifications of the precursor with carbon and boron as seen in Figure VI-2.

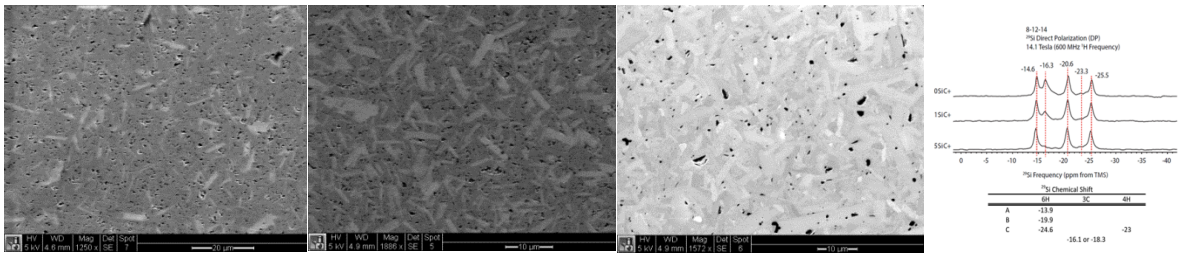

Figure VI-2 SEM & ^{29}Si MAS NMR observations (0, 1 & 5 wt% left to right) of excess carbon and polytypes

The appearance of elongated needle-like grains is representative of abnormal grain growth present in the hot pressed SiC sample with the decaborane modified SMP-10 polymeric precursor. The elongated grains are indicative of a hexagonal polytype, more specifically 6H (determined from XRD analysis). It can be seen that with increasing concentration of carbon there is increasing concentration of the 6H phase. Therefore suggesting that carbon is controlling the stability of the resultant polytype. Furthermore, it can also be shown using Nano-SIMS that increasing concentration of carbon from 1-5 wt % shows coarsening of the species within the SiC structure Figure VI-3.

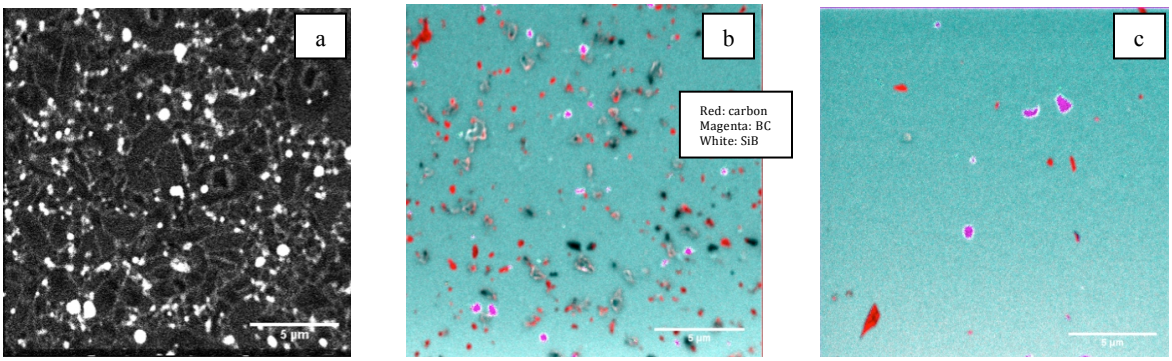

Figure VI-3 a)Intragranular incorporation of B, b)1 wt% excess C, c) 5 wt% excess C

These results are significantly difference than what has been previously reported in the literature for the processing of SiC using boron and carbon as sintering additives. In which the addition of boron in the form of amorphous boron or boron carbide is shown to stabilize the 4H polytype. As shown in Figure VI-4 it can be seen that when the exact same amount of boron and carbon is added to the system with the only variation being the method of boron addition, drastically different results are achieved.

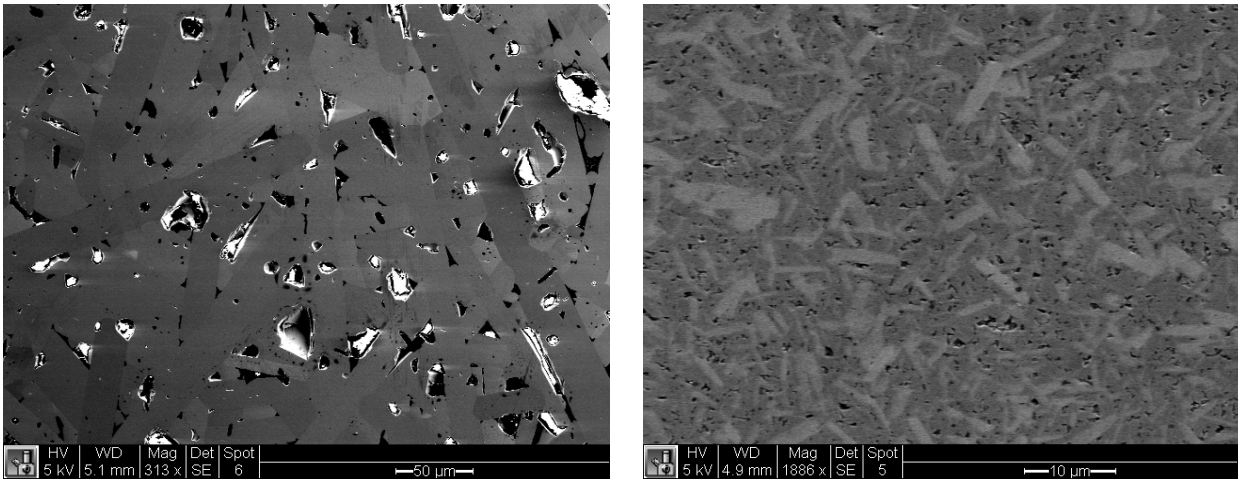

Figure VI-4 Amorphous boron in SiC (4H) (left), Polymer modifications w/ B (3C & 6H) (right)

VI.3 Radiation Stability of Polymer Derived Silicon Carbide Ceramics

Ion accelerator experiments were performed at EMSL to determine the effects of processing and microstructure properties. The swelling of the material due to point defect accumulation was explored using the AFM to determine any step height changes from the masked and unmasked regions of the samples. SiC compositions of the exact same stoichiometries (1 wt% excess C and 1 wt% B in SiC) but varying methods of boron incorporation (added molecularly to the precursor

vs. added to the powder) were compared in their ability to mitigate radiation damage from ion bombardment. It was observed that boron added at the molecular level demonstrated an increased ability in mitigating radiation defects as evidenced by significantly reduced step height changes associated with point defect swelling between masked and un-masked Figure VI-5 and Figure VI-6.

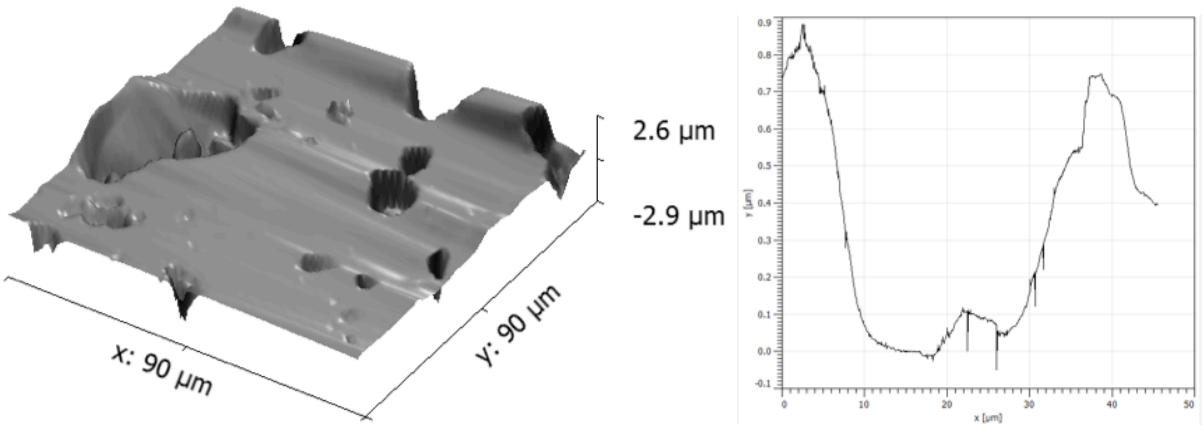

Figure VI-5 SiC with amorphous boron step height changes of irradiated regions

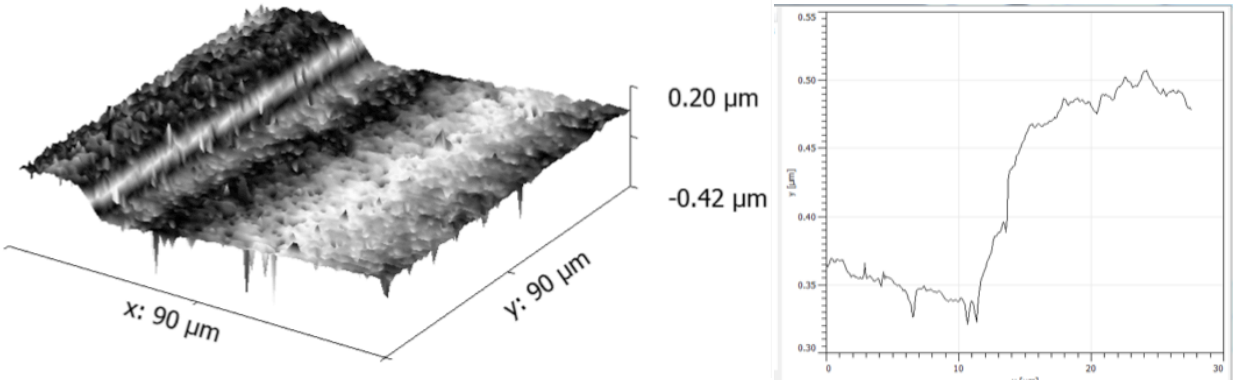

Figure VI-6 Molecular modified precursors step height changes from ion irradiation

Chapter VII Planned Future Work

A novel class of SiC ceramics with controlled microstructures has been developed through tailoring of the molecular architecture of the starting precursor (allylhydridopolycarbosilane, Starfire® SMP-10). This approach allowed the possibility to molecularly control and design the composition of the ceramic. Nanostructural features in the form of graphene layers were incorporated via excess carbon from the addition of divinylbenzene (0-5 wt%) to the liquid SMP-10. The utilization of PDCs also made possible the integration of sintering additives at the molecular level through a hydroboration reaction of SMP-10 with decaborane. It can be observed through SEM and ^{29}Si MAS NMR analysis that increasing concentrations of carbon increases the 6H SiC polytype at the expense of 3C polytype Figure VII-1.

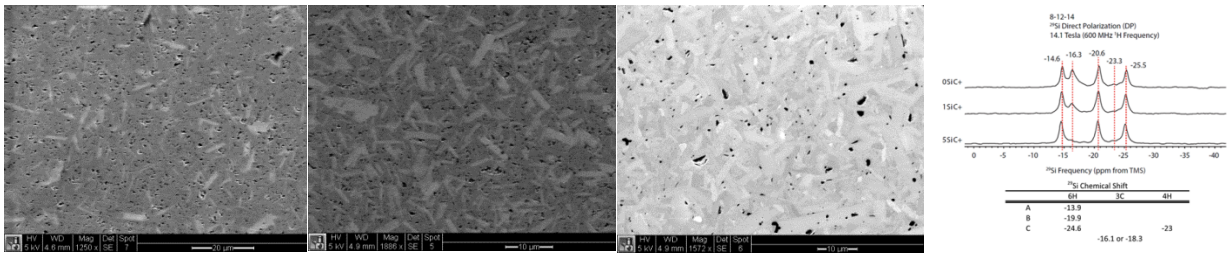

Figure VII-1 SEM & ^{29}Si MAS NMR observations (0, 1 & 5 wt% left to right) of excess carbon and polytypes

The presence of elongated needle-like grains in the matrix represents abnormal grain growth of the 6H hexagonal phase in the PDC SiC. The hypothesis that emerges from this research is that graphite nanodomains within the material dictate and control the resultant polytype. For example, the morphology of the carbon phase with respect to the 6H SiC phase can be studied using high-resolution transmission electron microscopy (HRTEM). The bonding associated with

the carbon nanodomains can be analysed using scanning transmission electron microscopy energy electron loss spectroscopy (STEM EELS). In the nuclear literature, 3C SiC has been extensively explored for its sustainability in the nuclear environment. The results of this work allow the ability to explore the role of SiC polytypes (3C:6H) along with the effects of increasing interfaces with graphene nanodomains and their stability in the next generation of accident damage tolerant nuclear reactors.

With respect to performance in the nuclear environment, the hypothesis is that these carbon nanodomains will mitigate radiation damage by enhancing local recombination of defects at the engineered interfaces. With that, it is essential to determine the size and extent of these nanodomains through Small Angle X-ray Scattering (SAXS). With that, this project will continue for 8 more weeks through the East Asia and Pacific Summer Institute (EAPSI) National Science Foundation (NSF) Fellowship. At at the University of Queensland, St. Lucia, Australia (UQ), Center for Microscopy and Microanalysis (CMM) SAXS will be conducted to characterize the interfacial relationship of SiC & graphene with radiation, a key component of this research.

The low temperature ion radiation experiments were conducted using EMSL facilities at PNNL. In this work, the microstructures of the ceramics have been designed to mitigate severe neutron radiation effects through increasing interfaces within the material. The nature of radiation defects are only visualized through transmission electron microscopy (TEM) analysis, specifically using the weak-beam method. This method allows the observation of defects in one specific crystallographic orientation (plane). This is done for various planes, followed by comparison of

images to allow for observation of defects and their plane of origin. This technique is extraordinarily challenging and requires the input of an expert in the field. Professor John Drennan, the director of the CMM at UQ and his staff are experts in determining microstructure/physical property relationships in a wide variety of ceramics using electron microscopy. As such the EAPSI Fellowship, will allow the opportunity to characterize the radiation-induced defects in SiC.

In summary, in the immediate future the following investigations will be conducted through the EAPSI Fellowship:

- Explore the role of the carbon bonding and morphology in relation to SiC polytypes using TEM. Complete microstructural analysis of the various polytypes and graphene interfaces.
- Learn Techniques for Weak Beam method of TEM for analysis of ion-damaged samples. Analyze the nature of atomistic point defects in samples exposed to varying doses of ions
- Learn SAXS techniques. Determine size of nanodomains in samples processed under different conditions and with varying carbon content
- Write up results and complete any pending analyses necessary prior to departure.

Chapter VIII Suggested Future Work

VIII.1Polymer Derived SiC Stability in the Nuclear Environment

In the nuclear literature, 3C SiC has been extensively studied for its sustainability in the nuclear environment. We postulate that SiC polytypes (3C:6H) along with the effects of increasing interfaces with graphene nanodomains has potential to improve performance under conditions anticipated in the next generation of accident damage tolerant nuclear reactors. It has been shown that increasing interfaces in the form of stacking faults allows a sink for mobile vacancies Figure VIII-1

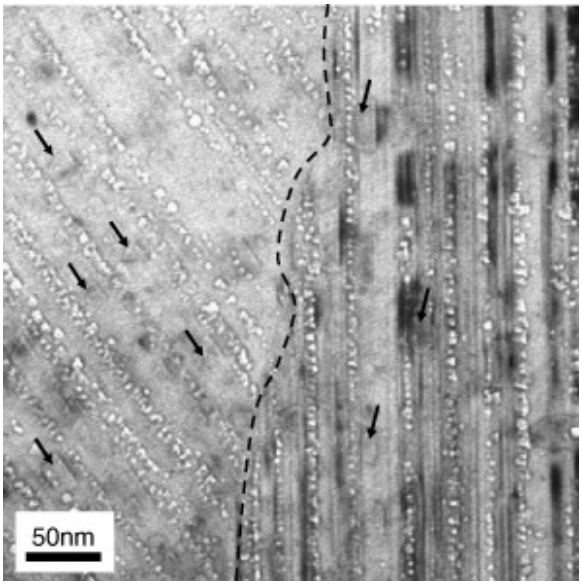

Figure VIII-1 Void swelling from mobile vacancies [58]

Processing

The unique method of molecularly modifying the precursor with C and B allows the intragranular incorporation of boron in the form of boron carbide, with a silicon boride outer layer within the SiC grains as demonstrated using Nano-SIMS (Figure VIII-2). Furthermore, it can also be shown using Nano-SIMS that increasing concentration of carbon from 1-5 wt % shows coarsening of the species within the SiC structure (Figure VIII-2). The effects of non-stoichiometry can be further confirmed through analysis of total carbon content following pyrolysis. This can be determined through a combustion/non-dispersive infrared gas analysis method using the C,H,N,S analyzer. Likewise, it is necessary to quantify the remaining concentration of boron in the system following pyrolysis through use of ICP-MS. Finally, ordering of the free carbon phase with increasing the temperature (up to 2000°C) for the various Si:C ratios should be characterized with Raman Spectroscopy. In addition to characterizing the samples with excess carbon it will also be important to observe the Raman intensity prior to thermal treatment of SMP-10 alone. The combination of these tools gives great insight into the sintering mechanisms as well as the self-assembly mechanisms associated with non-stoichiometry and impurity atoms during densification and processing in general.

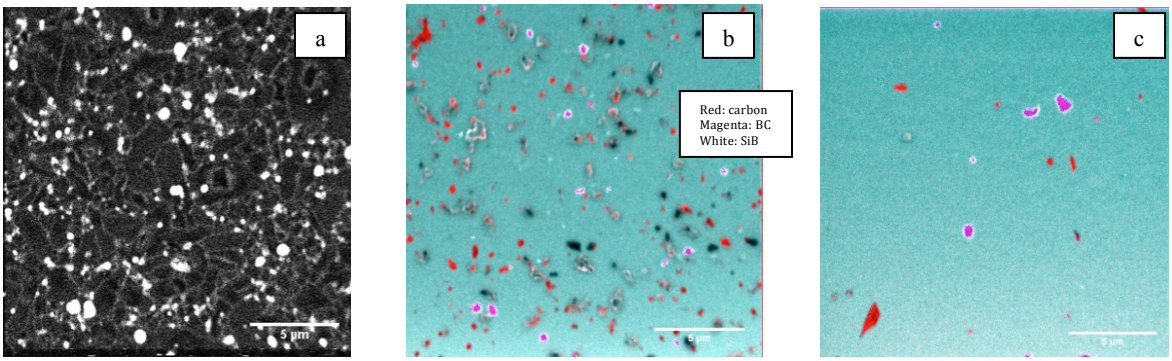

Figure VIII-2 a)Intragranular incorporation of B, b)1 wt% excess C, c) 5 wt% excess C

It can be appreciated that introducing boron using traditional ceramic processing routes of amorphous boron powder additions to SiC powders allows for incorporation of boron at the grain boundaries as demonstrated using ToF-SIMS at EMSL (

Figure VIII-3). ^{29}Si MAS NMR analysis at EMSL also revealed the presence of the 4H SiC polytype and the complete absence of the 3C SiC polytype (

Figure VIII-3).

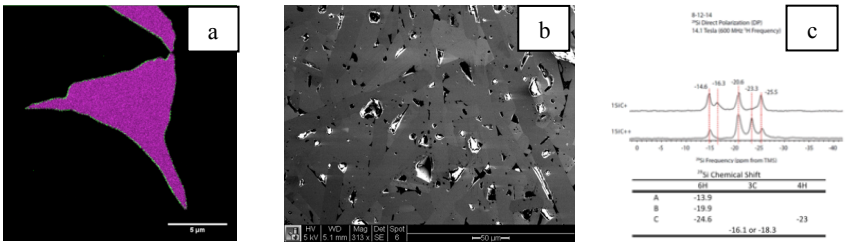

Figure VIII-3 Amorphous B added to SiC powders a) ToF-SIMS b) SEM c) ^{29}Si MAS NMR

The SEM, ToF-SIMS, Nano-SIMS and MAS-NMR characterization techniques yield information on the distribution of the dopants and the microstructure. This can be used to develop an understanding of the sintering mechanisms and grain growth associated with non-

stoichiometry and impurity atoms during densification of PDC SiC. Further sintering studies can confirm the transport mechanisms (lattice diffusion vs. grain boundary diffusion) leading to the morphological evolution of the microstructure during sintering. In these studies, attention can be focused on minimizing boron usage while maintaining full density. This will lead to a systematic understanding of how to couple processing and microstructure properties for nuclear applications. Due to the broad range of SiC applications, this work is also of interest for: semiconductors, body armor, abrasives/cutting tools, and extreme environments in which high temperature structural and wear resistant materials are needed.

Properties

Preliminary ion accelerator experiments were performed at EMSL to determine the effects of processing and microstructure on properties. The swelling of the material due to point defect accumulation was explored using the Asylum MFP-3D AFM. Compositions of the exact same stoichiometries (1 wt% excess C and 1 wt% B in SiC) but varying methods of boron incorporation (added molecularly to the precursor vs. added to the powder) were compared in their ability to mitigate radiation damage from ion bombardment. It was observed that boron added at the molecular level demonstrated an increased ability in mitigating radiation defects as evidenced by significantly reduced step height changes associated with point defect swelling between masked and un-masked regions as shown in Figure VIII-4 and Figure VIII-5.

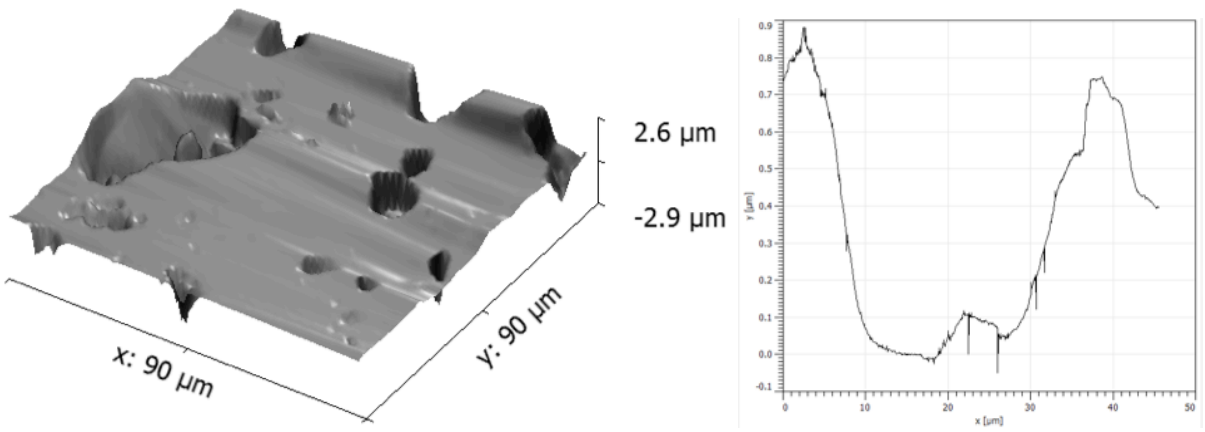

Figure VIII-4 Radiation damage in SiC in which B is added as a powder

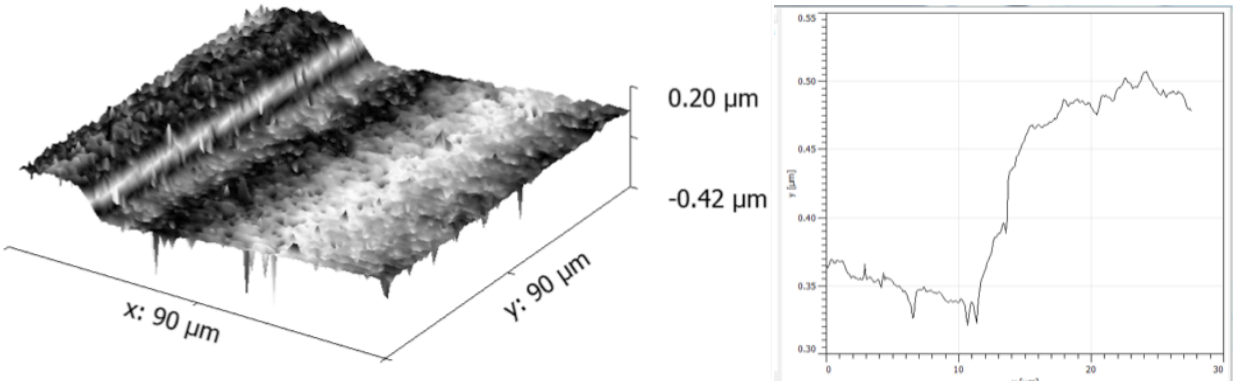

Figure VIII-5 Radiation damage in SiC in which B is added as a molecular precursor

The neutron stability of these materials can be explored through strategic placement of the systematically controlled polymer derived SiC ceramics in the High Flux Isotope Reactor (HFIR) located at the Oak Ridge National Laboratory (ORNL) (Figure VIII-6).

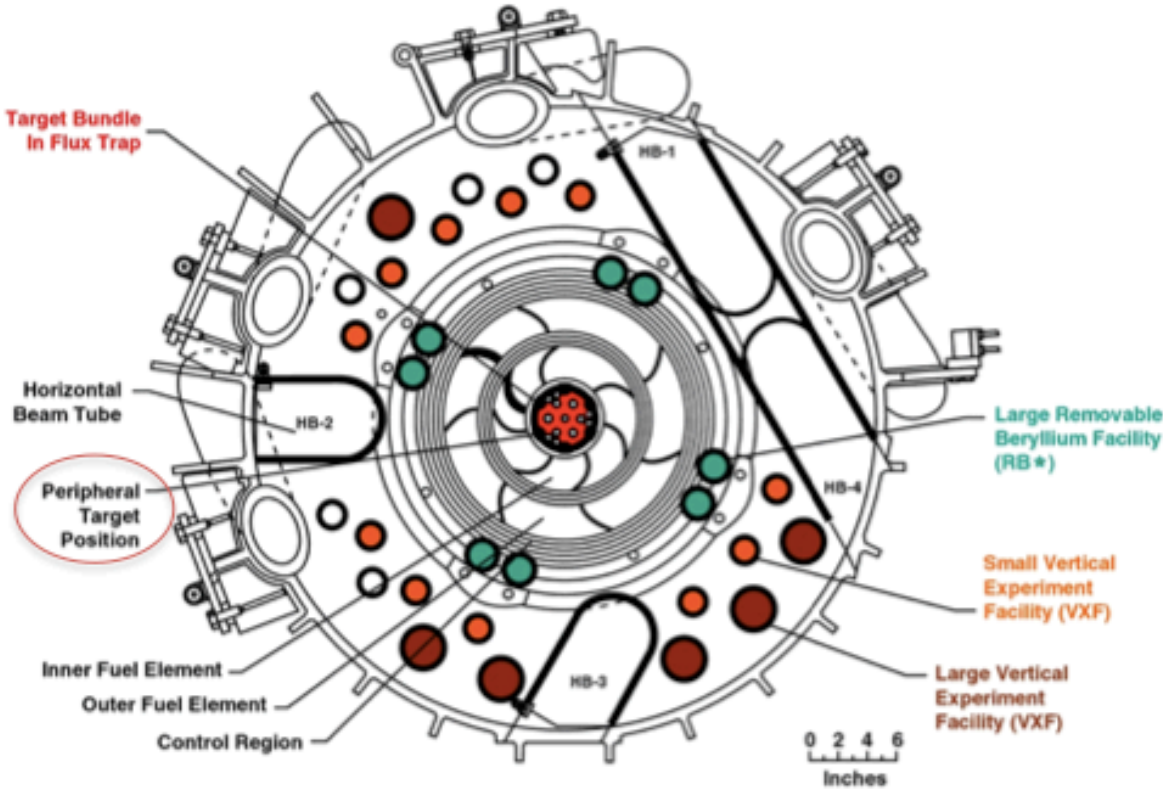

Figure VIII-6 High Flux Isotope Reactor (ORNL)

Through placement of the polymer derived SiC ceramics (with varying stoichiometries as well as boron concentration) in the peripheral target position of the HFIR, rapid neutron radiation experiments can be designed. The HFIR is an 85 MW research reactor yielding the highest steady-state neutron flux in the western world. The HFIR generates a peak thermal flux of 2.5×10^{15} n/cm^2-s and a peak fast flux of 1.1×10^{15} n/cm^2-s.[129] The HFIR is an ideal reactor to irradiate the various SiC samples due to its ability to quickly generate isotopes that require multiple neutron captures and perform materials irradiations that simulate lifetimes of power reactor use in a fraction of the time in a single cycle lasting between 23 and 26 days. This study would allow rapid screening and optimization of the composition.

The advanced test reactor (ATR) at the Idaho National Laboratory is an ideal reactor system for determination of the long-term stability the PDC SiC ceramics. The ATR is a water-cooled, high-flux test reactor that allows large power variations among its flux traps. As such in a single trap it is possible to achieve varying temperatures and fluxes. Specifically, the “B” positions in Figure VIII-7, in the ATR allow for the highest possible fluxes and temperatures.

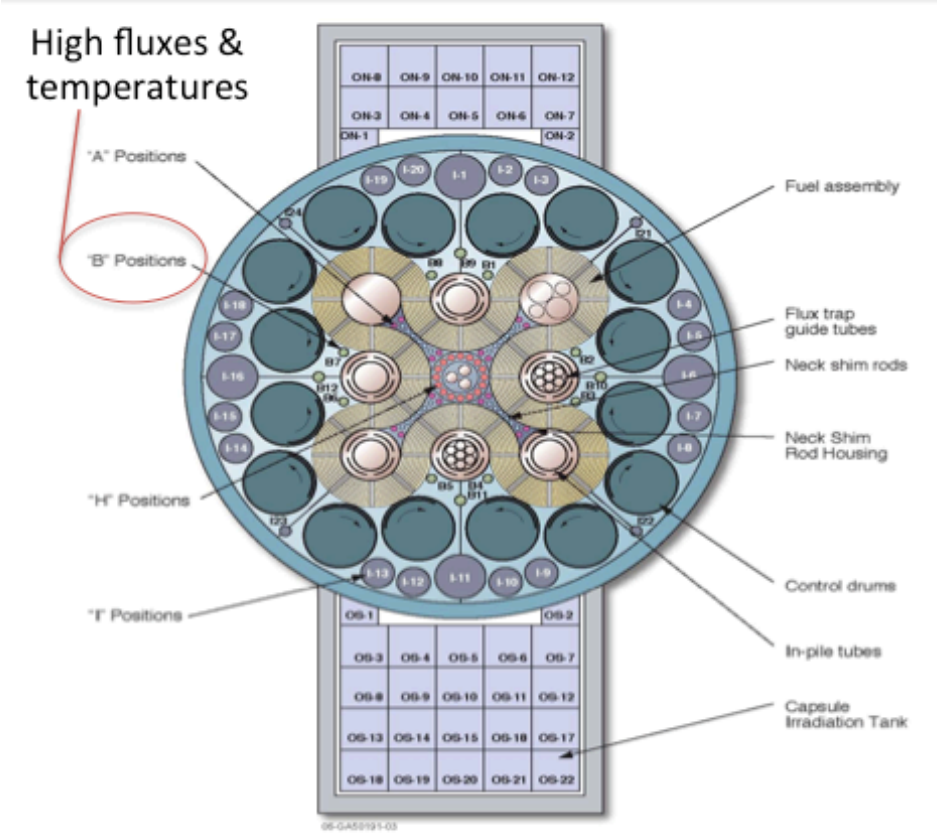

Figure VIII-7 Advanced Test Reactor at INL

Through utilization of the ATR at INL the compositions that were determined the most stable from the HFIR can be further evaluated. Here we can determine how the radiation damages the material at varying fluences as well as temperatures. It is also possible to do bend stress relaxation experiments in situ to determine the radiation creep, where thin strip samples are bent to a fixed radius during irradiation (Figure VIII-8).

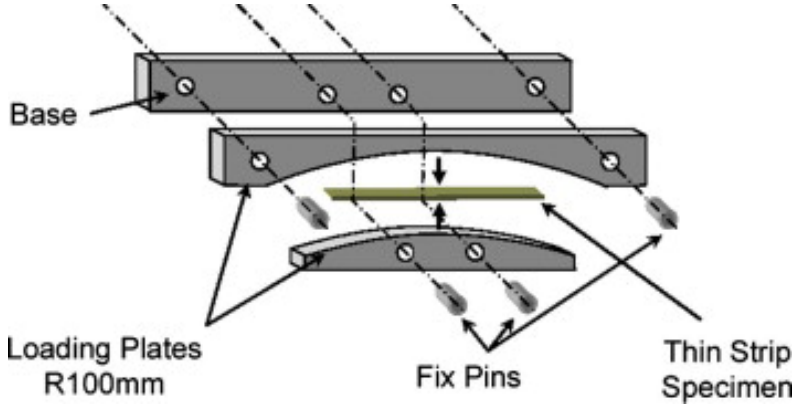

Figure VIII-8 Fixture of Bend stress relaxation experiment

This is done through machining the dense PDC SiC ceramics into thin strip samples of approximate dimensions of 40 mm x 0.1 mm x 1.0 mm. The initial and final stresses σ_0 and σ_a, respectively are calculated using the measured initial (constrained) bend radius (R_0), and the unconstrained residual bend radius after irradiation. Further details of this test are provided in section II.4.3.

The results of this study are threefold: to understand the effects of molecularly controlled intragranular boron, determine the role of increasing interfaces within SiC, and to establish a

systematic understanding of SiC crystal structures (3C:6H) in the mitigation of radiation defects. We hypothesize that increased radiation stability will arise with decreased concentration of boron and finer dispersions thereof. This is due to the potential negative effects associated with (n,α) reactions with boron leading to He accumulation at the grain boundaries causing embrittlement and failure of the material.

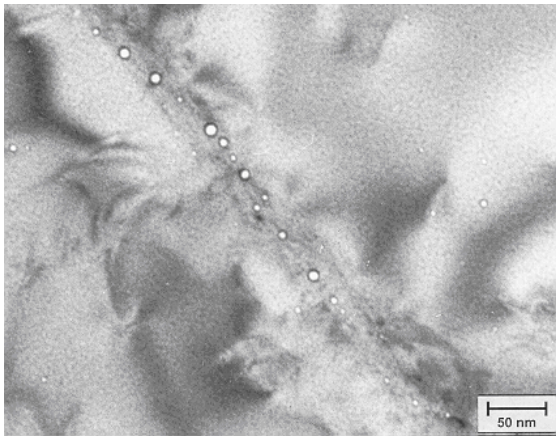

Figure VIII-9 Grain boundary embrittlement [130]

The hypothesis for this part of the research is that the incorporation of nanostructured interfaces within SiC will allow a center for point defect recombination in the mitigation of radiation defects detrimental to the lifetime of SiC in the neutron environment. The studies in the literature have focused solely on one SiC polytype, but none of mixed. Here a range of microstructures will be studied to understand their functionality in the prevention of deleterious microstructural evolution due to radiation damage processes. These experiments will explore the relationship of processing with microstructure properties in the neutron environment.

Using a radiological ^{29}Si MAS NMR and radiological powder XRD (located at EMSL facilities) the resultant polytypes (or SiC amorphization) can be examined following neutron radiation leading to an understanding of polytype stability in the neutron environment. The radiological AFM can allow the determination of surface roughness due to swelling of the material as a function of processing conditions. The nature of radiation defects is only visualized through transmission electron microscopy (TEM) analysis. A radiological FIB will allow the preparation of the irradiated SiC samples to study in the radiological TEM (ARM). The weak beam method of TEM analysis will allow the observation of defects in one specific crystallographic orientation (plane). This is done for various orientations, followed by comparison of images to allow for observation of defects and their planes of origin. This combination of techniques (TEM, AFM, XRD and NMR) will allow determination of the microstructure/physical property relationships in irradiated nanostructured SiC ceramics. The ability to study the radiation defects will substantially improve our understanding of the optimum operating temperature window for this new class of SiC for the next generation nuclear power plants that are anticipated to operate under high radiation fluxes and at elevated temperatures.

Summary of the suggested work for determining the stability of polymer derived SiC stability in the neutron environment:

- Explore the role of the carbon bonding & morphology in relation to SiC polytypes using TEM.
- Design experiments to induce neutron damage to polymer derived SiC ceramics at varying temperatures and fluences within the ATR at INL

- Design in-situ creep testing experiment during exposure to neutron damage to investigate creep mechanisms
- Utilize weak beam method of TEM for analysis of neutron-damaged samples. Analyze the nature of atomistic point defects in SiC ceramics exposed to neutron irradiation at varying locations within the ATR.
- Develop an understanding of the interfacial relationship of SiC polytypes (3C and 6H) with graphene when exposed to neutron radiation using TEM techniques

VIII.2 Porous PDC SiC

Porous SiC ceramics are useful in the nuclear field and elsewhere including: filters, catalytic supports, separation membranes, thermoelectric energy conversion, storage and retention of gases and reinforcement of composites.[103 131] In order to meet design demands of these applications, the properties over a range of porosities must be understood. In this research a novel processing technique to control the pore distribution, pore morphology and pore size of SiC porous monoliths was developed. Due to the many applications and the novel processing route of this material, there is great potential for this technology, including commercial applications and therefore many opportunities for further exploration.

The porous SiC ceramics were engineered using a polymeric route, followed by thermal conversion to the ceramic phase The preceramic polymer SMP-10 was modified by

incorporating a foaming agent azodicarbonamide (ADA). In order for this foaming reaction to be controlled, a variety of processing parameters were investigated and optimized. These include: holding temperature, rate of curing, dispersal mechanism, colloidal system, and concentration of foaming modifiers (decaborane & divinylbenzene) and foaming agent. For example, as seen in Figure VIII-10 pore morphology can be controlled through modifications of the polymeric system.

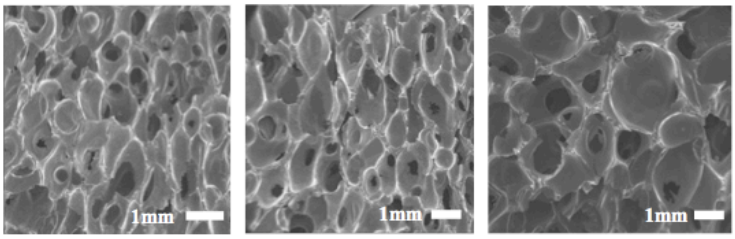

Figure VIII-10 0,0.5 & 1 wt% decaborane in 1wt% ADA respectively L-R

The pore morphology of the boron-modified SMP-10 system was tailored by varying the concentration of decaborane. This method of foaming produced porous SiC monoliths with a controllable trend from elliptical to spherical pores oppositely, increasing the concentration of the foaming agent ADA yielded a decrease in pore size and a change in pore morphology from spherical to ellipsoidal

.

The tailoring of these variables allowed the development of a systematic processing route to control pore morphology, pore distribution and excess carbon in the material system. Although the engineering of these ceramics has been realized, a scientific understanding of the reaction kinetics and mechanisms has not yet been developed. This research can be advanced by

understanding the governing reactions associated with time and temperature dependence of the bubble nucleation and bubble growth associated with the crosslinking mechanisms in the molecularly modified polymeric system. Additionally, the thermal and gas storage properties associated with the controlled porous PDC SiC structures can be explored to investigate the performance of the porous SiC.

The kinetics of the polymer cross-linking can be studied by determining the viscoelastic properties of the system as a function of the processing variable and time. This will provide an understanding of the diffusion of the gaseous species through the polymer melt, leaving behind the porous monolith. The evolution of these gaseous species with temperature can be evaluated using Thermogravimetric Analysis coupled with Fourier Transform Infrared Spectroscopy (TGA/FTIR). In order to conduct these studies, a viscometer with the ability to achieve temperatures up to 300°C in an inert atmosphere and thermal analysis equipment that can evaluate the composition of the evolved gases is needed.

As demonstrated previously through SEM images, the pore morphology of the bulk porous SiC structures can be tailored by controlling the molecular architecture of the polymeric system. However, SEM imaging is limited to a 2D cross section and is not representative of the bulk. It would be ideal to generate 3D images using micro X-ray computed tomography (μCT). With this technique, it is possible to characterize the pore density, pore distribution, average strut connectivity, cell size distribution and the strut thickness distribution. Ideally the μCT studies would be complimented with mercury intrusion porosimetry (MIP) experiments. This will allow

the determination of pore volume, surface area and density of the resultant ceramic structures. The proposed characterization techniques will allow the determination of the effects of the processing variables on the resultant porous SiC structures.

The applicability of the porous ceramics can be examined through observations of their gas storage ability and thermal conductivity. The gas permeability within the foamed system can be determined using a laboratory designed gas flow meter device. These studies could be coupled with the cell window size determined from the μCT results to more effectively examine the effect of microstructure on gas permeability. The thermal conductivity studies will allow the determination of the effects of the graphene network introduced into the porous SiC system in the form of excess carbon to the SMP-10 precursor. These studies will give necessary information on the relationship of processing on the properties of the porous polymer derived SiC ceramics.

Summary of the suggested future work in the area of porous polymer derived SiC

- Investigate the role of viscosity and stabilization of the polymer melt for the following processing variables: holding temperature, rate of curing, dispersal mechanism, colloidal system and concentration of foaming modifiers (decaborane & divinylbenzene) and foaming agent (ADA)
- Using TGA/FTIR determine the evolution temperature and chemical nature of the evolved gaseous species.

- Investigate the pore volume, surface area and densities of the variety of porous materials using mercury intrusion porosimetry.
- Experimentally determine the ability of these materials to store and retain gaseous products.
- Investigate the thermal properties of the varying pore morphologies and additionally the effect of the carbon nanodomains of the porous SiC ceramics
- Determine: pore density, pore and cell size distribution, connectivity, strut thickness distribution using μCT

VIII.3 Hot Pressing Partially Pyrolyzed powders

Partially pyrolyzed powder SiC samples should be milled thoroughly after thermal treatment to assure uniform particle sizes. Additionally, the dicumyl peroxide should be added to the SMP-10 precursor to assist in the crosslinking of oligomers that would otherwise come off as hydrocarbons during pyrolysis. It would additionally be beneficial to attempt to hot press the crosslinked powders once more with the new pressure regime where the pressure is added only once the final temperature has been achieved. This is in opposition to the one originally used where full pressure was applied on the sample immediately. This has the possibility of leaving the crosslinked powders with some reactivity for sintering.

VIII.4 Crystalline vs Amorphous SiC for High Temperature Nuclear Applications

It is well appreciated that crystalline materials are preferred to amorphous materials for high temperature nuclear applications. However, one of the benefits of using PDCs for generating SiC is that the amorphous ceramics that result from their polymers are very stable at high temperatures. However, the nuclear stability of amorphous polymer derived SiC has not been studied. It is therefore important to not only prepare fully crystalline SiC ceramics, but also to look at various degrees of crystalline SiC by heat treating the PDCs at different temperatures and testing their mechanical and radiation resistant properties. This will allow the determination as to whether amorphous, crystalline or partially crystalline materials are ideal for high temperature nuclear applications.

VIII.5 Effect of Stoichiometry on Mechanical and Radiation Stability

Systematically investigate the mechanical and thermal properties of nanostructured polymer derived SiC ceramics with controlled polytypes as a function of temperature is needed. In addition, the mechanical and thermal properties, both at room and elevated temperatures can be studied for the various Si:C ratios prepared. This can be done to develop a relationship between nanostructure and composition on the mechanical properties of the materials.

The modulus as a function of the temperature for different nanostructures can be experimentally determined from mechanical measurements and also using a high temperature nanoindenter.

Ideally, this would be completed before and after ion implantation of crystalline dense SiC samples. Room temperature and high temperature strength can be measured using a 4-point flexure tests and the room temperature fracture toughness can be measured using the single edge V notch beam technique.

Creep resistance should be explored to determine the suitability of the SiC ceramics under extended operation at elevated temperature. The compressive creep resistance of selected nanostructured materials should be determined as a function of temperature and stress, and will be analyzed using standard approaches. These experiments can be conducted in argon in the temperature range of 1575 K to 1650 K as a function of stress (100 to 250 MPa range).

It would also be ideal to develop a larger range of polytypes and explore mixed polytypes as a function of thermal conductivity and compare this to the literature values in Figure VIII-11.

Thermal conductivity, χ ($W\,cm^{-1}\,K^{-1}$)	Polytype	Comments
3.2	3C	poly-3C
3.7	4H	-
3.6	6H	$N_N = 8 \times 10^{15}\,cm^{-3}$ at 300 K
3.6	6H	$N_N = 5 \times 10^{16}\,cm^{-3}$ at 300 K
3.6	6H	$N_N = 1 \times 10^{19}\,cm^{-3}$ at 300 K
2.31	6H	$N_{Al} = 5 \times 10^{19}\,cm^{-3}$ at 300 K
4.9	6H	-

N_N = nitrogen doping concentration
N_{Al} = aluminium doping concentration

Figure VIII-11 Thermal conductivity of SiC polytypes [124]

VIII.6 Experimental Studies on Radiation Effects

Energetic ion irradiation was used to produce displacement damage to simulate the neutron environment. Ideally, various temperatures could be utilized to couple the radiation fluence levels to better understand the tolerance of the newly developed structures and their associated mechanical properties. Following this study the irradiated samples at varying temperatures can be examined for damage accumulation using Grazing Incidence X-Ray Diffraction. This characterization technique can be used to study the degree of crystallinity and the nanostructure before and after irradiation. This study has the possibility of being correlated back to the polytypes present in the samples prior to irradiation damage.

The ion implantation studies can also be extended to study lower weight ions that are more representative of the neutron environment (He and Kr) and thus the ability to contain these gases. In particular, the diffusivity of these species can be obtained by heating the specimens in the ion beam analysis station and using Rutherford Backscattering (RBS) to monitor the depth profile of the He and Kr in the Si-C nanostructures. TEM can be used to explore the inert gas retention in more detail, looking specifically for where the swelling occurs in the materials.

Chapter IX VI References

(1) Marra, J. In *IOP Conference Series: Materials Science & Engineering* 2011; Vol. 18, p 162001.

(2) Hittner, D.; Bogusch, E.; Fütterer, M.; de Groot, S.; Ruer, J. *Nuclear Engineering and Design* **2011**, *241*, 3490.

(3) Jiang, W.; Jiao, L.; Wang, H. *Journal of the American Ceramic Society* **2011**, *94*, 4127.

(4) Zinkle, S. J. In *Fusion Engineering & Design* 2005; Vol. 94.

(5) Griffith, G.; INL?CON-11-2318 ed.; Energy, U. S. D. o., Ed.; Enlarged Halden Programme Group Meeting: Idaho National Laboratory, 2011.

(6) Kim, B. G.; Choi, Y.; Lee, J. W.; Lee, Y. W.; Sohn, D. S.; Kim, G. M. *Journal of Nuclear Materials* **2000**, *281*, 163.

(7) Verrall, R. A.; Vlajic, M. D.; Krstic, V. D. *Journal of Nuclear Materials* **1999**, *274*, 54.

(8) S.J; Ghoniem, N. M. *Fusion Engineering and Design* **2000**, *51–52*, 55.

(9) Nozawa, T.; Hinoki, T.; Hasegawa, A.; Kohyama, A.; Katoh, Y.; Snead, L. L.; Henager Jr, C. H.; Hegeman, J. B. J. *Journal of Nuclear Materials* **2009**, *386–388*, 622.

(10) Rothaut, J.; Schroeder, H.; Ullmaier, H. *Philosophical Magazine B* **1983**, *47*, 781.

(11) Herderick, E. D. *American Ceramic Society Bulletin* **2013**, *92*, 32.

(12) Baba, M. *Radiation Measurements* **2013**, *55*, 17.

(13) Kryshev, II; Kryshev, A. I.; Sazykina, T. G. *Journal of Environmental Radioactivity* **2012**, *114*, 157.

(14) Buesseler, K. O. *Science* **2012**, *338*, 480.

(15) Chang, Y.-C.; Zhao, Y. *Marine Pollution Bulletin* **2012**, *64*, 897.

(16) Kim, C.-K.; Byun, J.-I.; Chae, J.-S.; Choi, H.-Y.; Choi, S.-W.; Kim, D.-J.; Kim, Y.-J.; Lee, D.-M.; Park, W.-J.; Yim, S. A.; Yun, J.-Y. *Journal of Environmental Radioactivity* **2012**, *111*, 70.

(17) Hamada, N.; Ogino, H. *Journal of Environmental Radioactivity* **2012**, *111*, 83.

(18) Buessler, K. O. J., S.R.; Fisher, N.S., Rypina, I.I., Baumann, H.; Baumann, Z.; Breier, C.F.; Douglass, E.M., Georger, J.; Macdonald, A.M.; Nishikawa, J.; Pike, S.M.; Yoshida, S. In *National Academy of Sciences* 2012; Vol. 109, p 5984.

(19) Murakami, M.; Oki, T. *Chemosphere* **2012**, *87*, 1355.

(20) Kritidis, P.; Florou, H.; Eleftheriadis, K.; Evangeliou, N.; Gini, M.; Sotiropoulou, M.; Diapouli, E.; Vratolis, S. *Journal of Environmental Radioactivity* **2012**, *114*, 100.

(21) Choi, H. *Annals of Nuclear Energy* **2011**, *38*, 2338.

(22) Lee, B. **2012**.

(23) Kiriyama, E.; Pickett, S. *Progress in Nuclear Energy* **2000**, *37*, 71.

(24) Tomanin, A. *Esarda Bulletin* **2009**, *41*.

(25) Members, M. N. F. C. C. *The Future of the Nuclear Fuel Cycle* MIT, 2011.

(26) Doug Chapin, S. K., Jim Nestell *MPR Associates Inc. Engineers* **2004**, 1.

(27) Ashbya, M.; Smidmana, M. **2011**.

(28) Moses, D. L.; Energy, D. o., Ed. Oak Ridge National Laboratory, 2010.

(29) Moses, D. L. *Nuclear Engineering and Design* **2012**, *251*, 216.

(30) Filippov, G. A.; Grishanin, E. I.; Konditerov, M. V.; Mastyukin, V. P.; Mel'kin, V. I.; Trubachev, V. M.; Fal'kovskii, L. N.; Fonarev, B. I.; Momot, G. V. *At Energy* **2006**, *101*, 722.

(31) Sasaki, K.; Maruyama, T.; Iseki, T. *Journal of Nuclear Materials* **1989**, *168*, 349.

(32) Fukuda, K.; Iwamoto, K. *Journal of Nuclear Science and Technology* **1975**, *12*, 181.

(33) Katoh, Y.; Hashimoto, N.; Kondo, S.; Snead, L. L.; Kohyama, A. *Journal of Nuclear Materials* **2006**, *351*, 228.

(34) Gao, F. W., W.J. *Philosophical Magazine. Structure and Properties of Condensed Matter* **2005**, *85*, 509.

(35) Heinisch, H. L.; Greenwood, L. R.; Weber, W. J.; Williford, R. E. *Journal of Nuclear Materials* **2004**, *327*, 175.

(36) Taguchi, T.; Igawa, N.; Miwa, S.; Wakai, E.; Jitsukawa, S.; Snead, L. L.; Hasegawa, A. *Journal of Nuclear Materials* **2007**, *367–370, Part A*, 698.

(37) Katoh, Y.; Snead, L. L.; Henager Jr, C. H.; Hasegawa, A.; Kohyama, A.; Riccardi, B.; Hegeman, H. *Journal of Nuclear Materials* **2007**, *367–370, Part A*, 659.

(38) Snead, L. L.; Nozawa, T.; Katoh, Y.; Byun, T.-S.; Kondo, S.; Petti, D. A. *Journal of Nuclear Materials* **2007**, *371*, 329.

(39) Hobbs, L. W. *Nuclear Instruments and Methods in Physics Research Section B: Beam Interactions with Materials and Atoms* **1994**, *91*, 30.

(40) Jesurum, C. E.; Pulim, V.; Hobbs, L. W. *Journal of Nuclear Materials* **1998**, *253*, 87.

(41) Hobbs, L. W.; Sreeram, A. N.; Jesurum, C. E.; Berger, B. A. *Nuclear Instruments and Methods in Physics Research Section B: Beam Interactions with Materials and Atoms* **1996**, *116*, 18.

(42) Hobbs, L. W. *Journal of Non-Crystalline Solids* **1995**, *182*, 27.

(43) Hobbs, L. W.; Clinard, F. W.; Zinkle, S. J.; Ewing, R. C. *Journal of Nuclear Materials* **1994**, *216*, 291.

(44) Katoh, Y.; Kishimoto, H.; Kohyama, A. *Materials Transactions* **2002**, *43*, 612.

(45) Kondo, S.; Katoh, Y.; Snead, L. L. *Applied Physics Letters* **2008**, *93*.

(46) Barbot, J. F.; Beaufort, M. F.; Texier, M.; Tromas, C. *Journal of Nuclear Materials* **2011**, *413*, 162.

(47) Ryazanov, A. I.; Klaptsov, A. V.; Kohyama, A.; Katoh, Y.; Kishimoto, H. *Journal of Nuclear Materials* **2004**, *329*, 486.

(48) Heinisch, H. L.; Gao, F.; Kurtz, R. J. *Journal of Nuclear Materials* **2004**, *329*, 924.

(49) Zinkle, S. J. *Fusion Engineering and Design* **2005**, *74*, 31.

(50) Hasegawa, A.; Kohyama, A.; Jones, R. H.; Snead, L. L.; Riccardi, B.; Fenici, P. *Journal of Nuclear Materials* **2000**, *283*, 128.

(51) Hojou, K.; Izui, K. *Journal of Nuclear Materials* **1988**, *160*, 147.

(52) Loveland, W. M., D.j.; Seaborg, G.T. *Modern Nuclear Chemistry*; Wiley-Interscience; 1 edition, 2005.

(53) Suzuki, T.; Iseki, T.; Mori, T.; Evans, J. H. *Journal of Nuclear Materials* **1990**, *170*, 113.

(54) Kim, J. H.; Kwon, Y. D.; Yonathan, P.; Hidayat, I.; Lee, J. G.; Choi, J. H.; Lee, S. C. *Journal of Materials Science* **2009**, *44*, 1828.

(55) Bonal, J.-P.; Kohyama, A.; van der Laan, J.; Snead, L. L. *MRS Bulletin* **2009**, *34*, 28.
(56) Katoh, Y.; Kishimoto, H.; Kohyama, A. *Journal of Nuclear Materials* **2002**, *307*, 1221.
(57) Pramono, Y.; Imai, M.; Yano, T. *Journal of Nuclear Science and Technology* **2003**, *40*, 531.
(58) Kondo, S.; Katoh, Y.; Snead, L. L. *Journal of Nuclear Materials* **2009**, *386–388*, 222.
(59) Kondo, S.; Katoh, Y.; Snead, L. L. *Journal of Nuclear Materials* **2008**, *382*, 160.
(60) Demkowicz, M. J. *MIT News* **2009**.
(61) Zheng, S.; Beyerlein, I. J.; Carpenter, J. S.; Kang, K.; Wang, J.; Han, W.; Mara, N. A. *Nature communications* **2013**, *4*, 1696.
(62) Chandler, D. *MIT News Office* **2013**.
(63) Katoh, Y.; Snead, L.; Golubov, S. In *Mechanical Properties and Performance of Engineering Ceramics and Composites III*; John Wiley & Sons, Inc.: 2009, p 297.
(64) Katoh, Y.; Kondo, S.; Snead, L. L. *Journal of Nuclear Materials* **2008**, *382*, 170.
(65) Katoh, Y.; Snead, L. *Fusion Science and Technology* **2009**, *56*, 1045.
(66) Colombo, P.; Mera, G.; Riedel, R.; Soraru, G. D. *Journal of the American Ceramic Society* **2010**, *93*, 1805.
(67) **2001**, 1.
(68) Lee, R. **2009**, 1.
(69) Saha, A.; Raj, R.; Williamson, D. *Journal of the American Ceramic Society* **2006**, *89*, 2188.
(70) Wang, Z. C.; Aldinger, F.; Riedel, R. *Journal of the American Ceramic Society* **2001**, *84*, 2179.
(71) Greil, P. *Advanced materials* **2002**, *14*, 709.
(72) Rocha, R. M. G., P.; Bressiani, J.C.; Almeida Bressiani, A.H. *Materials Research* **2005**, *8*, 191.
(73) Bernard, S.; Weinmann, M.; Cornu, D.; Miele, P.; Aldinger, F. *Journal of the European Ceramic Society* **2005**, *25*, 251.
(74) Vakifahmetoglu, C.; Menapace, I.; Hirsch, A.; Biasetto, L.; Hauser, R.; Riedel, R.; Colombo, P. *Ceramics International* **2009**, *35*, 3281.
(75) Colombo, P.; Bernardo, E.; Biasetto, L. *Journal of the American Ceramic Society* **2008**, *87*, 152.
(76) Colombo, P. M., G.; Soraru, G.D.; Kleebe, H.J. *Polymer Derived Ceramics from Nano-Structure to Applications*; DEStech Publications: Lancaster, PA, 2009.
(77) Dernovsek, O.; Bressiani, J. C.; Bressiani, A. H. A.; Acchar, W.; Greil, P. *Journal of Materials Science* **2000**, *35*, 2201.
(78) Kaindl, A.; Lehner, W.; Greil, P.; Kim, D. J. *Materials Science and Engineering a-Structural Materials Properties Microstructure and Processing* **1999**, *260*, 101.
(79) Bernardo, E.; Parcianello, G.; Colombo, P.; Adair, J. H.; Barnes, A. T.; Hellmann, J. R.; Jones, B. H.; Kruise, J.; Swab, J. J. *Journal of the European Ceramic Society* **2012**, *32*, 1329.
(80) Ly, H. Q.; Taylor, R.; Day, R. J.; Heatley, F. *Journal of Materials Science* **2001**, *36*, 4037.

(81) Idesaki, A.; Sugimoto, M.; Tanaka, S.; Narisawa, M.; Okamura, K.; Itoh, M. *Journal of Materials Science* **2004**, *39*, 5689.

(82) Varshneya, A. K. *Fundamentals of Inorganic glasses*; Academic Press Inc.: San Diego, CA, 1994.

(83) Hattar, K.; Demkowicz, M. J.; Misra, A.; Robertson, I. M.; Hoagland, R. G. *Scripta Materialia* **2008**, *58*, 541.

(84) Demkowicz, M. J.; Hoagland, R. G.; Hirth, J. P. *Physical Review Letters* **2008**, *100*.

(85) Lara-Curzio, E. *Mechanical Properties and Performance of Engineering Ceramics and Composites III*; John Wiley & Sons: Daytona Beach, FL, 2007.

(86) Kleebe, H. J.; Blum, Y. D. *Journal of the European Ceramic Society* **2008**, *28*, 1037.

(87) Knight, D. S.; White, W. B. *Journal of Materials Research* **1989**, *4*, 385.

(88) Kleebe, H.; Blum, Y. *Journal of the European Ceramic Society* **2008**, *28*, 1037.

(89) Pantano, C. G.; Singh, A. K.; Zhang, H. X. *Journal of Sol-Gel Science and Technology* **1999**, *14*, 7.

(90) Tavakoli, A. H.; Gerstel, P.; Golczewski, J. A.; Bill, J. *Acta Materialia* **2010**, *58*, 6002.

(91) Sickafus, K. E.; Grimes, R. W.; Valdez, J. A.; Cleave, A.; Tang, M.; Ishimaru, M.; Corish, S. M.; Stanek, C. R.; Uberuaga, B. P. *Nature Materials* **2007**, *6*, 217.

(92) Shen, T. D.; Feng, S.; Tang, M.; Valdez, J. A.; Wang, Y.; Sickafus, K. E. *Applied Physics Letters* **2007**, *90*.

(93) Zhang, J. M.; Lian, J.; Fuentes, A. F.; Zhang, F. X.; Lang, M.; Lu, F. Y.; Ewing, R. C. *Applied Physics Letters* **2009**, *94*.

(94) Lian, J.; Zhang, J. M.; Namavar, F.; Zhang, Y. W.; Lu, F. Y.; Haider, H.; Garvin, K.; Weber, W. J.; Ewing, R. C. *Nanotechnology* **2009**, *20*.

(95) Muller, A.; Gerstel, P.; Weinmann, M.; Bill, J.; Aldinger, F. *Journal of the European Ceramic Society* **2000**, *20*, 2655.

(96) Jalowiecki, A.; Bill, J.; Friess, M.; Mayer, J.; Aldinger …, F. *Nanostructured ...* **1995**.

(97) Somiya, S. I., Y. *Silicon Carbide Ceramics*; Elsevier Applied Science: New York, NY, 1991.

(98) Bereciartu, A.; Ordás, N.; García-Rosales, C.; Moroño, A.; Malo, M.; Hodgson, E. R.; Abellà, J.; Sedano, L. *Fusion Engineering and Design* **2011**, *86*, 2526.

(99) Sharafat, S.; Aoyama, A.; Ghoniem, N.; Williams, B.; Katoh, Y. *IEEE Transactions on Plasma Science* **2010**, *38*, 2993.

(100) Riccardi, B.; Giancarli, L.; Hasegawa, A.; Katoh, Y.; Kohyama, A.; Jones, R. H.; Snead, L. L. *Journal of Nuclear Materials* **2004**, *329–333, Part A*, 56.

(101) Colombo, P. *Journal of the European Ceramic Society* **2008**, *28*, 1389.

(102) Takahashi, T.; Colombo, P. *Journal of Porous Materials* **2003**, *10*, 113.

(103) Zeschky, J.; Höfner, T.; Arnold, C.; Weißmann, R.; Bahloul-Hourlier, D.; Scheffler, M.; Greil, P. *Acta Materialia* **2005**, *53*, 927.

(104) Greil, P. *Journal of the American Ceramic Society* **1995**, *78*, 835.

(105) She, J. H.; Ueno, K. *Materials Research Bulletin* **1999**, *34*, 1629.

(106) Rahaman, M. N. *Ceramic Processing and Sintering*; 2 ed.; CRC PRess, Taylor & Francis Group: Boca Raton, FL, 2003.

(107) Prochazka, S. In *Mass Transport Phenomena in Ceramics*; Cooper, A. R., Heuer, A. H., Eds.; Springer US: 1975; Vol. 9, p 421.

(108) Herrmann, M.; Neher, R.; Brandt, K.; Hoehn, S. *Journal of the European Ceramic Society* **2010**, *30*, 1495.

(109) Prochazka, S.; Scanlan, R. M. *Journal of the American Ceramic Society* **1975**, *58*, 72.

(110) Omori, M.; Takei, H. *Journal of the American Ceramic Society* **1982**, *65*, c92.

(111) van Rijswijk, W.; Shanefield, D. J. *Journal of the American Ceramic Society* **1990**, *73*, 148.

(112) S, P.; Google Patents: 1974.

(113) Clegg, W. J. *Journal of the American Ceramic Society* **2000**, *83*, 1039.

(114) Prochazka, S.; Charles, R. J. In *Fracture Mechanics of Ceramics*; Bradt, R. C., Hasselman, D. P. H., Lange, F. F., Eds.; Springer US: 1974, p 579.

(115) Hasegawa, Y. *Composites Science and Technology* **1994**, *51*, 161.

(116) Kaur, S.; Riedel, R.; Ionescu, E. *Journal of the European Ceramic Society* **2014**, *34*, 3571.

(117) Pirouz, P.; Yang, J. W. *Ultramicroscopy* **1993**, *51*, 189.

(118) Kelly, A. A.; Knowles, K. M. *Crystallography and crystal defects*; John Wiley & Sons, 2012.

(119) Jepps, N. W.; Page, T. F. *Progress in Crystal Growth and Characterization* **1983**, *7*, 259.

(120) Nakashima, S.-i.; Higashihira, M.; Maeda, K.; Tanaka, H. *Journal of the American Ceramic Society* **2003**, *86*, 823.

(121) Nakashima, S. i.; Higashihira, M.; Maeda, K.; Tanaka, H. *Journal of the American ceramic society* **2003**, *86*, 823.

(122) Florian, M.; Carvalho, L. E. d.; Cairo, C. A. A. *SiCf/SiC Composite: Attainment Methods, Properties and Characterization*, 2011.

(123) Lundqvist, D. *Acta Chemica Scandinavica* **1948**, *2*, 177.

(124) Harris, G. L. *Properties of silicon carbide*; Iet, 1995.

(125) Freyhardt, H. C., Muller, G. *Growth and Defect Structures*; Springer Berlin Heidelberg, 1984.

(126) Shaffer, P. *Acta Crystallographica Section B* **1969**, *25*, 477.

(127) Inomata, Y. *Thermal Stability of Wurtzite and Sphalerite Structures*, DTIC Document, 1971.

(128) .

(129) Garland, M. A.; Mirzadeh, S.; Alexander, C. W.; Hirtz, G. J.; Hobbs, R. W.; Pertmer, G. A.; Knapp Jr, F. F. *Applied Radiation and Isotopes* **2003**, *59*, 63.

(130) Kanne, W.; Louthan, M.; Rankin, D.; Tosten, M. *Materials characterization* **1999**, *43*, 203.

(131) Zeschky, J.; Goetz-Neunhoeffer, F.; Neubauer, J.; Jason Lo, S. H.; Kummer, B.; Scheffler, M.; Greil, P. *Composites Science and Technology* **2003**, *63*, 2361.